A.F. TECHNICAL REPORT 5853
PART III.

RECOVERY SYSTEMS FOR MISSILES AND TARGET AIRCRAFT

PART III.
HIGH SUBSONIC AND TRANSONIC TRACK BORNE PARACHUTE TESTS

J. ROBERT DOWNING
HAROLD V. HAWKINS
JOHN H. McCLOW, JR.
PAUL E. PEDERSEN

COOK RESEARCH LABORATORIES
A DIVISION OF COOK ELECTRIC COMPANY
CHICAGO, ILLINOIS

DECEMBER 1956

WRIGHT AIR DEVELOPMENT CENTER

NOTICES

When Government drawings, specifications, or other data are used for any purpose other than in connection with a definitely related Government procurement operation, the United States Government thereby incurs no responsibility nor any obligation whatsoever; and the fact that the Government may have formulated, furnished, or in any way supplied the said drawings, specifications, or other data, is not to be regarded by implication or otherwise as in any manner licensing the holder or any other person or corporation, or conveying any rights or permission to manufacture, use, or sell any patented invention that may in any way be related thereto.

- - - - -

Qualified requesters may obtain copies of this report from the ASTIA Document Service Center, Knott Building, Dayton 2, Ohio.

- - - - -

Copies of WADC Technical Reports and Technical Notes should not be returned to the Wright Air Development Center unless return is required by security considerations, contractual obligations, or notice on a specific document.

A.F. TECHNICAL REPORT 5853
PART III.

AD-122635

RECOVERY SYSTEMS FOR MISSILES AND TARGET AIRCRAFT

PART III.

HIGH SUBSONIC AND TRANSONIC TRACK BORNE PARACHUTE TESTS

J. ROBERT DOWNING
HAROLD V. HAWKINS
JOHN H. McCLOW, JR.
PAUL E. PEDERSEN

COOK RESEARCH LABORATORIES
A DIVISION OF COOK ELECTRIC COMPANY
CHICAGO, ILLINOIS

DECEMBER 1956

PARACHUTE BRANCH, EQUIPMENT LABORATORY
CONTRACT No. AF 33(038)-10653
PROJECT No. 6069-61520

WRIGHT AIR DEVELOPMENT CENTER
AIR RESEARCH AND DEVELOPMENT COMMAND
UNITED STATES AIR FORCE
WRIGHT-PATTERSON AIR FORCE BASE, OHIO

Carpenter Litho & Prtg. Co., Springfield, O.
200 - February 1957

FOREWORD

This report was prepared by the Cook Research Laboratories, a Division of Cook Electric Company, Chicago, Illinois, in compliance with Contract AF 33(038)-10653. Work by the Cook Research Laboratories was conducted under Project 6069-61520 by the Parachute Branch of the Equipment Laboratory, Wright Air Development Center, with Mr. R. J. Berndt as Project Officer. The work at Cook Research Laboratories was conducted under the supervision of Dr. J. R. Downing, Director of the Laboratories, with Mr. J. H. McClow, Jr., as Project Engineer. This report, the third of a series issued on this project, was compiled by Mr. P. E. Pedersen and edited by Mrs. T. A. Dunbar.

Staff members of Cook Research Laboratories who have contributed to the project include:

Dr. H. V. Hawkins	Assistant Director and Technical Head - Aerodynamics Section
R. O. Fredette	Assistant Director of Research
S. C. Henjum	Engineer in Charge - Field Test Section
P. E. Pedersen	Aeronautical Engineer - Aerodynamics Section
P. R. Hoffman	Aeronautical Engineer - Aerodynamics Section
J. L. Musil	Aerodynamicist - Aerodynamics Section
F. A. Ruprecht	Supervisor - Parachute Section

Others who have rendered valuable assistance to the project include:

Dr. H. G. Heinrich	Wright Air Development Center
T. W. Knacke	Parachute Development Test Group El Centro, California
J. P. Sturrock	Capt. USAF, Flight Research Laboratory Wright Air Development Center
R. L. King	Chief, Experimental Track Branch Air Force Flight Test Center Edwards AFB, California
R. F. Gompertz	Chief, Rocket Branch AFFTC, Edwards AFB, California
W. E. Harrison	Chief, Photo Branch AFFTC, Edwards AFB, California
C. C. Baldridge	Supervisor, Motion Picture Branch AFFTC, Edwards AFB, California
J. Bridges	AMC Liaison Office AFFTC, Edwards AFB, California
A. S. Feld	AMC Liaison Office AFFTC, Edwards AFB, California

ABSTRACT

The operating characteristics of Guide Surface, FIST Ribbon, and Rotafoil parachutes tested in the high subsonic and transonic speed range from 450 to 862 mph are described. Associated problems such as deployment systems and harness design, encountered in parachute operation, are also discussed. Operational and design information obtained from the various parachutes tested is intended for application to the design of parabrakes capable of withstanding initial high velocity deployment, and decelerating a high velocity missile to a relatively low-speed range where a larger parachute can be deployed to accomplish safe recovery. All test parachutes were designed to have a drag area of 28 sq ft. Material strengths and constructional details were varied throughout the test program to provide parachutes of minimum bulk and weight commensurate with adequate strength characteristics for operations at the desired velocities. The tests were conducted with a liquid fuel rocket powered vehicle on the 10,000 foot Free Air Test Facility Track at Edwards Air Force Base, Edwards, California. The data obtained during the test program included inflation times, opening shock factors, drag forces, inflated diameters, and stability of the parachutes at various velocities. This work is a continuation of the program reported in Air Force Technical Report 5853 (Parts I and II) in which similar tests were made for speed ranges up to 500 mph.

PUBLICATION REVIEW

This report has been reviewed and is approved

FOR THE COMMANDER:

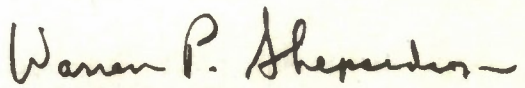

Warren P. Shepardson
Chief, Parachute Branch
Equipment Laboratory
Directorate of Development
Wright Air Development Center

TABLE OF CONTENTS

TABLE OF CONTENTS (cont'd)

LIST OF ILLUSTRATIONS

LIST OF ILLUSTRATIONS (cont'd)

LIST OF TABLES

LIST OF TABLES

LIST OF SYMBOLS

Quantity		Units
a^*	Speed of sound in air	fps
C_D	Drag coefficient of parachute based on theoretical projected area of canopy - (dimensionless)	
C_{D_o}	Drag coefficient of parachute based on total canopy area (S_o) - (dimensionless)	
D_o	Nominal diameter of parachute - equal to the diameter of a circle whose area is equal to the total canopy area (S_o) of the parachute	ft
D_p	Theoretical projected diameter of a fully inflated parachute	ft
$D_{p_1}{}^*$	Instantaneous projected diameter of parachute	ft
$(\frac{D_{p_1}}{D_p})_M{}^*$	Primary maximum diameter ratio	
$(\frac{D_{p_1}}{D_p})_A{}^*$	Average steady state diameter ratio	
F	Drag force of parachute as transmitted to sled	lb
F_o	Peak opening shock force	lb
$F_s{}^*$	Peak snatch force	lb
M	Mach number	lb
q	Dynamic pressure, $\frac{\rho v^2}{2}$	lb/sq ft
q_c	Impact pressure, compressible	

* Indicates that the definition is not included in the Parachute Handbook (Ref. 1) or that the definition in the Handbook has been modified.

LIST OF SYMBOLS
(cont'd)

Quantity		Units
q_o*	Dynamic pressure corresponding to the velocity of the sled at peak opening shock force	lb/sq ft
q_s	Dynamic pressure corresponding to the velocity of the sled at peak snatch force	lb/sq ft
F/qS	Instantaneous force ratio (S_o or S_p used as the case may be)	
R	Angular displacement of parachute from a longitudinal axis through attachment point	degrees
R_ω	Angular velocity of parachute about axis of revolution	rpm
S_o	Total design canopy area of parachute - for Guide Surface parachute, this includes area of ribs and skirt; for Ribbon and Rotafoil parachutes, S_o is the polygon area	sq ft
S_p	Theoretical projected area of inflated parachute	sq ft
t_f*	Time interval from occurrence of peak snatch force to the instant when parachute is inflated to primary maximum projected diameter	sec
t_{ml}*	Time interval from occurrence of peak snatch force to occurrence of peak opening shock	sec
t_s*	Time interval from initiation of deployment to occurrence of peak snatch force	sec
V	Instantaneous velocity	fps
V_d	Velocity of sled at instant parachute is deployed	mph

* Indicates that the definition is not included in the Parachute Handbook (Ref. 1) or that the definition in the Handbook has been modified

LIST OF SYMBOLS
(cont'd)

Quantity		Units
V_s	Velocity of sled at peak snatch force	fps
X*	Opening shock factor (dimensionless), $\left(\frac{F_o}{q_s C_D S_p}\right.$ or $\frac{F_o}{q_s C_{D_o} S_o}$ where the reference drag area is the average steady state value).	
λ_f	Cloth permeability of Guide Surface parachutes; equal to the number of cubic feet per minute of air passing through a square foot of fabric due to a pressure difference equivalent to 1/2 inch of water	
λ_g	Geometric porosity of the parachute. Considered equal to total porosity (λ_t) for parachutes of heavy construction	%
υ	Kinematic viscosity of air	sq ft/sec
ρ	Density of air	slugs/cu ft

* Indicates that the definition is not included in the Parachute Handbook (Ref. 1), or that the definition in the Handbook has been modified.

I. INTRODUCTION

The use of parachute recovery systems on supersonic test missiles and target aircraft is well established for effecting savings in expense and time as well as for the recovery of information not otherwise obtainable. In order to obtain data on parachute operation for such applications, a comprehensive research program was initiated. The majority of the effort has been spent on study and tests of small heavy duty parachutes suitable for deployment at high velocity as the first stage of a multistage recovery system. The operation of large parachutes such as would be employed at lower speeds as the final parachute in a multistage recovery system has been studied in conjunction with other problems, such as aerial cargo delivery.

This report, the third in the series concerned with development of parabrakes suitable for deployment in the transonic speed range, is a continuation of earlier tests conducted with rocket powered test vehicles on the 10,000 foot Free Air Test Facility Track at Edwards Air Force Base, California.

The first phase of the problem was concerned with parachutes of approximately 28 sq ft drag area, designed for operation at 400 mph with a factor of safety of 1.5. This series of tests was conducted with a trackborne solid fuel rocket propelled vehicle as described in Ref. 14, Part I. In order to validate the data obtained from the trackborne vehicle tests and obtain data on the effect of parameters that could not be varied on the sled program, a series of tests was conducted with a free-fall missile, carried to a predetermined release altitude by aircraft. Four general types of parachutes were considered, namely: the Guide Surface Stabilization, Guide Surface Ribless, FIST Ribbon, and Rotafoil. Several variations of each type were tested on the trackborne vehicle and the four parachutes which showed the best operational characteristics were tested on the free-fall vehicle, described in Ref. 14, Part II.

Manuscript released by the author December 1956 for publication as a WADC Technical Report.

Phase II of the project is concerned with high subsonic and transonic parachute tests conducted at the Free Air Test Facility, Edwards Air Force Base, California. These tests utilized a trackborne, liquid fuel rocket powered test vehicle as described in Appendix F.

The following is a report of these tests at deployment velocities up to 862 mph (Mach 1.11).

II. TEST CONDITIONS

A. Test Facility

In order to duplicate Phase IA test conditions, Phase II was conducted at the same 10,000 foot Free Air Test Facility Track at Edwards Air Force Base, California. Parachutes were tested by deploying them from a specially designed Liquid Fuel Rocket Powered test vehicle at a predetermined velocity and location along the track. A complete description of the vehicle is given in Appendix F.

B. Test Program

A series of 63 parachute tests was conducted at deployment velocities ranging from approximately 450 mph to 862 mph T.A.S. To determine operational limits and characteristics of each configuration tested, deployment velocity, structural details, and geometric parameters were varied in the tests. The first parachutes of each type tested were structurally strengthened versions of the best designs derived from Phase I tests. As the program continued, design changes were made to obtain improvements in operational and strength characteristics of the parachutes.

Various factors imposed limitations to the test program which should be considered when reference is made to the test data herein. These limitations are listed below:

(1) Parachute Size - limited to approximately 28 sq ft drag area

(2) Deployment Velocity - limited to increments between medium subsonic to mid-transonic, the upper range being determined by the maximum velocity of the test vehicle

(3) Altitude - limited to ground elevation at the test facility, (2300 feet above sea level)

(4) Parachute Stability - measured with respect to a fixed attachment point on the sled

(5) Infinite Mass - vehicle mass so great in comparison to parachute

area that little velocity change occurred during opening process.

Results of each test were included in the Cook Research Laboratories' progress reports (Ref. 15). General characteristics and performance of the parachute types tested are presented in Section IV of this report and detailed summaries of test results by parachute type are included in Appendices A, B, C, and D.

C. Parachutes

All parachutes tested in the program were designed to have a drag area of approximately 28 sq ft with ultimate structural quality able to withstand deployment and operation at transonic velocities.

Four general parachute types were considered:

(1) Guide Surface Stabilization

This type of parachute is manufactured from solid cloth and has a relatively flat roof canopy with a conical surface shaped as an inverted truncated cone below the roof portion of the canopy. Internal cloth ribs define the canopy shape and separate the suspension lines from the canopy, making the shape relatively independent of the suspension line arrangement. Several variations of this general type were considered during the test period. A description, together with test data obtained for these parachute types, is given in Appendix A.

(2) Guide Surface Ribless

The Guide Surface Ribless parachute, like the Guide Surface Stabilization, is manufactured in solid cloth form and has a conical surface shaped as an inverted truncated cone below the roof portion of the canopy. Instead of internal cloth ribs to contain the suspension lines, the roof and guide surface panels are fabricated so that the canopy assumes the proper geometric shape when inflated. Suspension lines are attached along the roof panel seams on the exterior of the parachute. A description of the various configurations tested and test data obtained for these parachute types are given in Appendix B.

(3) FIST Ribbon

The FIST Ribbon parachute is basically a flat circular canopy composed of concentric bands of ribbon parachute material, supported

by smaller, symmetrically spaced vertical ribbons and by radial bands at the side of each panel. These bands transmit the aerodynamic loads from the ribbons to the attached suspension lines. A complete description of a ribbon parachute panel assembly is given in Appendix C, together with test data and description of the various configurations studied in the program.

(4) Rotafoil

The term Rotafoil significantly describes the parachute type since it is a derivation from the words rotating air foil. This parachute is in the flat circular category with panels fabricated of solid cloth. Radial openings in each gore transform the canopy into a system of sails which cause rotation of the parachute during normal operation. Typical panel assemblies and geometric properties of this type of parachute are described in Appendix D. Test results of the two configurations investigated in the program are also presented in Appendix D.

D. Instrumentation

Complete instrumentation was carried on the test vehicle during each test.

A magnetic tape recording system provided records of the following parameters:

(1) Drag Force

(2) Impact Pressure

(3) Acceleration

(4) Time

(5) Position.

From these parameters other pertinent information such as opening shock force, inflation time, and velocity was determined. Measurements of parachute area and stability were obtained from sledborne high-speed motion picture camera films. These were synchronized to tape recorded information, by common time and position impulses.

Additional operational information was obtained with stationary still,

sequence, and high-speed motion picture cameras.

A detailed description of the instrumentation and photographic equipment employed in the tests is presented in Appendix G.

E. Deployment System

The parachute deployment system including associated harness and hardware, was considered to be operationally equal in importance to the parachutes being tested. During the program three basic methods of parachute deployment were utilized with variations in each method being introduced as needed. Generally, these three methods were:

(1) Forceful expulsion - rearward

(2) Projectile and pilot parachute deployment - rearward

(3) Forceful expulsion - perpendicular to airstream - to simulate a missile side deployment system.

A complete description of these systems as used in each test run is given in Appendix E together with pertinent details of associated harness and hardware utilized with each system. Also included is a description of the parachute attachment and separating device designed for the test vehicle and used throughout the test program.

III. CONCLUSIONS

The only parachutes which operated satisfactorily during the 13 tests conducted with the Guide Surface Ribless parachute were of the 12 gore heavy construction classification. These were tested at widely varying velocities. Steady state drag coefficient was 0.80 and opening shock factor averaged 1.55. Stability of the parachutes was good, with maximum displacements less than 5 degrees.

Average data cannot be given for the 16 gore version since all tests conducted with this configuration resulted in structural failure or incomplete inflation.

The maximum velocity at which a Guide Surface Ribless parachute was deployed with complete inflation and without major damage was 802 mph.

Within the limits of strength capabilities the Guide Surface Stabilization parachutes exhibited good operation characteristics. Steady state drag coefficient (C_D) averaged 1.05, and opening shock factor (X) was 1.19 for the 12 gore parachute and 0.94 for the 16 gore version. Stability for both configurations was excellent.

Although the general construction of the Guide Surface Stabilization parachute gives comparatively high weight and bulk for a given diameter, the high drag coefficient and low opening shock factor make it as efficient as the Ribless type.

The maximum velocity at which a Guide Surface Stabilization parachute was successfully operated was 753 mph.

Five of the 12 FIST Ribbon parachute types tested exhibited satisfactory performance characteristics in the transonic speed range. The five successful types had porosities between 21 and 24% with minor variations in vertical and horizontal ribbon spacing and had steady state drag coefficients between 0.45 and 0.55 when tested with standard $\left(\frac{L_s}{D_o} = 1\right)$ line lengths.

Tests of the Types 122 and 123 parachutes indicate that a change in

suspension line length from $\frac{L_s}{D_o} = 1$ to $\frac{L_s}{D_o} = 2$ resulted in an increase in drag coefficient of approximately 20%, no change in opening shock factor, and a slight decrease in stability.

The Type 124-17, with a porosity (λ_g) of 21.15% exhibited the best and most consistent over-all characteristics. Steady state drag coefficient (C_{D_o}) averaged 0.52 and opening shock factor (X) averaged 0.94.

Successful operation of FIST Ribbon parachutes was attained at velocities up to and including 838 mph.

Based on results of the five tests conducted with the Rotafoil parachutes it is evident that additional testing will be required to develop a structurally and aerodynamically efficient Rotafoil parachute capable of operation in the transonic speed range.

IV. PARACHUTE CHARACTERISTIC RESULTS

A. General

General geometric and aerodynamic performance characteristics of the parachute types which operated most satisfactorily during the test program are presented in the following paragraphs of this section of the report. Detailed summaries of test results are included, by parachute type, in the respective appendices of the report.

The parachute test program provided general design information about parachute performance in the velocity ranges tested and established preliminary designs for parachutes suitable for successful deployment in the transonic speed range. Design information obtained included drag coefficients, opening shock factors, inflated diameters, filling time, and stability characteristics of each parachute type. Values of these parameters for the parachute types successfully tested in the program are presented in Table 1.

A bar graph showing the deployment velocity ranges through which successful parachute deployment and operation was obtained is illustrated by general parachute category in Fig. 1. Exact deployment velocities of specific parachute types can be found in the following paragraphs in this section and in the corresponding parachute appendices of this report.

For ease of comparison of the inflation characteristics of the basic parachute types tested, idealized curves have been derived from the over-all inflation results of those tests of particular parachute types which exhibited the most favorable operational characteristics in their group. These are illustrated in the curves in Fig. 2 and are representative of the average opening characteristics of the parachute types presented. Additional specific information on the parachutes which exhibited most favorable performance results within each particular type group is presented in the paragraphs which follow. These paragraphs present the average performance characteristics for a particular type of parachute. Primarily, such items are given in tabular form and include the basic geometric properties as well as the pertinent performance parameters. In addition, average performance curves which represent the average of the summary data performance curves of a particular type parachute are presented with the tabulated data.

TABLE 1

GENERAL PARACHUTE CHARACTERISTICS

GUIDE SURFACE PARACHUTES

TYPE	NUMBER OF GORES	PROJECTED DIAMETER (Dp) FEET	PROJECTED AREA (Sp) SQ. FT.	DRAG COEFFICIENT C_D	OPENING SHOCK FACTOR 'X'	DIAMETER RATIO $(D_R/D_P) \times 100$ PERCENT		— STABILITY — ANGULAR DISPLACEMENT DEGREES		DEPLOYMENT VELOCITY RANGE TESTED (FT. / SEC)
						AVERAGE	PRIMARY MAX	MEAN	MAX.	
STABILIZATION TYPE III CLOTH	12	6.5	33.2	1.04	1.19	97.2	102.6	1.80	3.20	918 *
STABILIZATION TYPE III CLOTH	16	6.5	33.2	1.05	0.94	97.4	92.5	1.48	2.17	1104 *
RIBLESS TYPE III CLOTH	12	6.5	33.2	0.80	1.55	83.0	86.0	2.70	4.80	912 - 1176
RIBLESS TYPE III CLOTH	16	6.5	33.2	0.75	1.79	87.5	86.6	2.35	5.50	1151 - 1225 **

FIST RIBBON PARACHUTES

TYPE	GEOMETRIC POROSITY λ_g PERCENT	NOMINAL DIAMETER (Do) FEET	CANOPY AREA (So) SQ. FT	DRAG COEFFICIENT C_D	OPENING SHOCK FACTOR 'X'	DIAMETER RATIO $(D_R/D_P) \times 100$ PERCENT		— STABILITY — ANGULAR DISPLACEMENT DEGREES		DEPLOYMENT VELOCITY RANGE TESTED (FT/SEC)
						AVERAGE	PRIMARY MAX	MEAN	MAX.	
107	14.62	8.60	56.60	0.57	1.21	100.0	104.8	12.8	14.5	661 - 1128
122-123 (L_S/D=1)	23.10	8.51	55.46	0.50	1.04	99.4	101.5	3.1	4.6	1110 - 1227
122-123 (L_S/D =2)	23.10	8.51	55.46	0.60	1.04	107.2	111.9	4.6	7.2	1080 - 1119
124-10	21.15	8.60	56.60	0.53	1.05	101.7	105.5	5.6	8.2	923 - 1173
124-17	21.15	8.60	56.60	0.52	0.94	98.2	100.9	2.2	3.2	1203 - 1218
125	23.25	8.15	50.94	0.48	1.03	100.7	101.6	3.8	6.4	1174 - 1211
126	23.30	8.92	60.90	0.48	0.91	96.9	97.8	2.2	3.6	1057 - 1213

* ONE TEST ONLY

** AVERAGE OF TWO TESTS IN WHICH PARACHUTE NEVER FULLY INFLATED

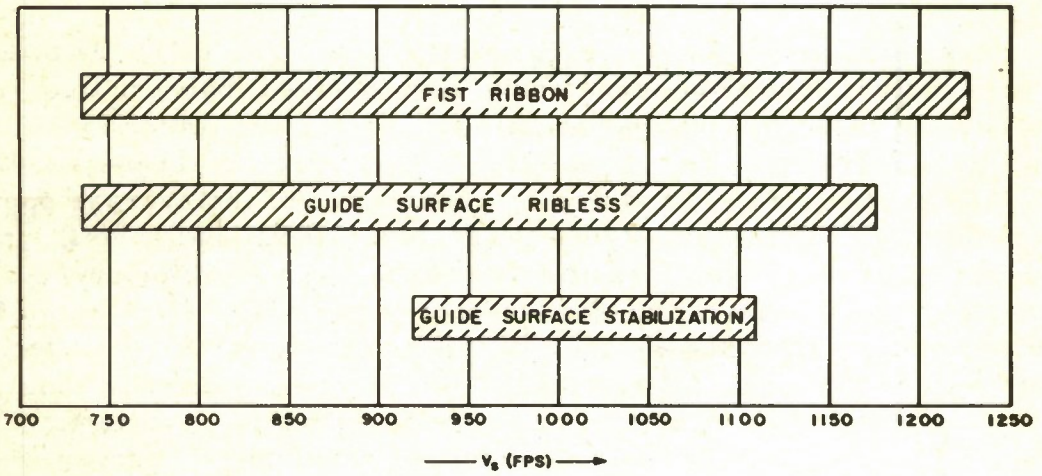

Figure 1 Range of Deployment Velocities Covered With Various Types of Parachutes in Test Which Resulted in Normal Deployments and no Parachute Damage

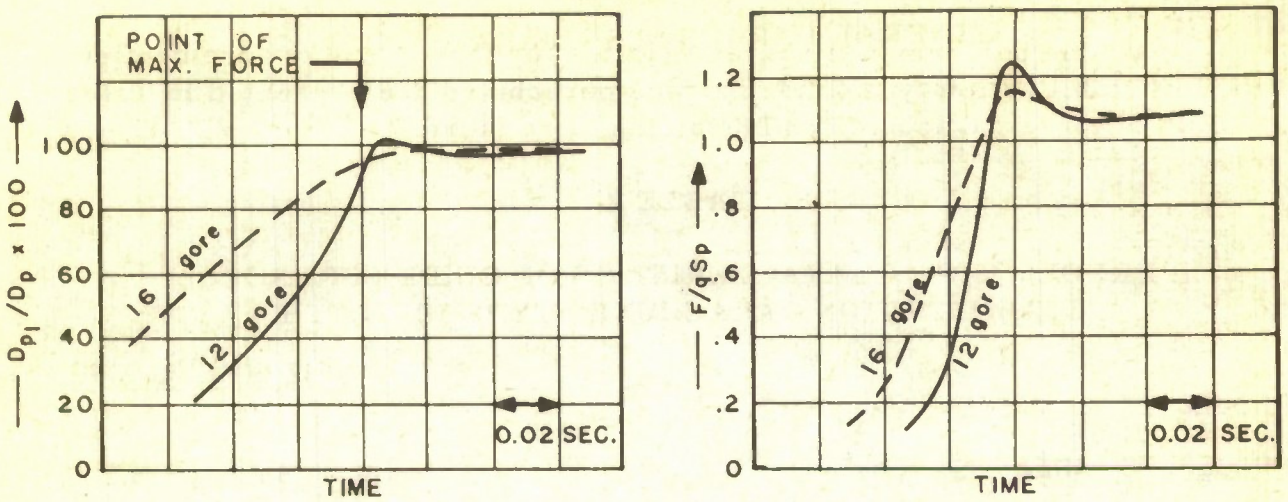

GUIDE SURFACE STABILIZATION (12 AND 16 GORE)

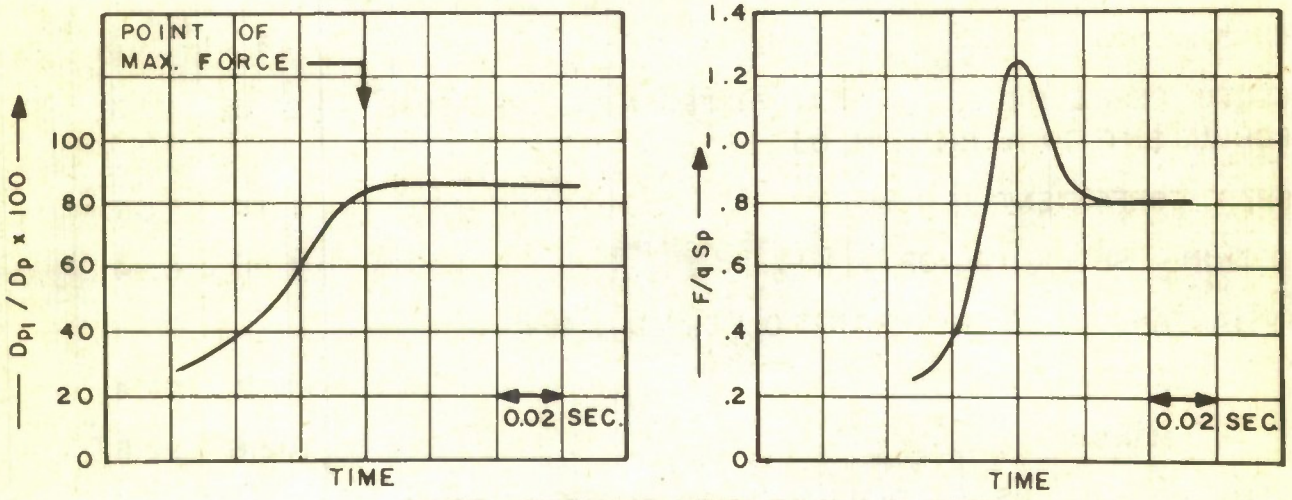

GUIDE SURFACE RIBLESS (12 GORE)

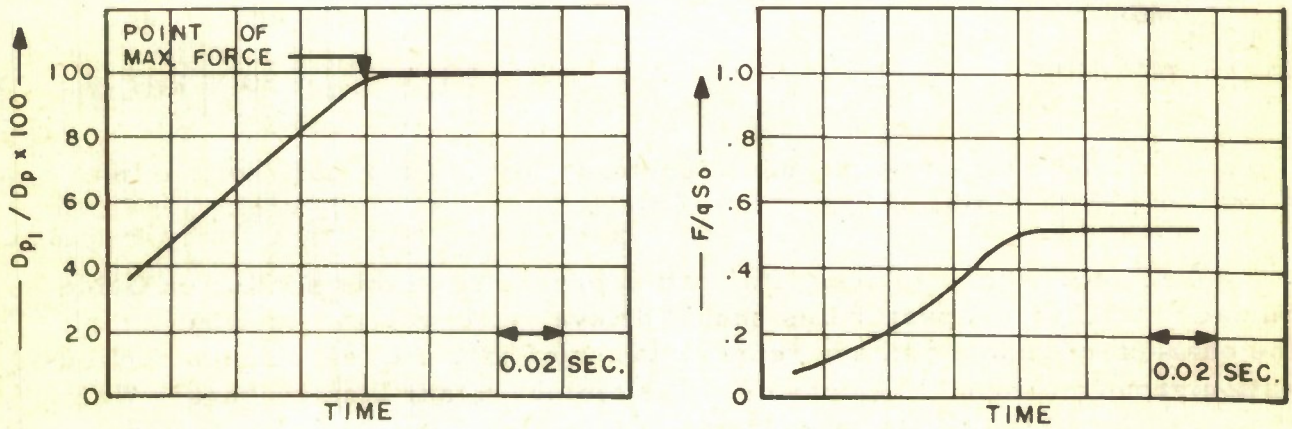

FIST RIBBON TYPE 124-17

Figure 2 Idealized Parachute Dynamic Characteristics

B. Guide Surface Stabilization Parachutes

Available performance characteristics for the 12 and 16 gore configuration of stabilization type Guide Surface parachutes are presented in Table 2. Both of these parachute configurations were fabricated from MIL-C-8021

TABLE 2

PERFORMANCE CHARACTERISTICS OF GUIDE SURFACE STABILIZATION PARACHUTE, TYPE III CLOTH

	12 GORE	16 GORE
PROJECTED DIAMETER, D_p (ft)	6.5	6.5
PROJECTED AREA, S_p (ft^2)	33.2	33.2
WEIGHT, (lbs)	27.1	33.0
BULK, (ft^3)	1.62	1.67
CLOTH PERMEABILITY, λ_f (AT DIFFERENTIAL PRESSURE EQUIVALENT TO ½ INCH H_2O)	22.3	22.3
DRAG COEFFICIENT, C_D	1.04	1.05
OPENING SHOCK FACTOR (X)	1.19	0.94
INSTANTANEOUS DIAMETER RATIO (D_{p_i}/D_p) %		
AVERAGE	97.2	97.4
MAXIMUM	102.6	92.5
STABILITY, RADIUS OF DISPLACEMENT, (R) DEGREES		
MEAN	1.80	1.48
MAXIMUM	3.20	2.17

Type III nylon cloth with a measured permeability of 22.3 cu ft/sq ft/min at a pressure differential of 1/2 inch of water.

Tabulated and graphical information presented in this section on Guide Surface Stabilization parachutes should be evaluated with the knowledge that the characteristics shown are representative of only one test in each configuration group and should be considered as typical rather than average. With the exception of the two tests presented in the summary all Guide Surface

Stabilization parachutes tested in the program suffered severe canopy or line damage during inflation.

The curves in Fig. 3 represent the general dynamic characteristics of

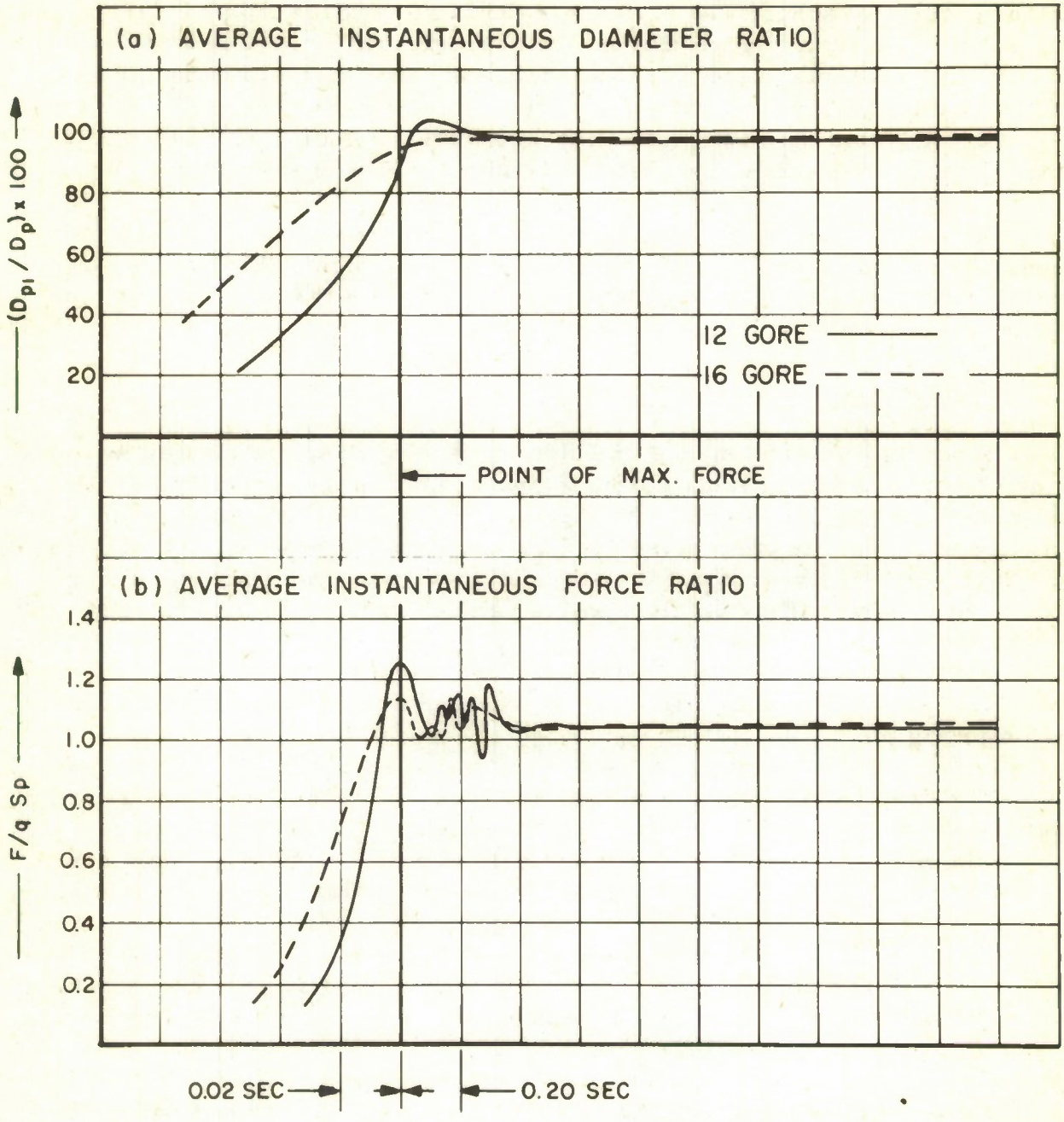

Figure 3 General Dynamic Characteristics - Guide Surface Stabilization Parachute

the 12 and 16 gore parachutes tested on test run Nos. 31 and 54, respectively. Averaged curves of the inflation process and transition to steady state operation are presented. As these curves indicate, both parachutes inflated to a steady state diameter ratio of approximately 97% and attained a steady state drag coefficient of approximately 1.05. Opening shock factor of the 12 gore parachute was 1.19 while the factor for the 16 gore parachute was 0.94. The latter figure may not be representative of the normal operation of this parachute since a hesitation was present in the inflation process, approximately at time of maximum force. This irregularity during opening is further substantiated by the fact that the instantaneous diameter ratio was lower at maximum force than that of the average steady state figure.

Stability of the Guide Surface Stabilization parachutes was generally good. As shown in Table 2, the tests considered indicate that the 16 gore parachute had slightly better stability characteristics than the 12 gore configuration.

C. Guide Surface Ribless Parachute

Satisfactory performance of Guide Surface Ribless parachutes was obtained on only two of 13 tests conducted with various configurations of the parachute. In the remaining tests the parachutes failed structurally or did not fully inflate. The parachutes used in the two tests in which satisfactory operation occurred were both 12 gore configurations, manufactured from MIL-C-8021, Type III nylon cloth with a permeability of 22.3 cu ft/sq ft/min at a differential pressure equal to 1/2 inch of water. Average performance characteristics for these parachutes from test run Nos. 30 and 40 are shown in Table 3. Average dynamic characteristics are graphically illustrated in Fig. 4.

The drag coefficient of 0.80 was identical for both tests although the opening shock factor of 1.55 was the average of a high and a low value. Parachute stability figures were of normal magnitudes attaining maximum displacements slightly under 5 degrees with mean values approximately half of this figure.

The average steady state drag coefficient of similar 12 gore parachutes which did not fully inflate was 0.75 with a corresponding opening shock factor, based on the low drag coefficient, of 1.22.

All tests conducted with the 16 gore Guide Surface Ribless parachutes resulted in structural failure of the parachute or incomplete inflation.

TABLE 3

PERFORMANCE CHARACTERISTICS OF THE 12 GORE GUIDE SURFACE RIBLESS PARACHUTES, TYPE III CLOTH

PROJECTED DIAMETER , D_p (ft)	6.5
PROJECTED AREA , S_p (ft^2)	33.2
WEIGHT , (lbs)	22.0
BULK , (ft^3)	1.25
CLOTH PERMEABILITY , λ_f (AT DIFFERENTIAL PRESSURE EQUIVALENT TO ½ INCH H_2O)	22.3
DRAG COEFFICIENT , C_D	0.80
OPENING SHOCK FACTOR (X)	1.55
INSTANTANEOUS DIAMETER RATIO (D_{p_1} / D_p) %	
AVERAGE	83.0
MAXIMUM	86.0
STABILITY , RADIUS OF DISPLACEMENT, (R) DEGREES	
MEAN	2.7
MAXIMUM	4.8

The graph presented in Fig. 5 shows a plot of opening shock force vs. dynamic pressure at peak snatch force for all tests in which Guide Surface Ribless test parachutes were successfully deployed. If the opening shock forces of test run Nos. 30 and 40 are based on an opening shock factor equal to the average factor attained in the two tests the opening shock force for average operation in this series of tests would fall on the solid line indicated in the graph. The locations of the various groups of points on the graph now become significantly related to the operational behavior of the various configurations tested. For example, the early 12 gore parachutes which did not fully inflate appear as an approximately linear group with opening shock force values approximately 30% below the average expected values. Similarly, the curve also shows that the latter group of 16 gore parachutes, which suffered structural failure during inflation, failed at or near the expected opening shock force values.

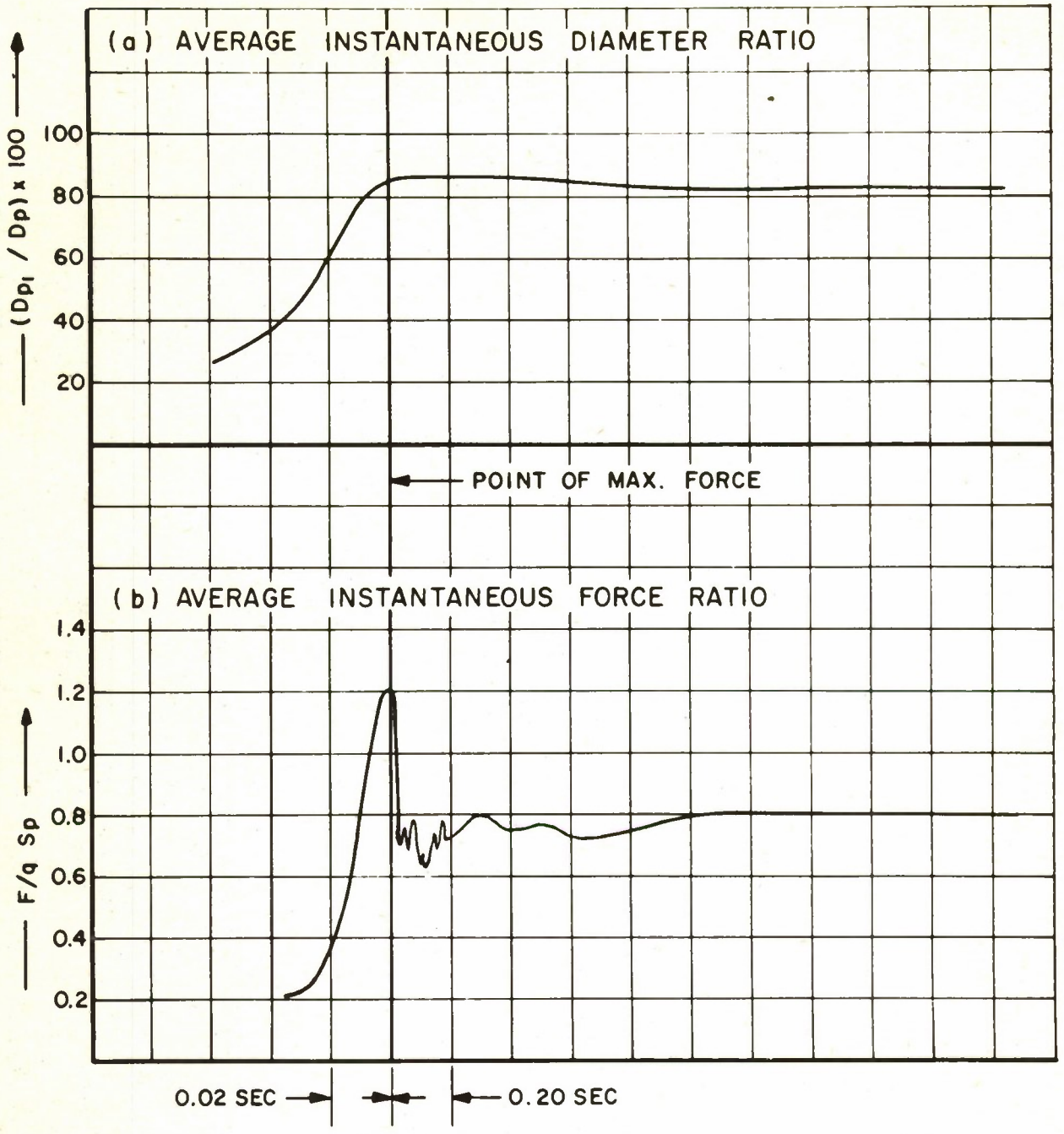

Figure 4 General Dynamic Characteristics - Twelve Gore Guide Surface Ribless Parachute

Figure 6 is a curve showing the relationship between time to maximum load t_{ml} (seconds) and the velocity at snatch force, V_s (fps). With the exception of one test in this series all values fell within the band shown in the curve.

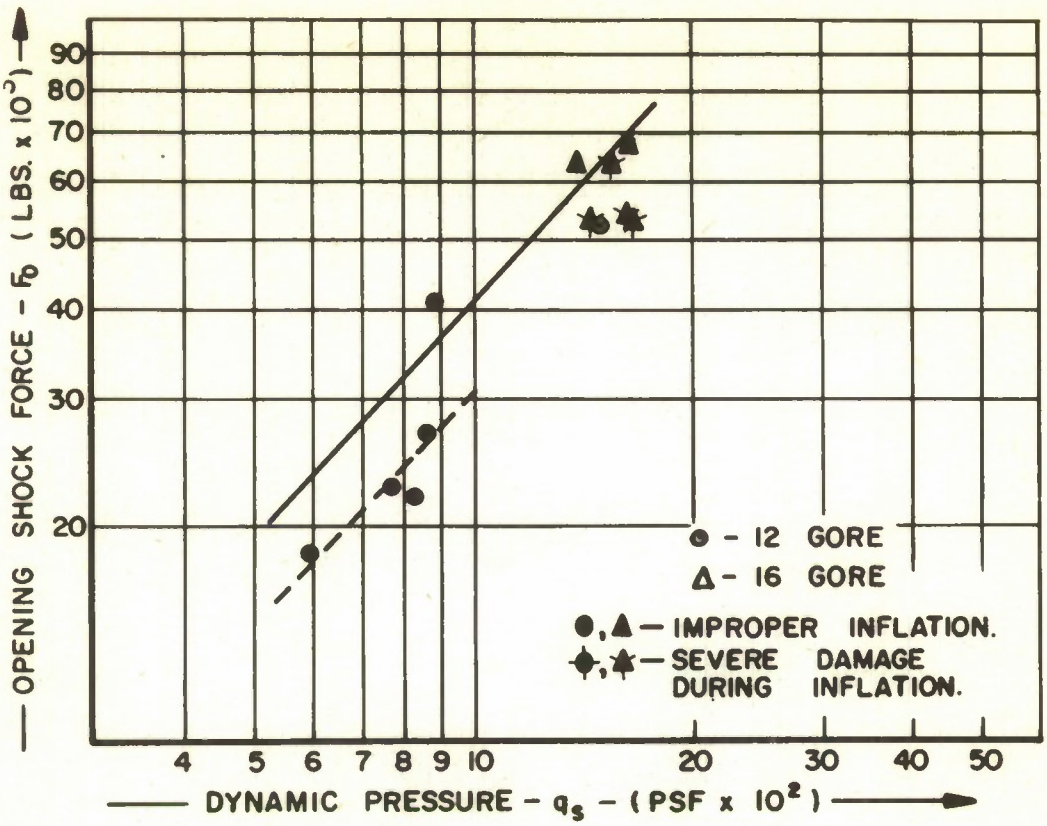

Figure 5 Opening Shock Force (F_o) vs. Dynamic Pressure at Snatch (q_s) for Guide Surface Ribless Parachutes

The bandwidth obtained by enclosing the normal scatter of points indicates that a variation of approximately ±0.01 second can be expected for normal operation within the velocity range covered by this series of tests.

D. FIST Ribbon Parachutes

Of the 12 types of FIST Ribbon parachutes tested in the program, the most favorable characteristics were exhibited by the Type 124 parachute constructed with 2 inch 1700 pound T. S. nylon horizontal ribbons and having a geometric porosity of 21.15%. Average performance characteristics for this parachute are presented in Table 4 and average dynamic characteristics are presented graphically in the curves in Fig. 7.

The similarity of inflation characteristics of the tests from which the average curve was derived are clearly evident in Parts (a) and (b) of the

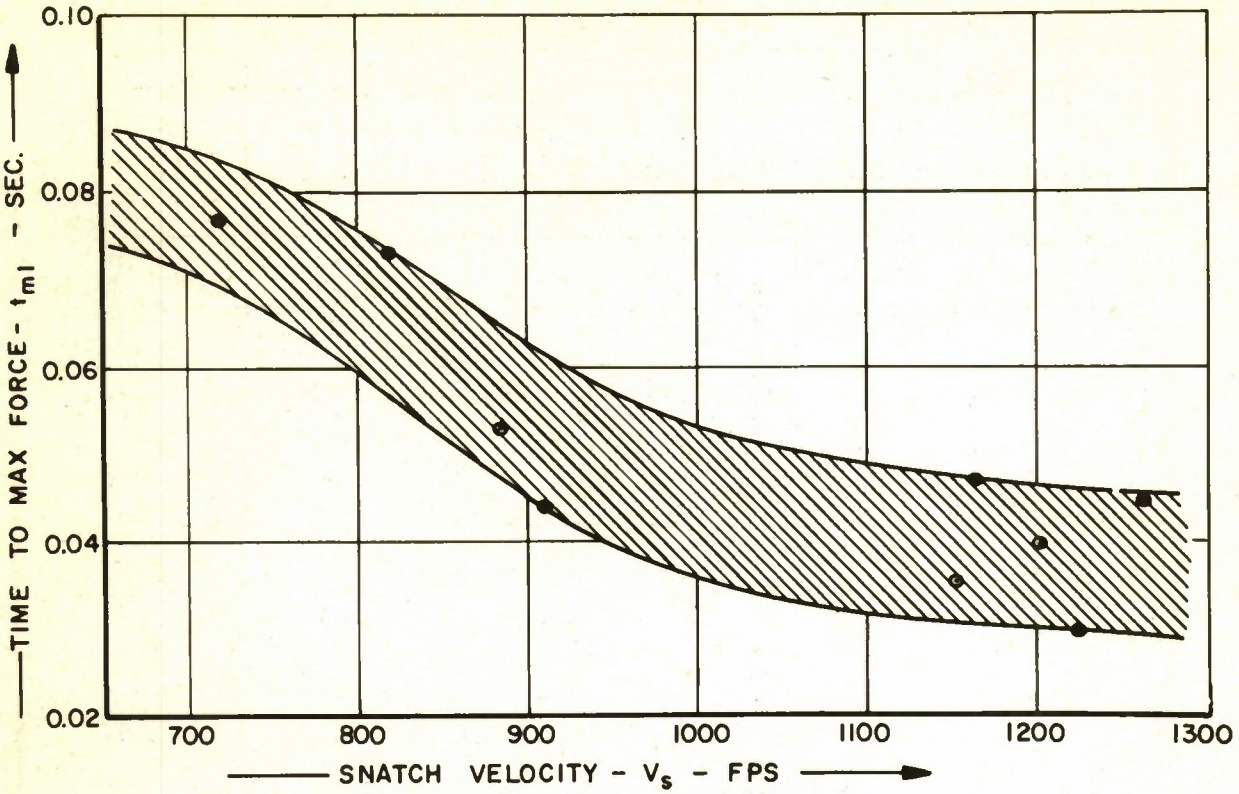

Figure 6 Relationship Between Time to Maximum Force (t_{m1}) and Deployment Velocity (V_s) for Guide Surface Ribless Parachutes

detailed performance curves in Fig. 39 of Appendix C. The drag coefficient, C_{D_o} based on the total polygon area of the parachute remained relatively constant over the velocity ranges of the tests and little difference is noted in the drag coefficient curves of the tests conducted. The average value of 0.52, shown in Table 4, is therefore considered quite reliable for this particular Ribbon parachute.

None of the FIST Ribbon type 124-17 parachutes tested in the program exhibited positive overshoot during inflation and opening shock factors were under 1.0 in all cases.

The velocity envelope shown in Fig. 8 illustrates the range of deployment velocities covered in this series of tests of FIST Ribbon parachutes, with respect to parachute type and geometric porosity. It is apparent from this graph that as test velocities were increased during the program, most successful parachute deployment and operation were obtained with parachutes

TABLE 4

PERFORMANCE CHARACTERISTICS OF THE FIST RIBBON TYPE 124-17 PARACHUTE

NOMINAL DIAMETER, D_o (ft)	8.60
POLYGON AREA, S_o (ft^2)	56.60
WEIGHT, (lbs)	21.5
BULK, (ft^3)	1.00
GEOMETRIC POROSITY, λ_g (%)	21.15
DRAG COEFFICIENT C_{D_o}	0.52
OPENING SHOCK FACTOR (X)	0.94
INSTANTANEOUS DIAMETER RATIO (D_{p_1} / D_p) %	
AVERAGE	98.20
MAXIMUM	100.90
STABILITY, RADIUS OF DISPLACEMENT, (R) DEGREES	
MEAN	2.20
MAXIMUM	3.20

in the higher porosity groups. The curve is included here to indicate the trend followed to obtain the most satisfactory operation rather than impose operational limits on any group of parachutes. It should be noted that none of the FIST Ribbon parachutes with geometric porosities over 20% had reached their structural limitations at the highest velocities tested in each group.

Several performance parameters illustrate a noted effect of porosity change. Paramount among these is perhaps the effects on parachute stability. In the illustration in Fig. 9, which shows the variation of average angular displacement for FIST Ribbon parachutes of various geometric porosities, it is readily apparent that the stability of the higher porosity parachutes was superior to that of the lower porosity types. The rate of increase in stability as porosity increases, is notably greater in the lower porosity region, diminishing with porosity increase until, at values of λ_g in the low 20's further

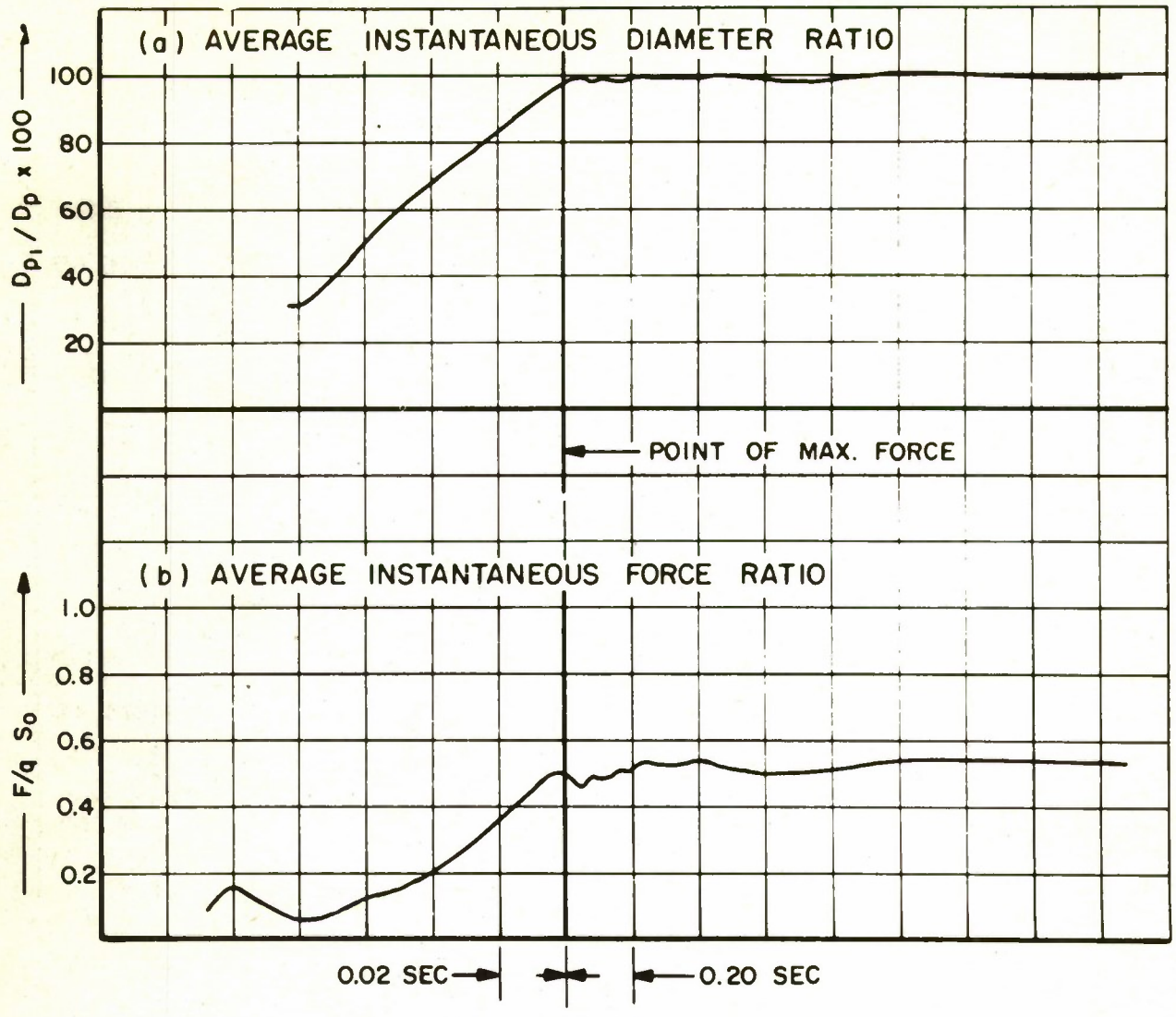

Figure 7 General Dynamic Characteristics - FIST Ribbon Type 124-17 Parachute

decreases of porosity apparently have minor effect on the stability characteristics of the parachute. It should be noted that the test points shown in Fig. 9 indicate the mean angular displacement for each test that they represent but do not indicate the magnitude of oscillatory variation about the mean point during each test. Therefore, the increase in bandwidth (shaded area on curve, Fig. 9) at the higher porosity end of the curve is not an indication of decreasing oscillatory stability but a function of the normal expected variation due to the number of tests made and the varying velocities at which they were conducted. If a greater number of test points were available at

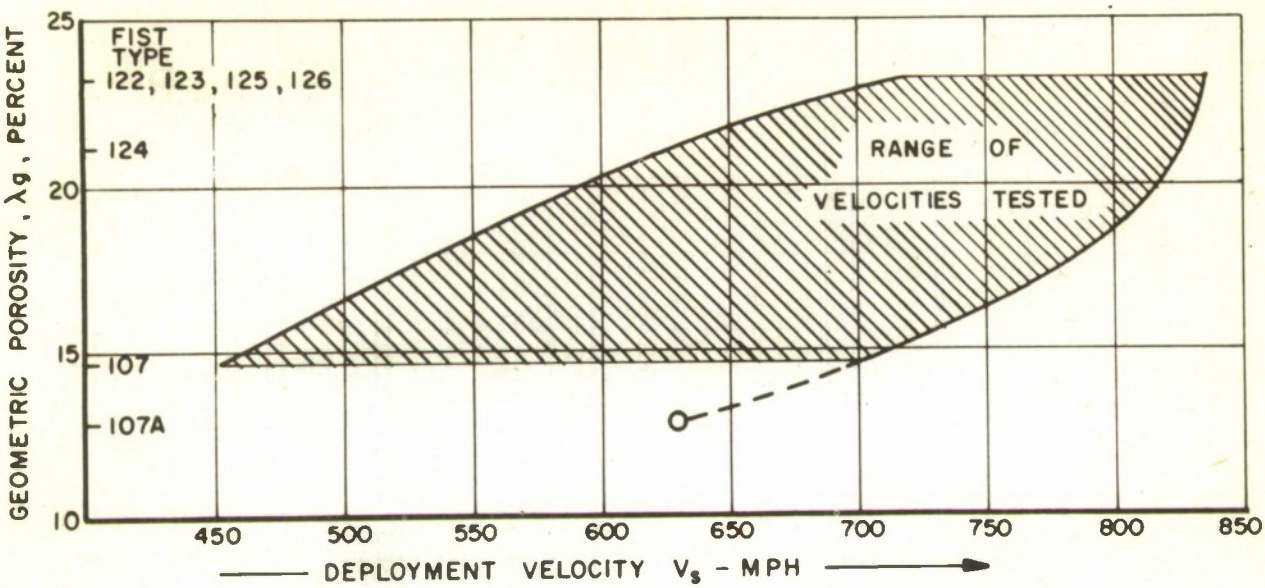

Figure 8 Range of Deployment Velocities for Various FIST Ribbon Parachute Types Tested

the low porosity end of the curve, it is probable that the normal data variation would present a more uniform bandwidth throughout the curve; however, the general trend and indicated average of angular displacement would not alter appreciably from the average presently shown.

Another parameter in which a noted effect of porosity was observed was in the drag coefficient. The average drag coefficient for all FIST Ribbon parachute tests in which satisfactory steady state information was obtained are plotted in Fig. 10 as a function of the geometric porosity. The resulting band shows that the average drag coefficient, C_{D_o}, decreases with increasing porosity, from an average value of approximately 0.58 at the low porosity end to an average value of approximately 0.50 at the high or porosity end. This corresponds to an average difference of approximately 15% in C_{D_o} values, between the high and low porosity parachutes. It appears, from this curve, that the average drag coefficient of 0.52 for the FIST Ribbon Type 124-17 parachute is consistent with general FIST Ribbon parachute characteristics and is a reliable figure for such a parachute having reasonable stability and inflation characteristics. It is also pertinent to note that there was essentially no variation of drag coefficient with dynamic pressure through the ranges of parachute test velocities.

Several tests were conducted with FIST Ribbon parachutes in which two different line length configurations were tested. These line length configuration changes were tested on Types 122 and 123 parachutes and were varied

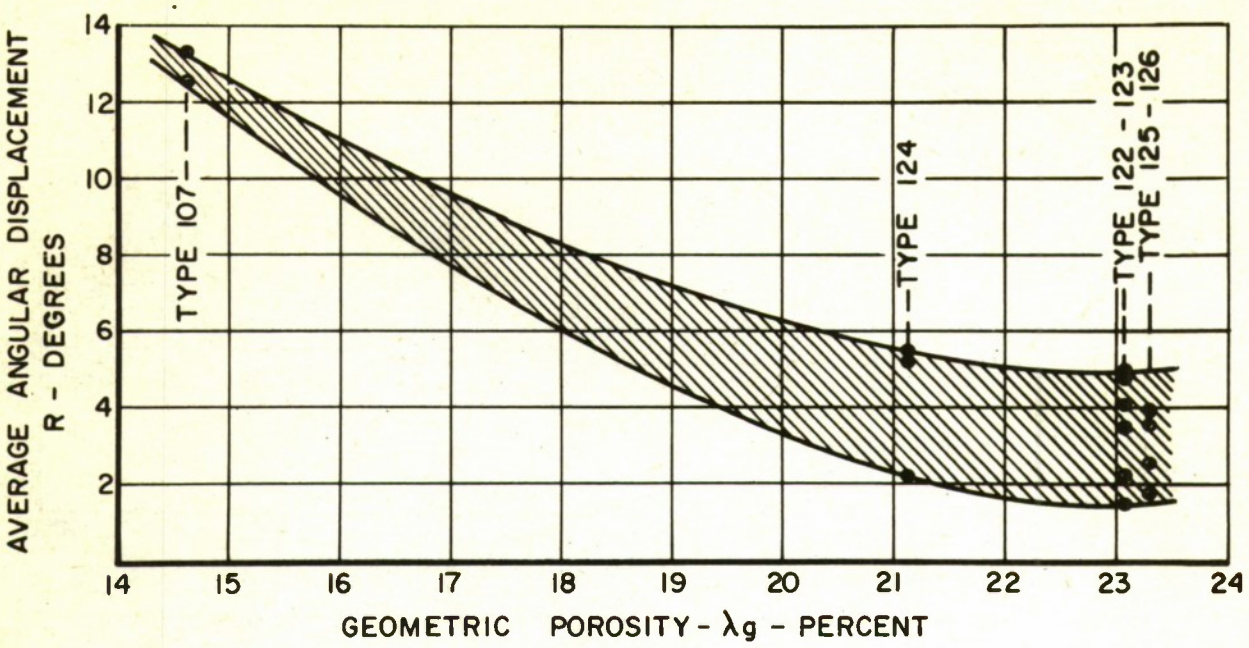

Figure 9 Variation of Average Angular Displacement (R) with Geometric Porosity (λ_g) - FIST Ribbon Parachutes

between the normal L_S/D ratio of one and L_S/D ratio of two. A summary of the average performance characteristics of the two line length configuration groups of Type 122 and 123 parachutes is tabulated in Table 5, and average dynamic characteristics of the two groups are graphically illustrated in the curves in Fig. 11.

From the information presented in the table and curves it is apparent that inflation characteristics vary considerably with L_S/D ratio. The long line group inflated to a 16% greater drag area than the similar short line group and reached the inflated state an average of 0.05 second, or approximately 30% faster than the group with the normal L_S/D ratio of one. A significant increase in drag coefficient is noted. The short line group averaged 0.50 while the long line group averaged 0.60. The average for all tests of both configurations was 0.54. Slightly less angular displacement (R) was observed for the short line parachutes. Mean displacement for this configuration was 3.1 degrees with oscillating variations of ±1.5 degrees while the long line configuration had an average displacement of 4.6 degrees with variations of ±2.6 degrees.

The only parameter which was identical for both groups was the opening shock factor (X) which averaged 1.04 in both groups.

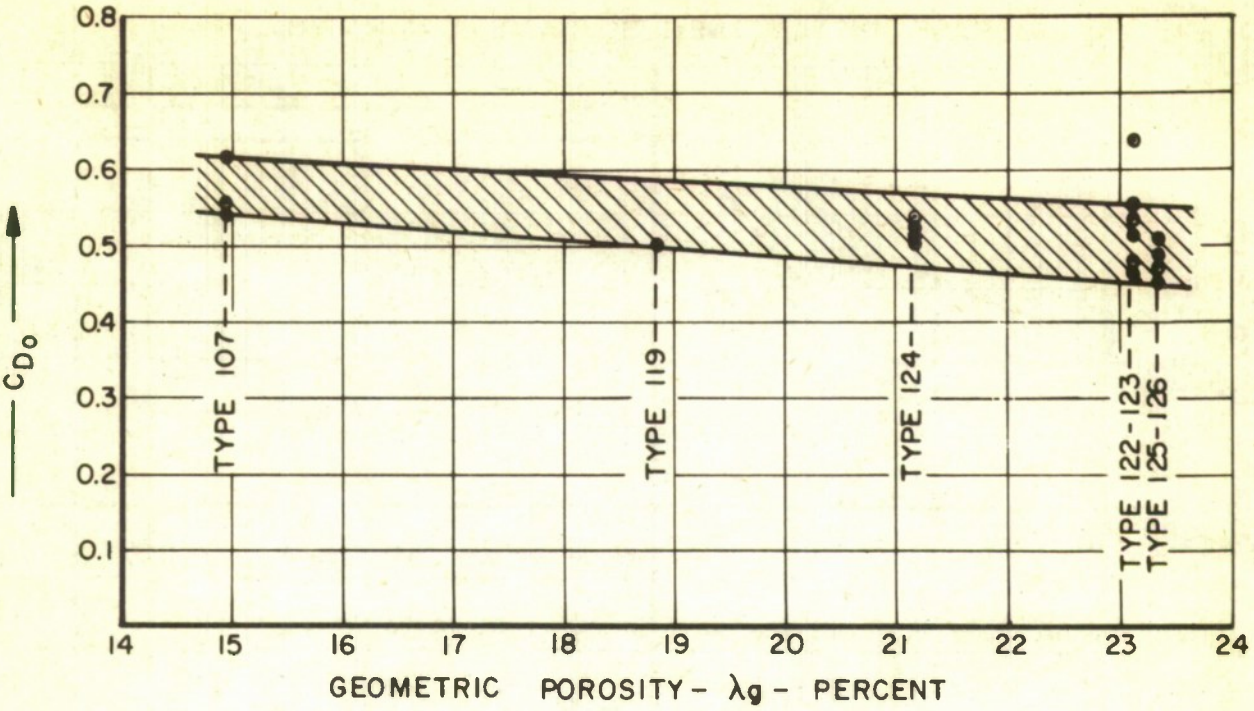

Figure 10 Variation of Steady-State Drag Coefficient (C_{D_o}) with Geometric Porosity (λ_g) for FIST Ribbon Parachute Types

TABLE 5

PERFORMANCE CHARACTERISTICS OF FIST RIBBON TYPE 122 AND 123 PARACHUTES

	TEST NO'S	C_D	X	t_f	D_{p_1}/D_p AVERAGE	R mean	R max.
$L_S/_D = 1$	28, 29, 33, 34, 35	0.50	1.04	0.14	99.5	3.1	4.6
$L_S/_D = 2$	36, 37	0.60	1.04	0.09	107.2	4.6	7.2
ALL TESTS		0.54	1.04	0.12	102.0	3.6	5.5

Detailed performance summaries of the individual tests in these groups are presented in Section C.7 of Appendix C.

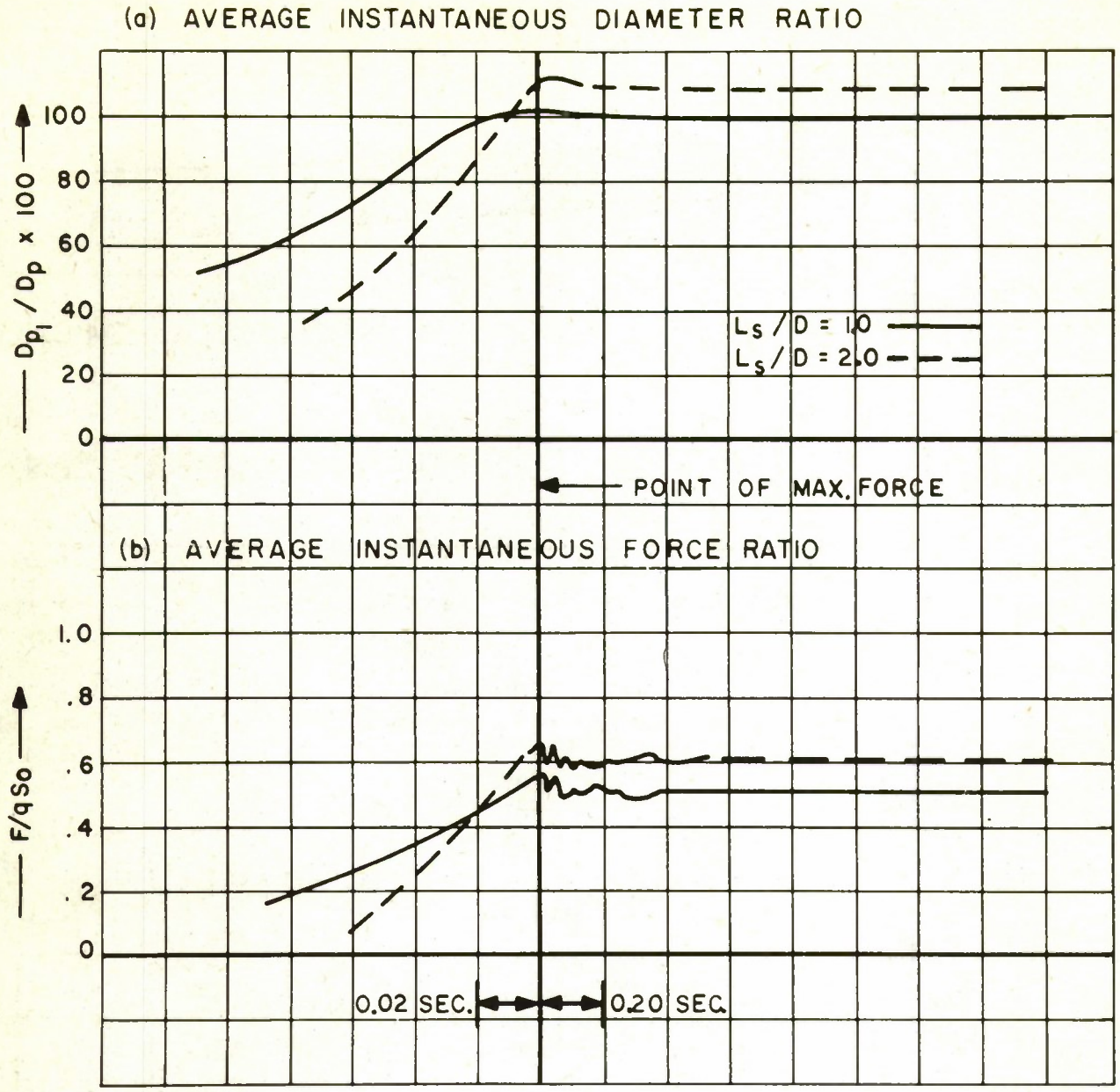

Figure 11 Average Dynamic Characteristics of FIST Ribbon Types 122 and 123 Parachutes With Different Line-Length Configurations

E. Rotafoil Parachutes

Five tests, details of which can be found in Appendix D, were conducted using Rotafoil test parachutes. In the tests of the original B7-8-20 configuration, suspension line system failure during inflation of the parachute led to

collapse and destruction of the parachutes.

The modified version of the Rotafoil B7-8-20 parachute, tested later in the program, suffered major canopy damage during inflation, and also resulted in collapse and destruction of the parachutes.

Since none of the Rotafoil parachutes tested in the program operated successfully in the steady state condition, aerodynamic parameters could not be obtained for comparison with other Rotafoil parachute information or with parachutes of other general classifications.

APPENDIX A

GUIDE SURFACE STABILIZATION PARACHUTE

A. Introduction

The Guide Surface Stabilization type of parachute is distinguished by a relatively long conical surface shaped as an inverted truncated cone below the roof portion of the canopy. Internal cloth ribs are used to separate the suspension lines from the canopy so that the canopy might form the Guide Surfaces and the flow separation edge required for stabilization. This also allows the canopy form to be variable, since the ribs define the canopy shape and make it independent of the suspension line arrangement. A typical parachute of this type is shown in operation in Fig. 12, and Fig. 13 shows the design profile. A complete description of the parachute is given by Heinrich (Ref. 3) and general specifications for the construction of the parachute are presented in Ref. 7.

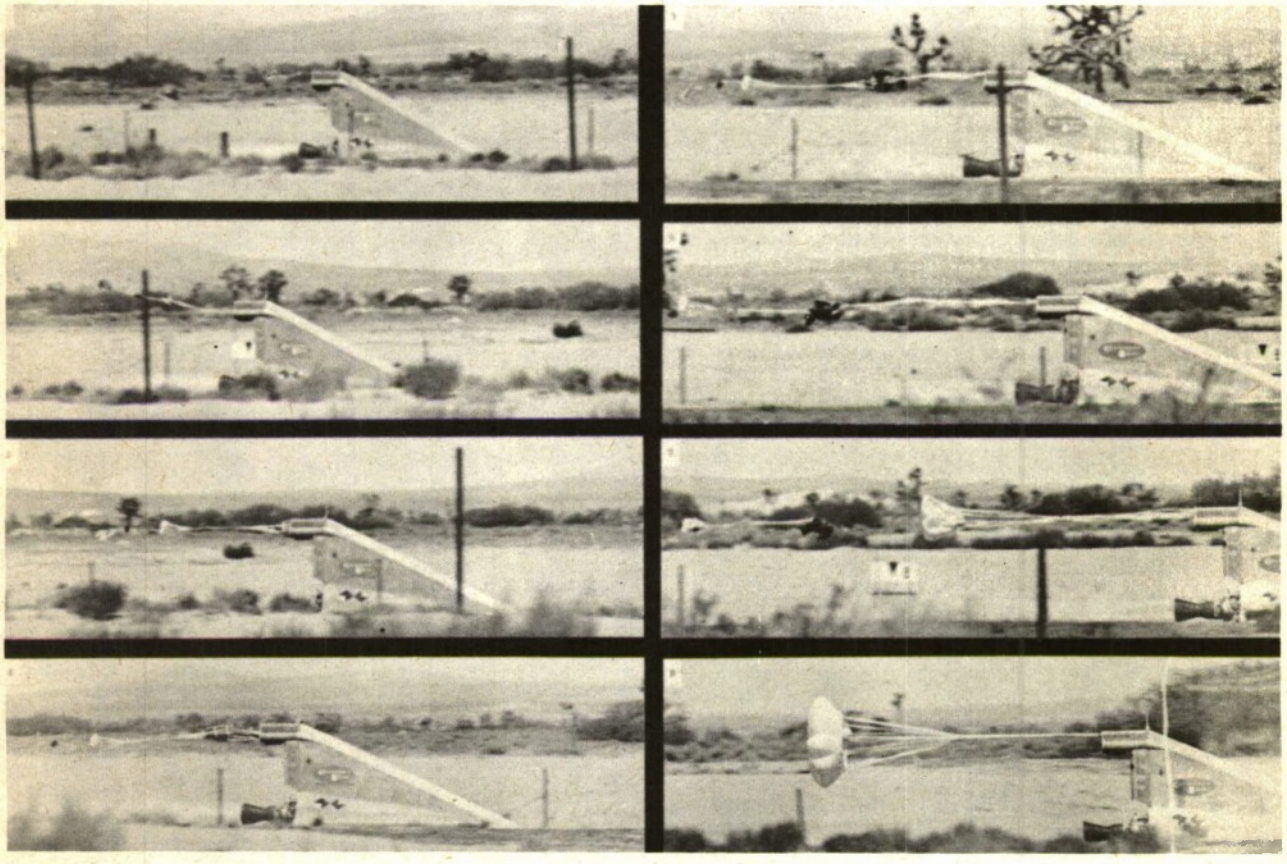

Figure 12 Deployment Sequence - Guide Surface Stabilization Parachute

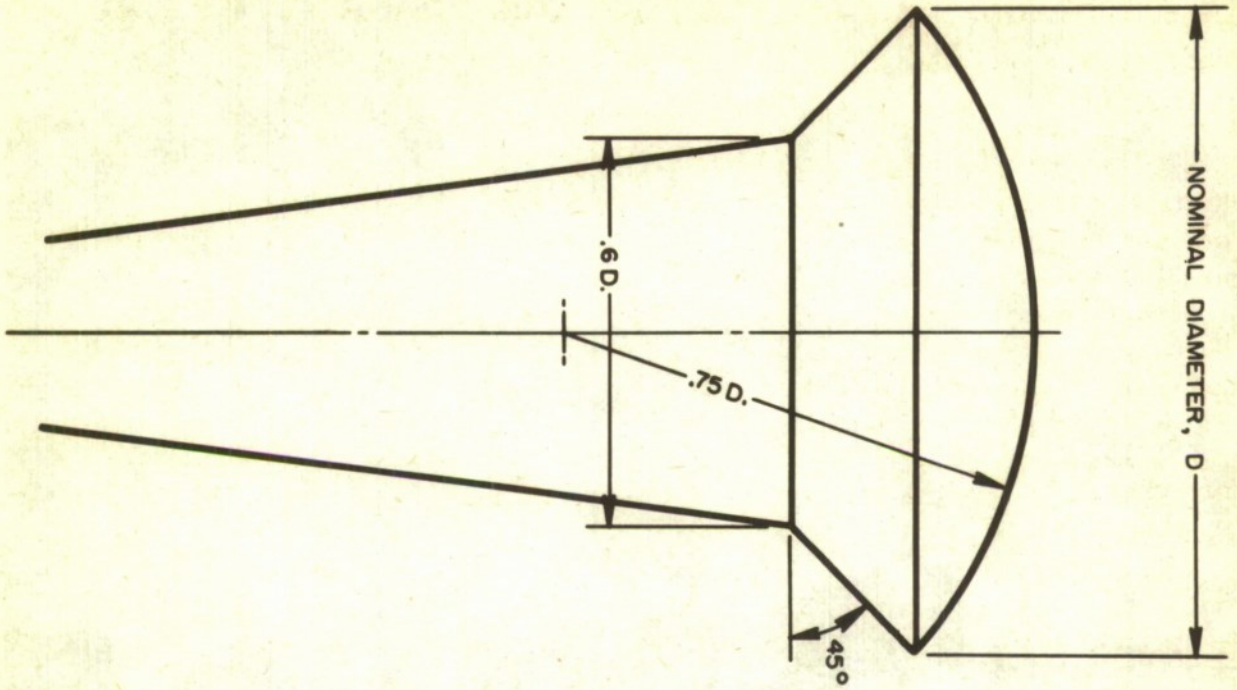

Figure 13 Design Profile - Guide Surface Stabilization Parachute

B. Test Program

Six tests were conducted in which Guide Surface Stabilization Test parachutes were deployed from a liquid fuel rocket powered test vehicle at velocities varying from 615 mph to 825 mph. All tests were performed on the 10,000 foot Free Air Test Facility Track at Edwards Air Force Base, California. The parachutes tested on the program were fabricated from MIL-C-8021 Type III nylon cloth in accordance with Military Specification MIL-P-5905A (Ref. 7), from design and revision information provided by the contracting agency. Parachute failures during the early part of the test program suggested the need for revisions in the thread sizes used on canopy seams and general improvement in suspension line attachment methods. Cook Research Laboratories engineers devised an improved suspension line attachment which incorporated a metal ring, similar to a reefing ring, and located at each line attachment point at the parachute skirt. This ring, which was attached to the skirt by a separate loop, allowed the suspension line to move unrestrained under normal loading conditions but restricted movement which would tend to tear the line away from the canopy. A photograph of a typical ring installation on a Guide Surface Stabilization parachute is shown in Fig. 14

Figure 14 Ring Type Skirt Connection for Guide Surface Stabilization Parachute

Other changes, which occurred later in the program, consisted of strengthening the vent band reinforcing and the use of higher tensile strength line webbing. Ultimately the number of gores in the parachute was increased from 12 to 16.

Physical details and material specifications of the Guide Surface Stabilization parachutes tested in this program are listed in Tables 6 and 7.

C. Parachute Performance

Guide Surface Stabilization parachute performance data as measured on the high-speed sled test program, are presented in Table 8 and graphically illustrated in Figs. 15 and 16.

The 12 gore version of the parachute operated successfully at 625 mph but severe canopy damage was incurred in attempted operation at 800 mph.

TABLE 6

PHYSICAL DETAILS OF GUIDE SURFACE STABILIZATION PARACHUTES

PARACHUTE DIAMETER - D_p - (ft)	6.5	6.5	6.5	6.5
DESIGN PROJECTED AREA - S_p - (ft^2)	33.2	33.2	33.2	33.2
NO. OF GORES AND SUSPENSION LINES	12	12	12	16
CANOPY MATERIAL	TYPE III-600 lb.	TYPE III-600 lb.	TYPE III-600 lb.	TYPE III-600 lb.
SUSPENSION LINE MATERIAL	I x 6000	I x 6000	I x 12000	I x 9000
SUSPENSION LINE LENGTH (ft)	8.125	8.125	8.125	8.125
VENT DIAMETER (IN.)	8.35	8.35	8.35	8.35
VENT LINE LENGTH (IN.)	6.83	6.83	6.83	6.83
VENT BAND REINFORCING	I x 3000	I x 3000	I x 6000	I x 6000
SLOT LENGTH (IN.)	NONE	NONE	NONE	NONE
THREAD SIZE (CANOPY SEAMS)	SIZE F	5 CORD	5 CORD	5 CORD
THREAD SIZE (LINE ATTACHMENT)	3 CORD	5 CORD	6 CORD	6 CORD
PATTERN DETAILS	A	A	A	A
WEIGHT (lbs)	21.9	21.9	27.1	33.0
BULK (ft^3)	1.20	1.20	1.62	1.67
USED ON RUN NO.	9	20	31,39	49,54

A - REFERENCE 7

The steady state drag coefficient, Fig. 15 (c), averaged 1.04 and the average opening shock factor for this parachute was 1.19. Excellent stability was exhibited by the parachute in the successful test, Fig. 15 (d). Early tests of the

TABLE 7

MATERIALS USED IN GUIDE SURFACE STABILIZATION PARACHUTES

PART	MATERIAL	SPECIFICATION	SIZE	TENSILE STRENGTH
CANOPY MATERIAL	CLOTH, NYLON	MIL-C-8021A TYPE III	14 oz./sq. yd.	600 lb/in
SUSPENSION LINES	WEBBING, NYLON	MIL-W-4088 TYPE XVIII	WIDTH-1 in	6000 lbs
	WEBBING, NYLON	MIL-W-4088 C TYPE XX	WIDTH - 1 in	9000 lbs
	WEBBING, NYLON	NON-SPECIFICATION	WIDTH - 1 in	12,000 lbs
THREAD	NYLON	MIL-T-7807	F 3 CORD 5 CORD 6 CORD	11 lbs 24 lbs 40 lbs 50 lbs
REINFORCING TAPE	WEBBING, NYLON TUBULAR	MIL-W-5625	WIDTH - 1 in	3000 lbs
	WEBBING, NYLON	MIL-W-4088 TYPE XVIII	WIDTH - 1 in	6000 lbs

12 gore Guide Surface Stabilization parachute suffered significant damage when deployed at 600 to 650 mph. The canopy seams of the first parachute of this type that was tested were sewn with size "F" thread and were severely damaged in the canopy. The following parachute was manufactured of identical material with 5 cord thread used in the canopy seams. This parachute was undamaged in the canopy but several of the 1 inch - 6000 pound suspension lines and risers failed. The possibility exists that if an improved keeper of the type described in Appendix E had been available the line failure might not have occurred. Since 1 inch - 9000 pound webbing was not yet being manufactured, the next parachute was fabricated with 1 inch - 12,000 pound suspension lines. Figure 12 shows the successful deployment and inflation of the 12 gore Guide Surface Stabilization parachute on run No. 31.

The Guide Surface Stabilization parachute was modified to the 16 gore

TABLE 8

TEST RESULTS OF GUIDE SURFACE STABILIZATION PARACHUTES

GUIDE SURFACE STABILIZATION TYPE		12 GORE - STANDARD PANEL				16-GORE STANDARD PANEL	
RUN NUMBER		9	20	31	39	49	54
VELOCITY F.P.S.	V_s AT PEAK SNATCH	APPROX. 950	APPROX. 900	918	1177	1208	1104
	V_o AT PEAK OPENING SHOCK	—	—	910	1167	1170	1082
DYNAMIC PRESSURE P.S.F.	q_s AT PEAK SNATCH	—	862	886	1520	1570	1297
	q_o AT PEAK OPENING SHOCK	—	845	870	1495	1473	1246
TIME INTERVAL SECONDS	t_s DEPLOYMENT TO PEAK SNATCH	—	0.298	0.357	0.330	0.232	0.200
	t_f SNATCH TO PRIMARY MAXIMUM INFLATION	—	0.092	0.098	0.050	0.067	0.080
	t_{ml} SNATCH TO MAXIMUM LOAD	—	0.067	0.042	0.040	0.115	0.076
FORCE LBS.	F_s SNATCH FORCE	—	8,950	12,700	17,750	30,150	26,050
	F_o OPENING SHOCK	—	29,050	36,300	62,600	51,400	42,500
DIAMETER RATIO PERCENT	$\left(\frac{D_{P_l}}{D_P}\right)_m$ MAXIMUM	—	74.7	102.6	86.8	84.6	92.5
	$\left(\frac{D_{P_l}}{D_P}\right)_a$ AVERAGE	—	—	97.2	—	—	97.4
STABILITY DEGREES	MEAN RADIUS OF DISPLACEMENT	—	—	1.80°	—	—	1.48°
	MAXIMUM RADIUS OF DISPLACEMENT	—	—	3.20°	—	—	2.17°
C_D AVERAGE DRAG COEFFICIENT		—	—	1.04	—	—	1.05
X OPENING SHOCK FACTOR		—	—	1.19	—	—	0.94
PARACHUTE DAMAGE	CANOPY	SEVERE DAMAGE THROUGHOUT	MINOR	NONE	SEVERE DAMAGE THROUGHOUT	6 PANELS SEVERELY DAMAGED	MINOR DAMAGE
	LINE	LINE DAMAGE	LINE DAMAGE	MINOR LINE DAMAGE	ALL LINES DAMAGED		
PARACHUTE OPERATION		NORMAL DEPLOYMENT / FAILED AT F_o	NORMAL DEPLOYMENT / FAILED 0.015 SEC. AFTER F_o	NORMAL	NORMAL DEPLOYMENT / DAMAGED DURING INFLATION	NORMAL DEPLOYMENT / DAMAGED DURING INFLATION	NORMAL
INSTRUMENTATION PREFORMANCE		RECORDERS & SLED CAMERAS JAMMED	NORMAL	NORMAL	NORMAL	NORMAL	NORMAL

configuration to secure greater canopy strength at the higher velocities by cutting down over-all panel sizes. The parachute as tested on test run Nos. 49 and 54 had material and constructional details similar to the final 12 gore

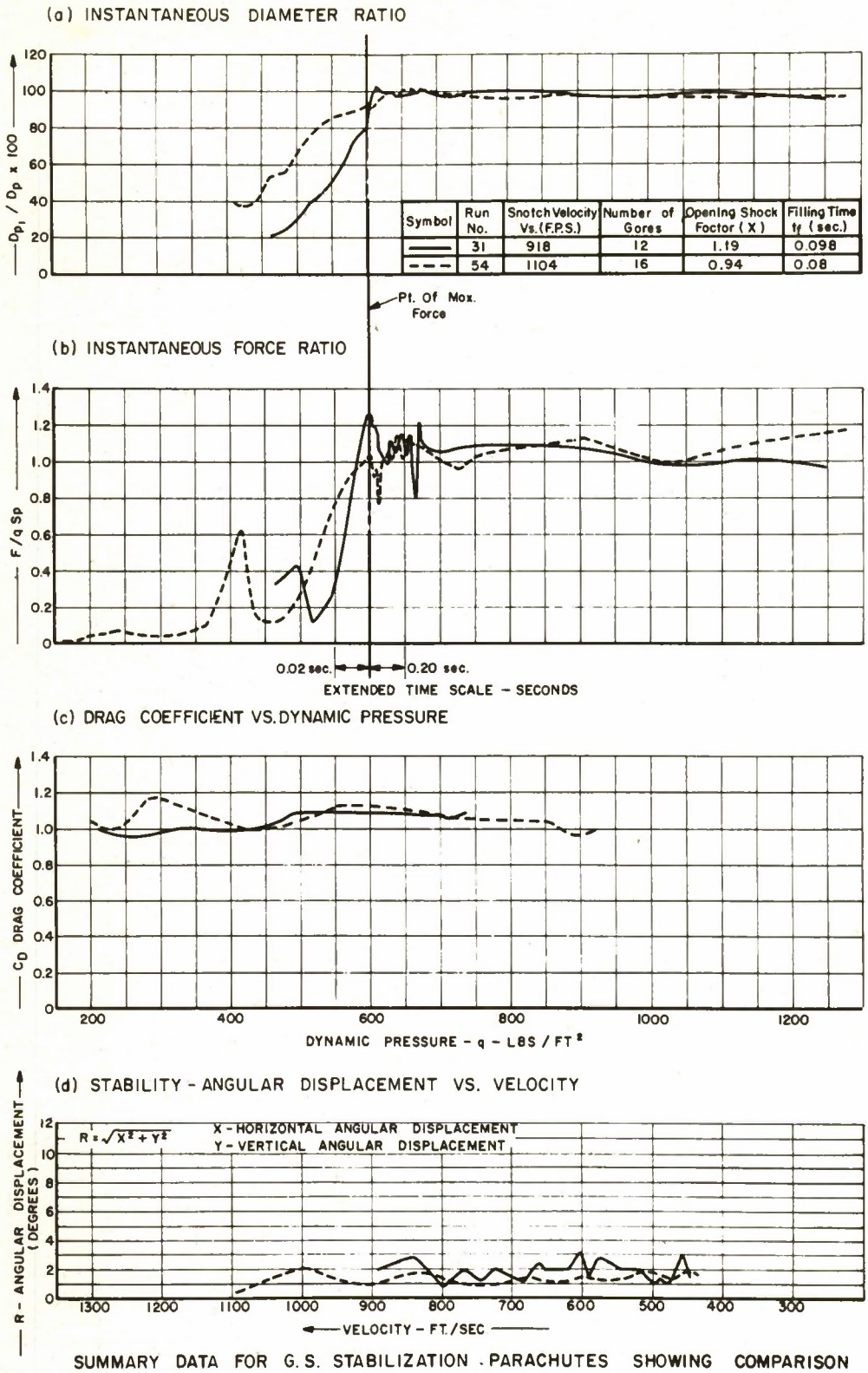

SUMMARY DATA FOR G. S. STABILIZATION PARACHUTES SHOWING COMPARISON OF PERFORMANCE ITEMS OBTAINED FROM S. S. SLED TESTS

Figure 15 Summary Data - Guide Surface Stabilization Parachutes (Test Run Nos. 31 and 54)

(a) INSTANTANEOUS DIAMETER RATIO

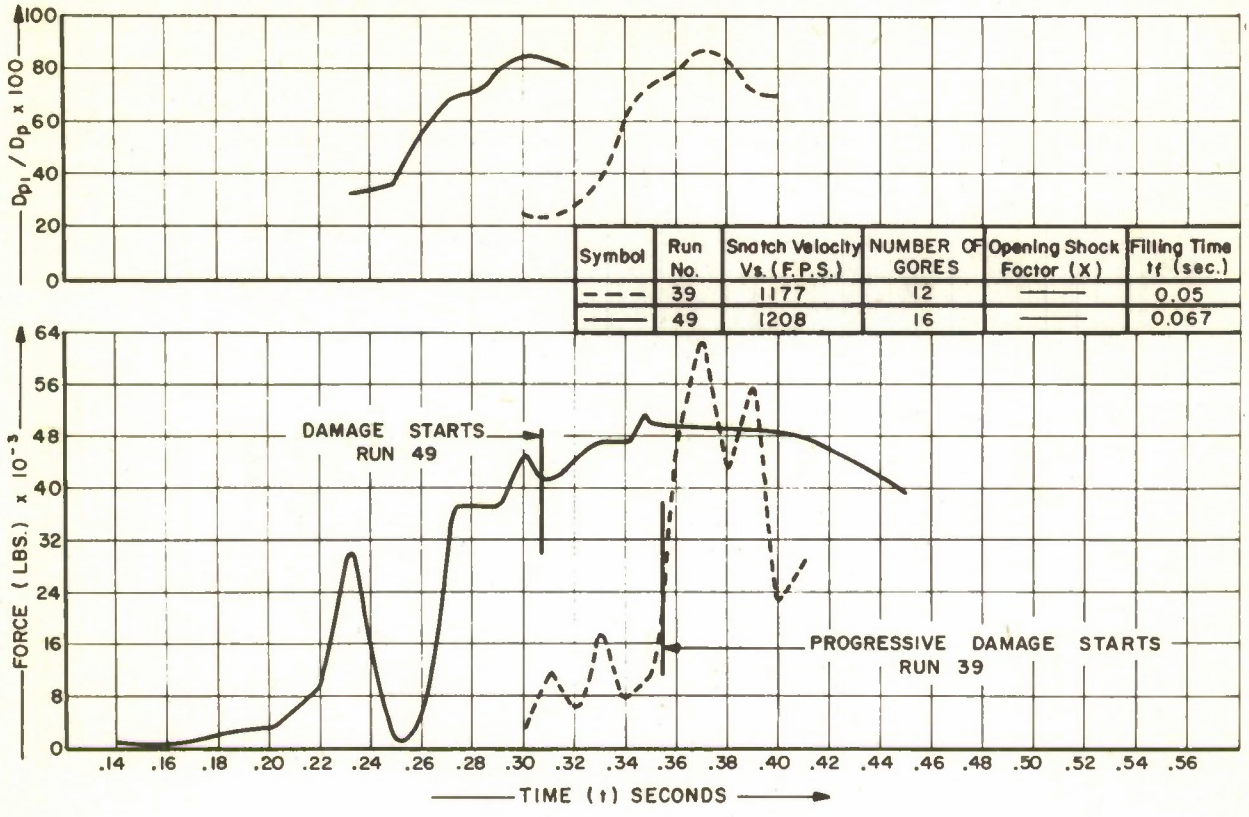

(b) INSTANTANEOUS FORCE RATIO

Figure 16 Summary Data - Guide Surface Stabilization Parachutes (Test Run Nos. 39 and 49)

version, except that the suspension lines were fabricated from the newly available 1 inch - 9000 pound nylon webbing. Satisfactory operation attained at a deployment velocity of 753 mph but severe canopy damage occurred during inflation at a deployment velocity of 824 mph.

The drag coefficient of the 16 gore parachute was 1.05, which is nearly identical to that of the 12 gore version. Opening shock factor, however, was 0.94 for the 16 gore parachute tested at 753 mph, or 25% lower than the opening shock factor of the 12 gore parachute tested at 626 mph. The lower opening shock factor for the 16 gore parachute was probably caused by an apparent hesitation in the opening process. At the time of maximum force the parachute had attained an inflated diameter of 92% of the design diameter. An additional 0.2 second elapsed before a true maximum diameter of 102% was reached. During this time increment the dynamic pressure, q, decreased approximately

200 psf (from 1246 psf to 1051 psf) because of vehicle deceleration. Stability of the 16 gore parachute, graphically presented in Fig. 15 (d), was excellent generally and slightly better than that of the 12 gore parachute.

On test run Nos. 39 and 49 in which canopy failure occurred, the parachutes had inflated to approximately 85% of their design diameter at time of failure. This is graphically illustrated in Fig. 16 (a).

APPENDIX B

GUIDE SURFACE RIBLESS PARACHUTE

A. Introduction

The Guide Surface Ribless parachute has a conical surface shaped as an inverted truncated cone below the roof portion of the canopy, which is similar to but slightly shorter than, the guide surface of the Stabilization type of parachute. As the name implies, there are no internal cloth ribs to contain and separate the suspension lines from the canopy. Instead, the roof and G. S. panels are fabricated so that the inflated shape of the canopy assumes the geometric form most conducive to good flow separation and stability. The suspension lines are rigidly attached to the exterior of the canopy along the roof panel seams.

The general shape of the roof and Guide Surface panels are shown in Fig. 17. Figure 18 shows a typical parachute of the Guide Surface Ribless type in operation.

B. Test Program

Thirteen tests were conducted in which Guide Surface Ribless test parachutes were deployed from a liquid fuel rocket powered test vehicle on the 10,000 foot Free Air Test Facility Track at Edwards Air Force Base, California. Test velocities ranged from 501 mph to 862 mph T.A.S. Specifications and revision information for fabrication of the parachutes tested on the program were provided by the contracting agency.

With the exception of one parachute manufactured from MIL-C-8021, Type II - 300 pound T. S. nylon cloth all test parachutes in this series were manufactured from MIL-C-8021 Type III - 600 pound T.S. nylon drag parachute cloth. Physical details and material specifications for the Guide Surface Ribless Parachutes are presented in Tables 9 and 10.

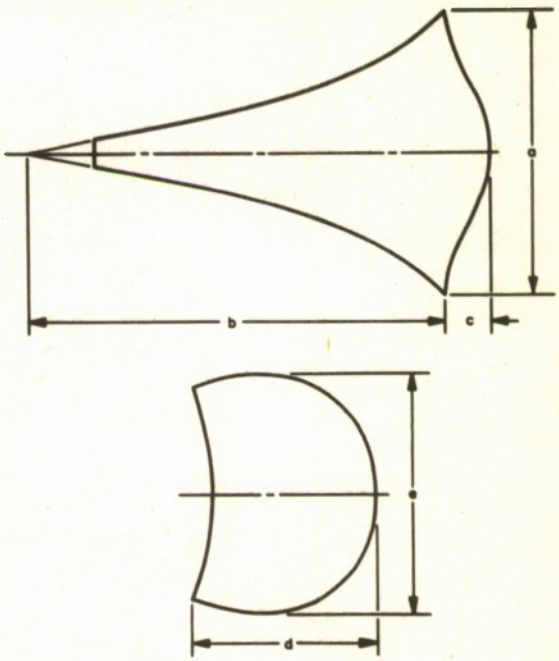

PATTERN DETAILS	a	b	c	d	e
	PERCENT OF PARACHUTE DIAMETER				
A	59.1	43.8	6.2	23.0	23.7
B	55.2	44.5	5.6	23.0	20.3
C	55.2	44.5	5.6	23.0	18.3

Figure 17 Panel Shapes and Basic Dimensions of the 12 and 16 Gore Guide Surface Ribless Parachute

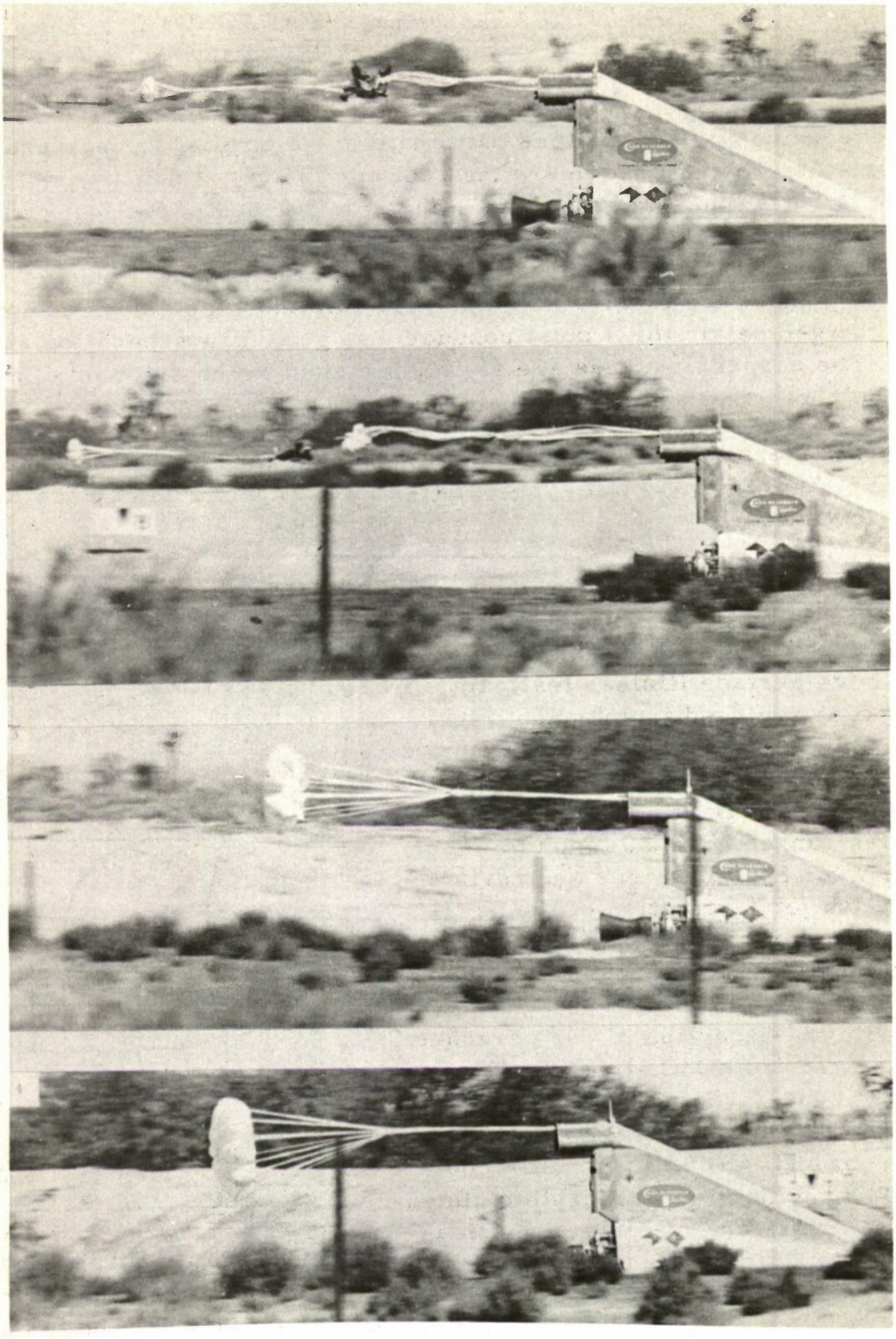

Figure 18 Deployment Sequence - Guide Surface Ribless Parachute

TABLE 9

PHYSICAL DETAILS OF GUIDE SURFACE RIBLESS PARACHUTES

PARACHUTE DIAMETER - D_p - (ft)	6.5	6.5	6.5	6.5	6.5	6.5	6.5	6.5	6.5	6.5
DESIGN PROJECTED AREA - S_p - (ft^2)	33.2	33.2	33.2	33.2	33.2	33.2	33.2	33.2	33.2	33.2
NO. OF GORES AND SUSPENSION LINES	12	12	12	12	12	12	16	16	16	16
CANOPY MATERIAL	TYPE III-600 lb.	TYPE II 300 lb	TYPE III-600 lb.	TYPE III-600 lb.	TYPE III-600 lb.	TYPE III-600 lb.	TYPE III-600 lb.	TYPE III-600 lb.	TYPE III-600 lb.	TYPE III-600 lb.
SUSPENSION LINE MATERIAL	1 x 6000	1 x 6000	1 x 6000	1 x 6000	1 x 12000	1 x 12000	1 x 9000	1 x 9000	1 x 9000	1 x 9000
SUSPENSION LINE LENGTH (ft)	8.125	8.125	8.125	8.125	8.125	8.125	8.125	8.125	8.125	8.125
VENT DIAMETER (IN.)	10.72	12.25	12.25	12.25	11.7 *	11.7	11.7	11.7	11.7	11.7
VENT LINE LENGTH (IN.)	8.83	6.83	6.83	6.83	9.75	9.75	9.75	9.75	8.75	8.75
VENT BAND REINFORCING	1 x 3000	1 x 3000	1 x 6000	1 x 6000	1 x 6000	1 x 6000	1 x 6000	1 ½ x 10000	1 ½ x 10000	1 ½ x 10000
SLOT LENGTH (IN.)	7.80	7.80	7.80	7.80	NONE	NONE	NONE	NONE	NONE	NONE
THREAD SIZE (CANOPY SEAMS)	SIZE F	3 CORD	5 CORD	5 CORD	5 CORD	6 CORD	6 CORD	6 CORD	6 CORD	6 CORD
THREAD SIZE (LINE ATTACHMENT)	3 CORD	3 CORD	5 CORD	5 CORD	6 CORD	6 CORD	6 CORD	6 CORD	6 CORD	6 CORD
PATTERN DETAILS	A	A	A	A	A	A	B	B	C	C
WEIGHT (lbs)	17.0	11.2	17.0	17.0	22.5	22.0	25.5	25.5	31	28
BULK (ft^3)	.92	.80	.92	.92	1.25	1.25	1.29	1.29	1.55	1.29
USED ON RUN NO.	11	15	17	19	30	40	45,52	58	60,62	61,63

* CAPPED VENT

TABLE 10

MATERIALS USED IN GUIDE SURFACE RIBLESS PARACHUTES

PART	MATERIAL	SPECIFICATION	SIZE	TENSILE STRENGTH
CANOPY MATERIAL	CLOTH, NYLON	MIL-C-8021A TYPE II	7oz./sq. yd.	300 lb/in
	CLOTH, NYLON	MIL-C-8021A TYPE III	14 oz./sq. yd.	600 lb/in
SUSPENSION LINES	WEBBING, NYLON	MIL-W-4088 TYPE XVIII	WIDTH - 1 in	6000 lbs
	WEBBING, NYLON	MIL-W-4088 C TYPE XX	WIDTH - 1 in	9000 lbs
	WEBBING, NYLON	NON-SPECIFICATION	WIDTH - 1 in	12,000 lbs
THREAD	NYLON	MIL-T-7807	3 CORD 5 CORD 6 CORD	24 lbs 40 lbs 50 lbs
REINFORCING TAPE	WEBBING, NYLON TUBULAR	MIL-W-5625	WIDTH - 1 in	3000 lbs
	WEBBING, NYLON	MIL-W-4088 TYPE XVIII	WIDTH - 1 in	6000 lbs
	WEBBING, NYLON	MIL-W-4088 TYPE XIX	WIDTH - 1 3/4 in	10,000 lbs

Structural changes were incorporated in the 12 gore parachutes tested in the early part of the program, because of suspension line failure, vent band failure, and/or noninflation of several roof and Guide Surface panels. When damage still occurred to the strengthened 12 gore version the number of gores in the parachute was increased to 16.

The 16 gore parachute was tested on seven test runs with three major modifications incorporated. Three of the tests were with a standard 16 gore pattern detail, two tests were with parachutes with Guide Surface widths reduced 10% from the standard, and two tests were with the latter parachute with 15% spoiler flaps added to the Guide Surface edges in alternate panels.

C. Parachute Performance

Guide Surface Ribless parachute performance data, as measured on the high-speed sled test program, are presented in Table 11 and graphically illustrated in the performance curves shown in Figs. 19 through 24. Where several tests have been made with parachutes of similar configuration and construction, multiple sets of performance curves have been plotted on the same graphs. This allows rapid comparison and quickly highlights the common characteristics as well as pointing out departures from normal operation.

In all the tests made with G. S. Ribless parachutes five basic configurations were tried, some having structural modifications without a configuration change. Performance of the five configurations is listed below in order of their changes.

1. 6.5 Foot Diameter, 12 Gore, Type II Cloth

Only one test run (No. 15) was conducted with this parachute at a deployment velocity of 501 mph. Two Guide Surface panels failed to inflate at deployment and remained uninflated throughout the major portion of the test. Although the parachute maintained a steady state diameter ratio of 80%, a relatively high drag coefficient of 0.82 was held through the corresponding time interval. This is 10 to 15% greater than might be expected for such operation but apparently little or no loss in drag force was experienced due to the pushed-in Guide Surfaces and lack of full inflation. Also, despite the unsymmetrical shape of the guide surfaces the average maximum and mean radius of displacement indicated excellent stability. Performance curves giving inflation, drag, and stability data from this test are shown in Fig. 19.

Since this parachute seems to be marginal in inflation characteristics, and doubtful structurally at higher velocities, no more tests were made with this configuration.

2. 6.5 Foot Diameter, 12 Gore, Type III Cloth

Five tests were made with parachutes in this category. In test run No. 11, suspension line failure at maximum force resulted in collapse of the canopy. In test run Nos. 17 and 19 roof and guide surface panels did not inflate in the normal way, and in test run Nos. 30 and 40 there were normal deployment and operation, with minor damage to parachute lines.

TABLE 11

TEST RESULTS OF GUIDE SURFACE RIBLESS PARACHUTES

GUIDE SURFACE RIBLESS TYPE		12 GORE – STANDARD PANEL						16 GORE – STANDARD PANEL			16 GORE 15% SPOILERS	16 GORE 90% G.S. WIDTH	16 GORE 15% SPOILERS	16 GORE 90% G.S. WIDTH
RUN NUMBER		11	15	17	19	30	40	45	52	58	60	61	62	63
VELOCITY F.P.S.	V_0 AT PEAK SNATCH	891	735	834	883	912	1176	1166	1225	1151	1204	110	1264	1238
	V_0 AT PEAK OPENING SHOCK	886	736	822	877	906	1162	1151	1211	1127	1184	–	1256	1241
DYNAMIC PRESSURE P.S.F.	q_0 AT PEAK SNATCH	826	399	768	860	881	1487	1540	1630	1366	1453	–	1608	1638
	G_0 AT PEAK OPENING SHOCK	821	600	743	848	870	1451	1500	1593	1329	1405	–	1568	1594
TIME INTERVAL SECONDS	t_0 DEPLOYMENT TO PEAK SNATCH	0.304	0.253	0.277	0.317	0.373	0.296	0.338	–	0.208	0.205	–	0.189	0.190
	t_f SNATCH TO PRIMARY MAXIMUM INFLATION	0.046	–	0.123	0.083	0.080	0.084	0.062	0.050	0.052	0.045	–	0.045	0.053
	t_{mi} SNATCH TO MAXIMUM LOAD	0.046	0.077	0.073	0.053	0.044	0.084	0.048	0.030	0.036	0.040	–	0.045	0.053
FORCE LBS.	F_0 SNATCH FORCE	6,900	7,400	8,900	11,800	13,800	11,000	21,400	36,500	27,800	27,500	–	26,000	37,300
	F_0 OPENING SHOCK	21,700	18,400	22,800	26,800	40,800	52,800	62,800	66,100	63,100	52,500	–	53,800	52,100
DIAMETER RATIO PERCENT	$\left(\frac{D_{P_L}}{D_P}\right)_m$ MAXIMUM	78.4	–	84.7	80.0	86.0	83.6	84.4	86.7	86.4	78.5	–	78.7	82.6
	$\left(\frac{D_{P_L}}{D_P}\right)_0$ AVERAGE	–	80.3	84.3	77.8	85.6		–	87.7	87.4	–	–	–	–
STABILITY DEGREES	MEAN RADIUS OF DISPLACEMENT	–	2.8	3.3	2.3	2.7	–	–	1.5	3.2	–	–	–	–
	MAXIMUM RADIUS OF DISPLACEMENT	–	3.4	4.0	6.2	4.8	–	–	3.0	8.0	–	–	–	–
C_D AVERAGE DRAG COEFFICIENT		–	0.82	0.72	0.77	0.80	0.80	–	0.83	0.68	–	–	–	–
X OPENING SHOCK FACTOR		–	1.12	1.24	1.21	1.78	1.33	–	1.47	–	–	–	–	–
PARACHUTE DAMAGE	CANOPY	MINOR DAMAGE	NONE	NONE	NONE	NONE	VENT BAND BROKEN	3 PANELS TORN	MINOR DAMAGE	MINOR DAMAGE	SEVERE DAMAGE	DESTROYED BY DRAGGING ALONG TRACK	SEVERE DAMAGE THROUGHOUT	SEVERE DAMAGE THROUGHOUT
	LINES	3 LINES BROKEN NEAR KEEPER				MINOR LINE DAMAGE	MINOR LINE DAMAGE	VENT BAND FAILED	VENT BAND BROKEN	NO LINE DAMAGE	6 LINES TORN FROM CANOPY		MAJOR LINE DAMAGE	VENT BAND BROKEN
								NO LINE DAMAGE	NO LINE DAMAGE					NO LINE DAMAGE
PARACHUTE OPERATION		1 PANEL IN COLLAPSED CONDITION, FAILED AT MAX. LOAD	2 G.S. PANELS PRESSED IN	2 PANELS HESITATED INFLATING	2 PANELS & G.S. NOT INFLATED FIRST 2 SEC.	NORMAL DEPLOYMENT DECREASING OSCILLATORY FREQUENCY	NORMAL	NORMAL DEPLOYMENT DAMAGED DURING INFLATION	NORMAL DEPLOYMENT 15 PANELS INFLATED AFTER 4.0 SEC	PARACHUTE NEVER FULLY INFLATED	NORMAL DEPLOYMENT FAILED 0.018 SEC AFTER F_0	DEPLOYED LOW VELOCITY	NORMAL DEPLOYMENT DAMAGED DURING INFLATION	NORMAL DEPLOYMENT DAMAGED DURING INFLATION
INSTRUMENTATION PERFORMANCE		NORMAL	NORMAL	NORMAL	NORMAL	NORMAL	NORMAL	NORMAL	NORMAL	NORMAL	NORMAL	NORMAL	NORMAL	NORMAL

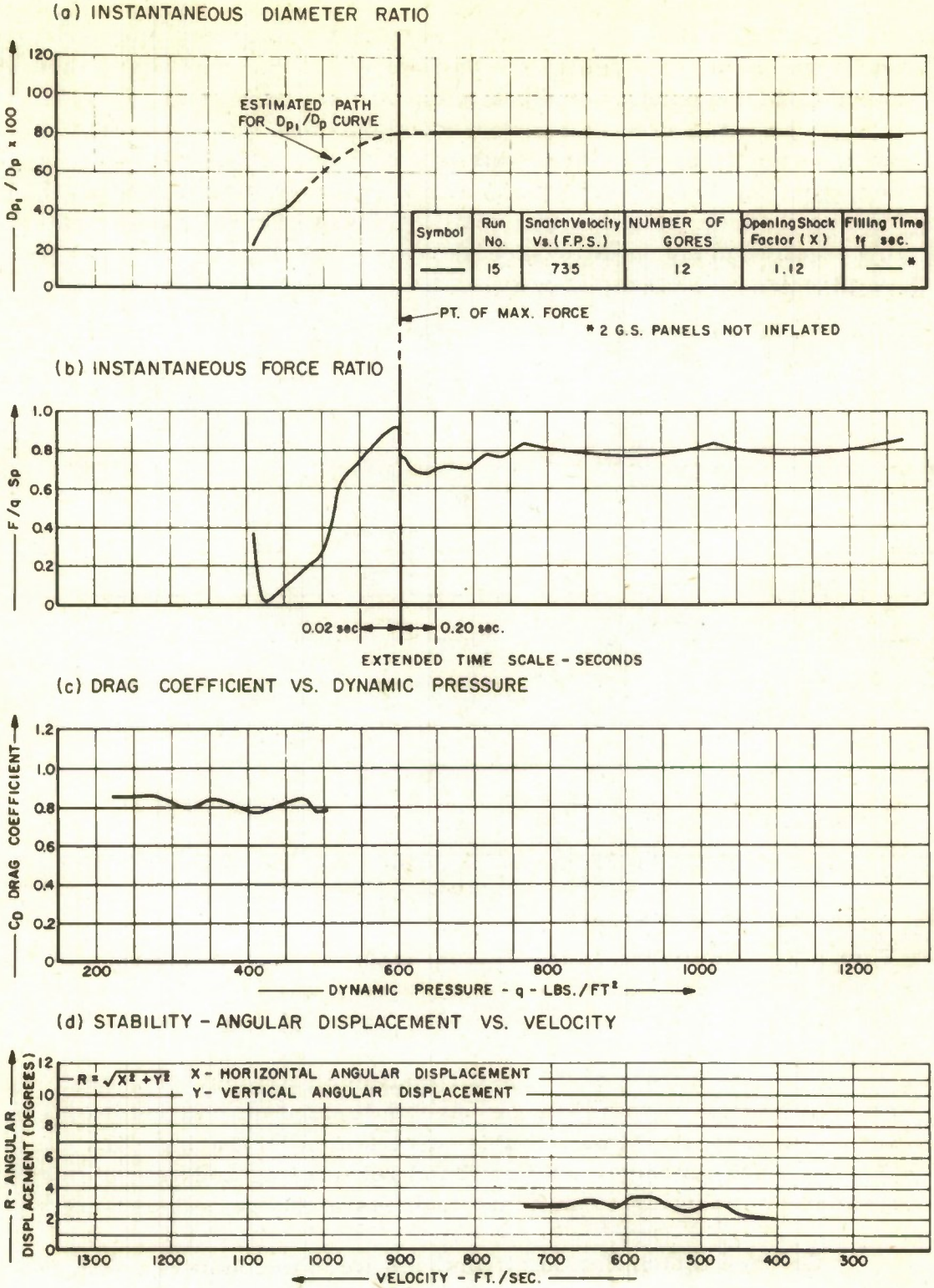

Figure 19 Summary Data - Guide Surface Ribless Parachute (Test Run No. 15)

Test run No. 11, the initial test in this category and parachute type, was made at a deployment velocity of 608 mph. Since three 6000 pound T.S. suspension lines failed at a maximum force of 21,715 pounds, it is pertinent to note that the inflation process was abnormal, with one panel in a collapsed position during inflation. This may have caused unsymmetric load distribution, allowing a few lines to absorb the opening shock force and ultimately fail. Curves of the diameter ratio and force ratio during inflation are shown in Fig. 20.

(a) INSTANTANEOUS DIAMETER RATIO

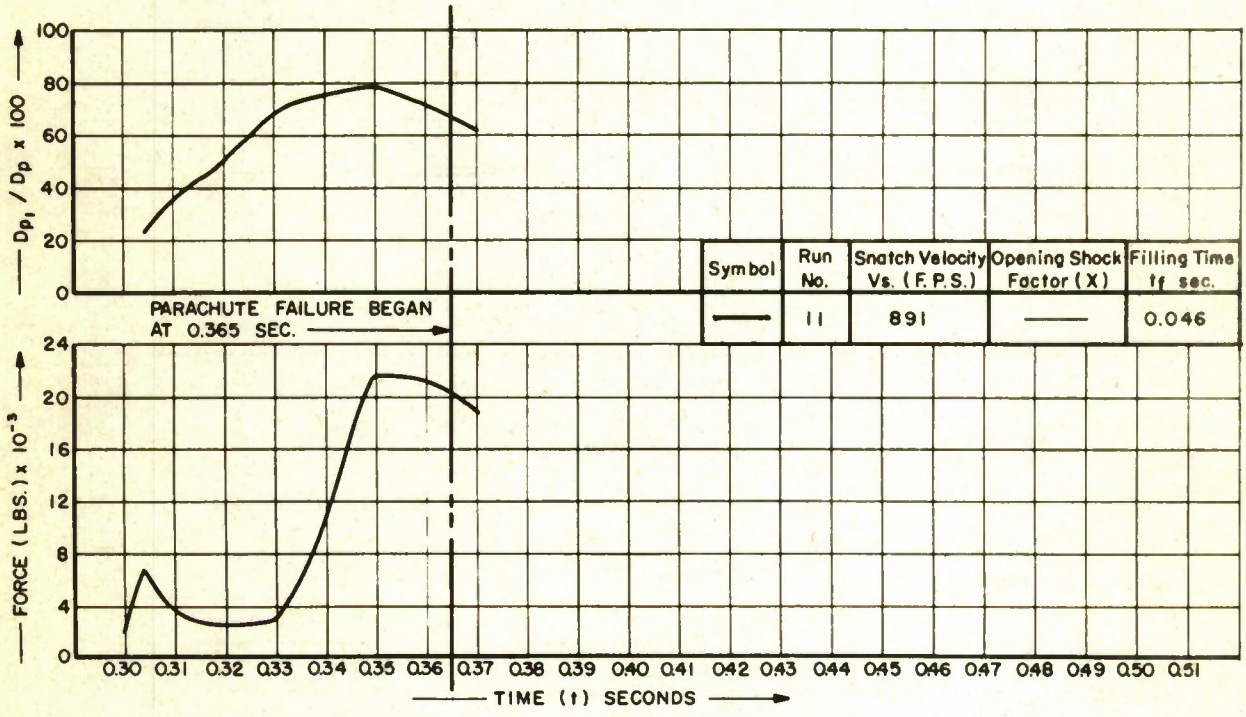

(b) INSTANTANEOUS FORCE RATIO

Figure 20 Summary Data - Guide Surface Ribless Parachute (Test Run No. 11)

With the exception of the utilization of straight cut rather than bias cut canopy material in the parachute used on test run No. 17, structurally identical parachutes were tested on test run Nos. 17 and 19. Both had strengthened vent band reinforcing and vent diameter increases contributing to an added fullness at the parachute vent.

On each test inflation difficulties were encountered with two panels. The parachute on test run No. 17, hesitated slightly during the inflation process, after which apparent normal operation was resumed.

On test run No. 19, two roof and guide surface panels remained uninflated for the first 2 seconds of operation. After this time the guide surface panels inflated but over-all panels did not inflate until low velocity end of test was reached. Steady state diameter ratios averaged 84.3% on test run No. 17 and 77.8% on test run No. 19 with corresponding average drag coefficients of 0.72 and 0.77. For their respective test runs these figures are reverse of what would be expected, although the generally reduced average drag coefficients correspond to the reduced average inflation figures. Opening shock factors for the two runs were nearly identical, 1.21 and 1.24. Performance curves for these two test runs are shown in Fig. 21.

Two more parachutes within this configuration group were tested on test run Nos. 30 and 40. These parachutes had no pressure relief slots in the round seam, and the central vent was covered on the parachute tested on test run No. 30. Increasing velocities and higher expected opening shock forces suggested changes in the suspension line assemblies to withstand the anticipated load increases. Although 9000 pound T.S. webbing would undoubtedly have been strong enough it was not commercially available at that time, so 1 inch - 12,000 pound T.S. webbing was used on these parachutes. It was also suspected that the original four line keeper was contributing to uneven line elongation and loading, due to its inherent four line method of attachment. This was alleviated by installing an improved keeper, which attached to all lines going through the confluence point. Both of these keepers are described in detail in Appendix E. Dimensional changes, decreasing the fullness at the vent of the parachute, was also made to the parachutes on these two tests.

The most satisfactory operation of a G.S. Ribless type of parachute in the test program was obtained with this configuration in test run Nos. 30 and 40. Both tests yielded a steady state drag coefficient of 0.80 although the opening shock factor from the two tests varied widely. On test run No. 30, which deployed at a velocity of 622 mph, the opening shock factor was 1.78 while on test run No. 40 which was deployed at the higher velocity of 802 mph the opening shock factor was 1.33. If a relationship between deployment velocities, or dynamic pressure, and opening shock force can be assumed it is evident that the opening shock force producing the high opening shock factor can be found in the inflation process, which shows that the parachute reached its peak force in approximately half the time required for the corresponding higher deployment velocity of test run No. 40 and approximately two-thirds the time of other comparable tests. This is graphically illustrated on the performance curves for these two tests, shown in Fig. 22.

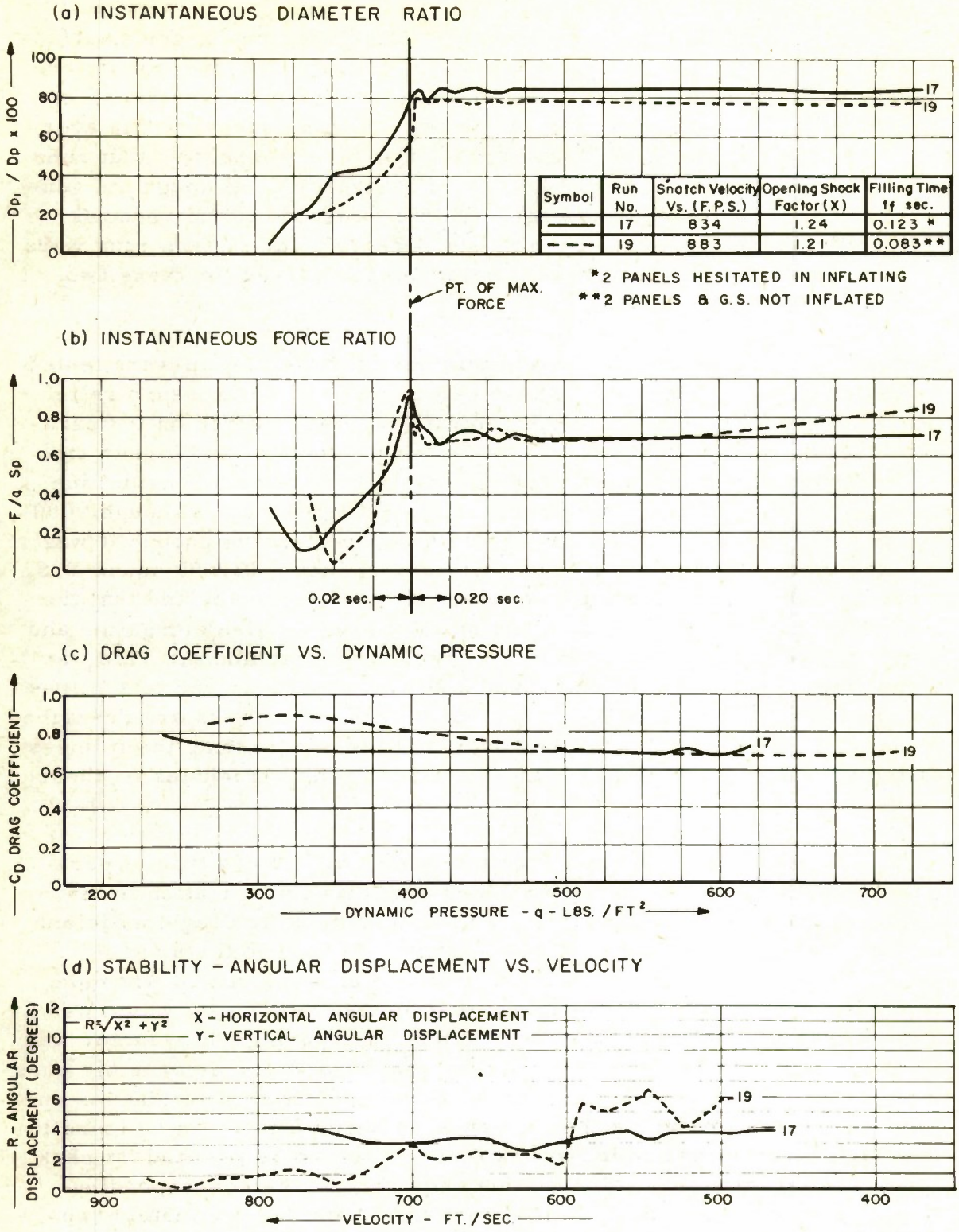

Figure 21 Summary Data - Guide Surface Ribless Parachute (Test Run Nos. 17 and 19)

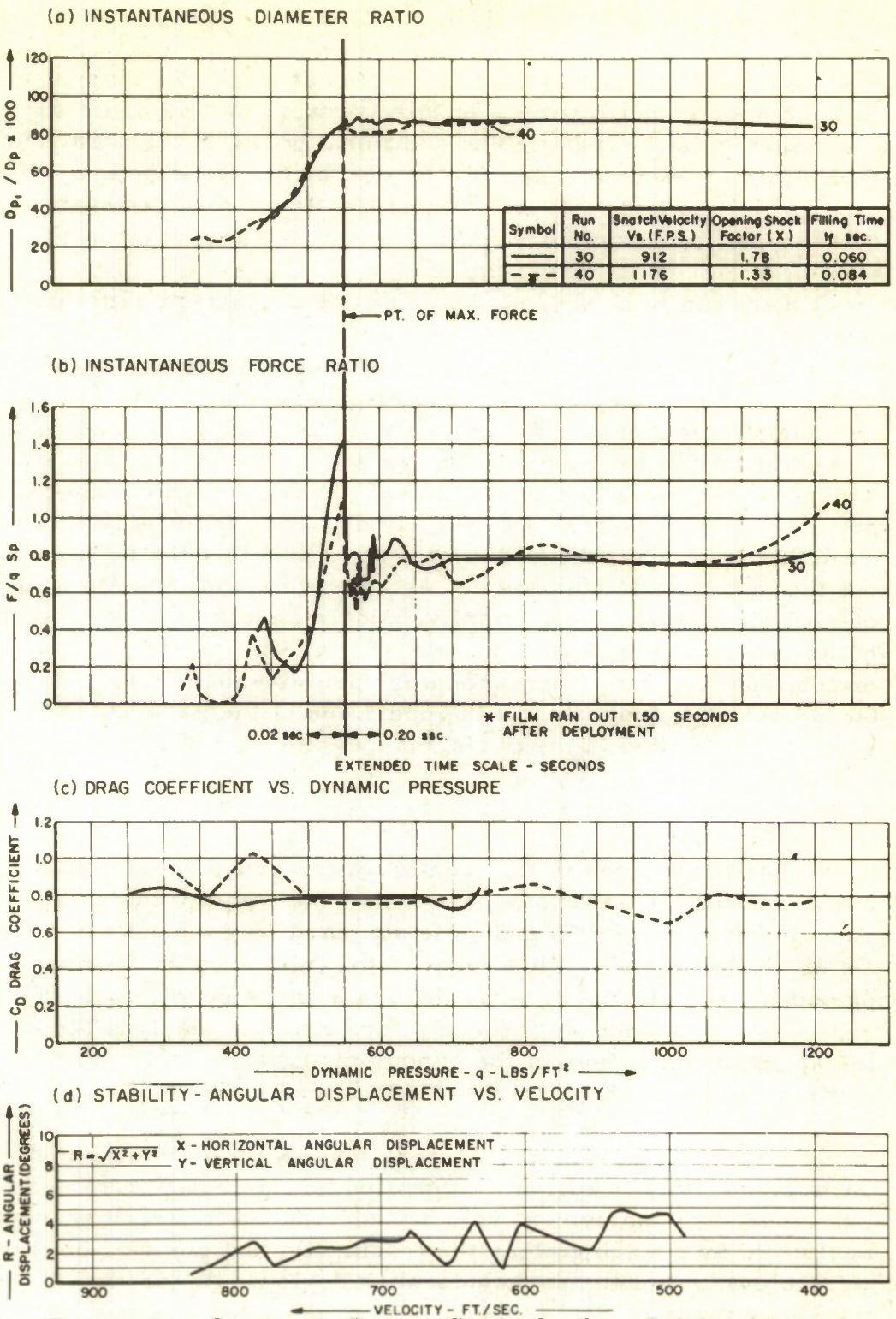

Figure 22 Summary Data - Guide Surface Ribless Parachute (Test Run Nos. 30 and 40)

3. 6.5 Foot Diameter, 16 Gore, Type III Cloth

Since considerable over-all strain damage was evident in the final 12 gore configuration a 16 gore version was designed to continue the higher velocity tests. The additional gores in the parachute were theoretically to add strength to the unit by decreasing over-all panel size as well as add total line strength. Basic gore dimensions for the standard 16 gore configuration are shown in Detail "B" in Fig. 17.

Test run Nos. 45, 52, and 58 were performed with this configuration at deployment velocities of 795, 835, and 785 mph, respectively. On test run No. 45 the parachute was severely damaged at opening shock. On test run Nos. 52 and 58 the parachutes suffered minor damage during inflation and did not fully inflate. Four seconds was required to inflate all panels of the parachute on test run No. 52 during which time the dynamic pressure had decreased from 1630 psf to 287 psf. This corresponds to a velocity decrease from 1225 to 514 fps T.A.S. On test run No. 58 a total of 13 panels were inflated throughout the test. Both tests yielded an average steady state diameter ratio of 87.5%. Despite the partically inflated condition of the parachutes on both tests an average steady state drag coefficient of 0.83 was realized on test run No. 52. Corresponding opening shock factor was 1.47. Graphical representation of the operation of the parachutes in this group is presented in the performance data summary curves in Fig. 23.

4. 6.5 Foot Diameter, 16 Gore, Type III Cloth, 90% G. S. Width

The parachutes in this configuration group were identical to the standard 16 gore parachute except that the width of the guide surface panels was reduced 10% from the standard 16 gore pattern as shown in Detail "C", Fig. 17. This reduced the inlet area at the mouth of the parachute and slightly altered the angle of the cone formed by the guide surfaces. Introduction of these alterations was designed to eliminate the apparent looseness of the canopy material in an attempt to induce full inflation at high deployment velocities.

Test run Nos. 61 and 73 were made with the modified 16 gore parachute. Rocket engine malfunction on test run No. 61, resulted in extremely low deployment velocity and caused the test parachute to be destroyed by dragging along the track. On test run No. 63 five panels were blown out of the parachute when deployed at 858 mph. The opening shock force of 52,149 pounds, corresponded to a maximum diameter ratio of 82.6% at time of failure. It is interesting to note that the opening shock force causing failure of this parachute was approximately 20%

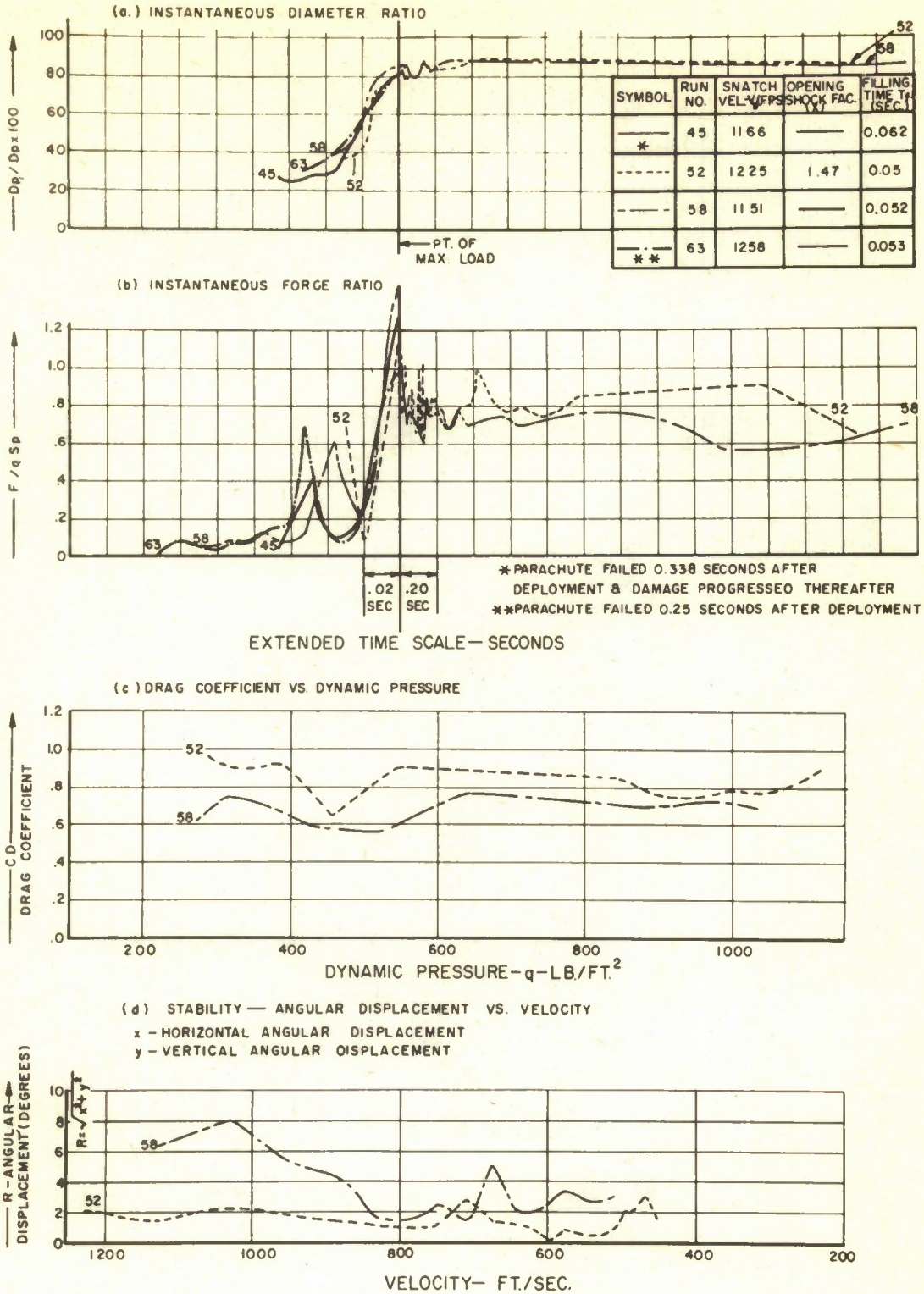

Figure 23 Summary Data - Guide Surface Ribless Parachute (Test Run Nos. 45, 52, 58, and 63)

below that of the standard 16 gore parachute which did not inflate fully under similar conditions.

5. 6.5 Foot Diameter, 16 Gore, Type III Cloth (90% G.S. Width - 15% Spoiler Flaps)

This configuration, tested on test run Nos. 60 and 62, was a modified 16 gore parachute as described in paragraph 4 above, with the addition of spoiler flaps measuring 0.15D in length and placed in alternate gores, below the guide surface panels and between adjacent suspension lines. A photograph of this type of parachute is shown in Fig. 24.

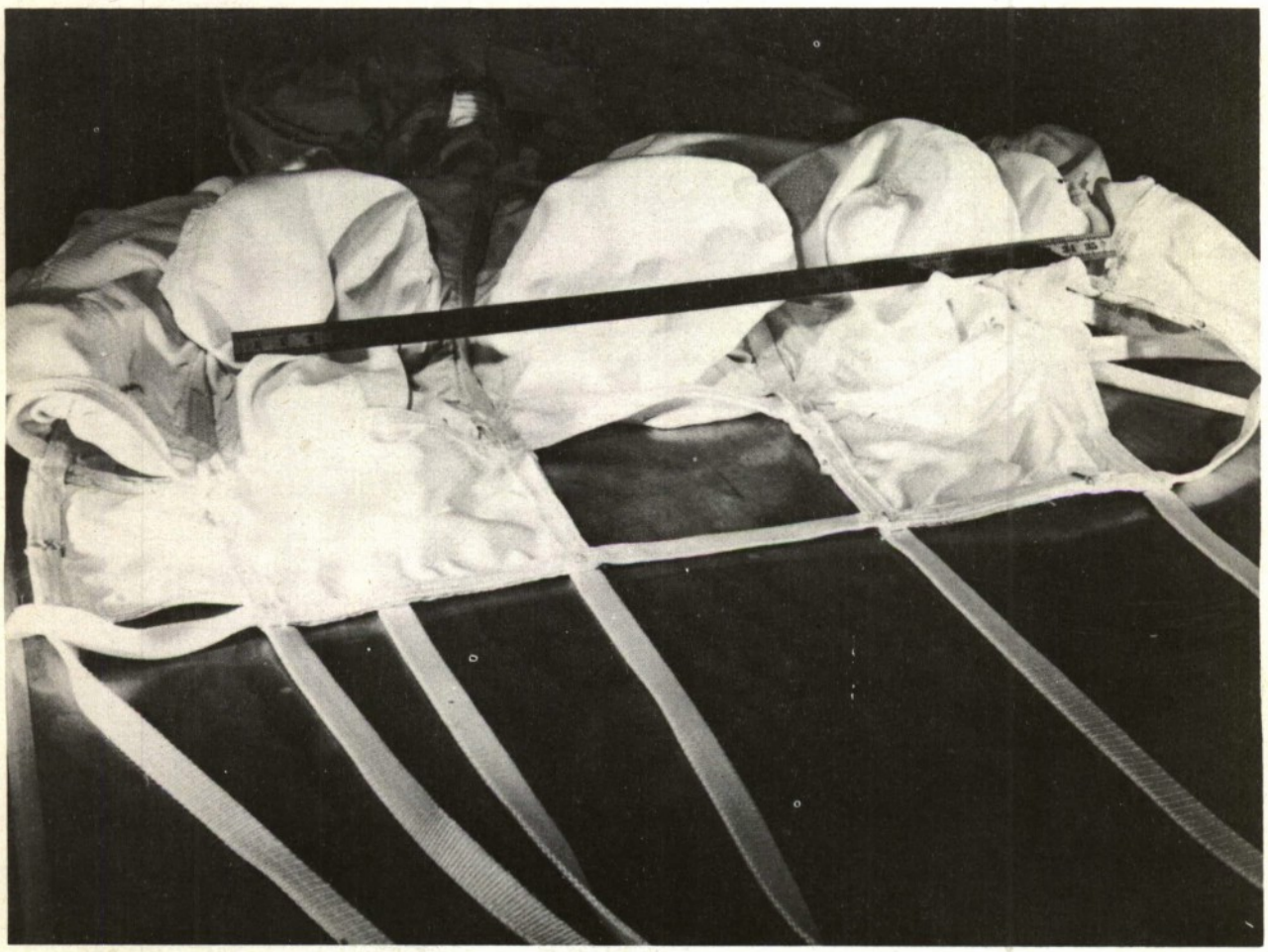

Figure 24 Guide Surface Ribless Parachute with Spoiler Flaps

Both of the tests with this parachute resulted in severe damage to the canopy and lines during inflation. The inflation and force curves shown in Fig. 25 are unique in that they illustrate almost identical characteristics of the two parachutes up to time of failure. Also pertinent,

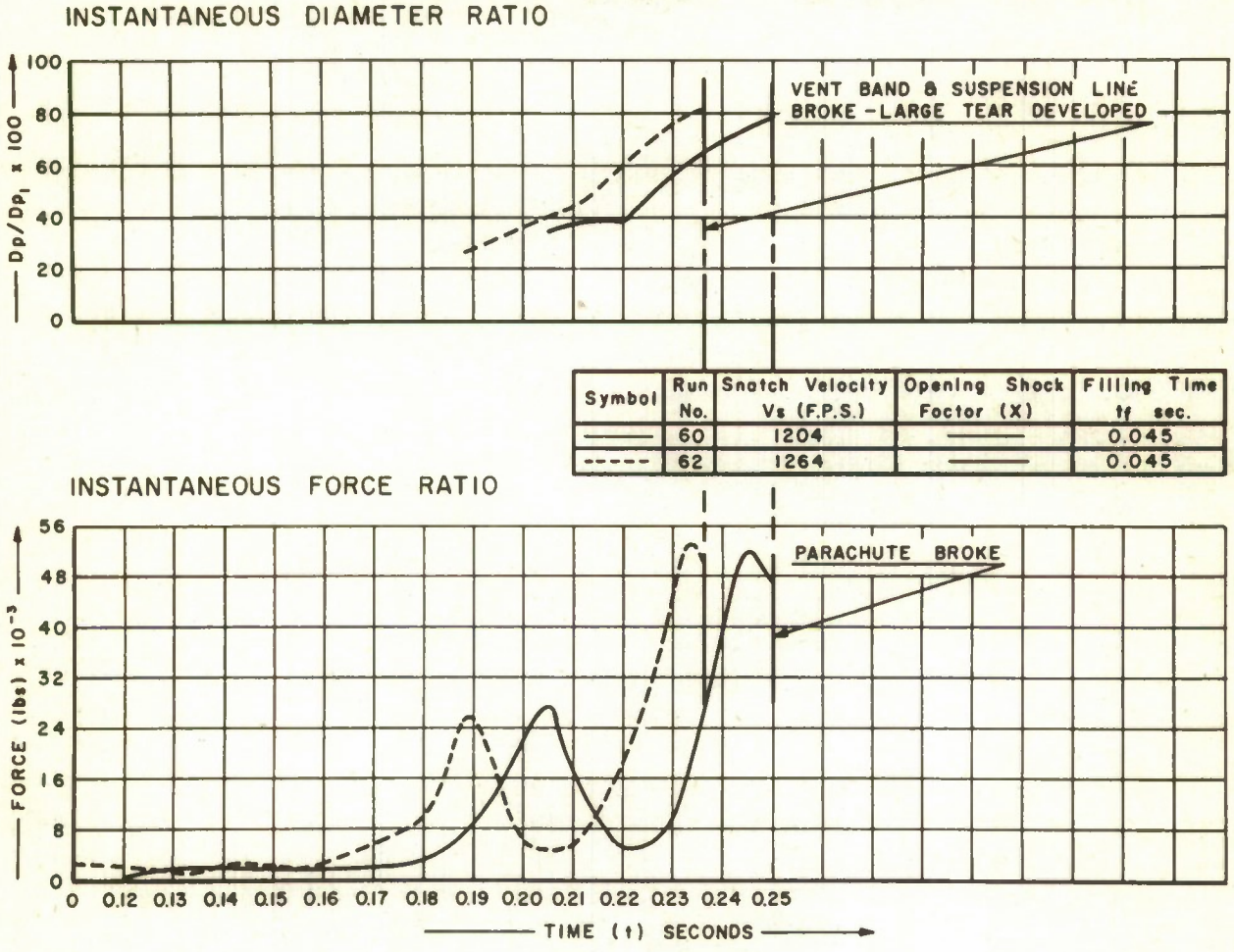

Figure 25 Summary Data - Guide Surface Ribless Parachute (Test Run Nos. 60 and 62)

is the fact that the two parachutes with spoiler flaps, which are intended to slow the opening process and reduce opening shock, had opening shock forces approximately equal to the identical parachute without spoiler flaps, under comparable test conditions.

APPENDIX C

FIST RIBBON PARACHUTE

A. Introduction

The FIST Ribbon parachute is basically a flat parachute, assembled from triangular panels which form the regular polygon configuration of the parachute. Each panel is a grid of horizontal ribbons spaced and retained at close intervals by one or more vertical ribbons. Radial bands, extending from vent to skirt at the sides of each panel, join the panels together and transfer the forces developed in the canopy to the suspension lines. A typical FIST Ribbon parachute is shown in operation in Fig. 26. Figure 27 illustrates a typical panel assembly. A complete description of the FIST Ribbon parachute is presented by Knacke (Ref. 5) and general specifications for the construction of the parachute are given in Ref. 8.

B. Test Program

A series of 33 tests was conducted in which various configurations of FIST Ribbon type parachutes were tested on the 10,000 foot Free Air Test Facility Track at Edwards Air Force Base, California. All tests were performed with the liquid fuel rocket powered test vehicle described in Appendix F at deployment velocities ranging from 450 and 840 mph T.A.S. The parachutes tested in the program, with the exception of a 6.57 foot special purpose design, ranged in size from 8.06 to 8.92 feet in diameter. Fabrication was in accordance with military specification MIL-P-6635 (Ref. 8) with design and revision information being furnished by the contracting agency. Major dimensional details, materials, and material specifications of the various FIST Ribbon parachutes tested in the program are listed in Tables 12 and 13. Geometric variations in the series of parachutes tested included diameter, number of panels, and the number and spacing of horizontal and vertical ribbons. The latter factors are primary determinants of the geometric porosity and influence some of the important operational characteristics of this type of parachute. Variations in these geometric parameters during the test program resulted in a total of 12 parachute types with geometric porosities ranging from 12.86% to 23.30%.

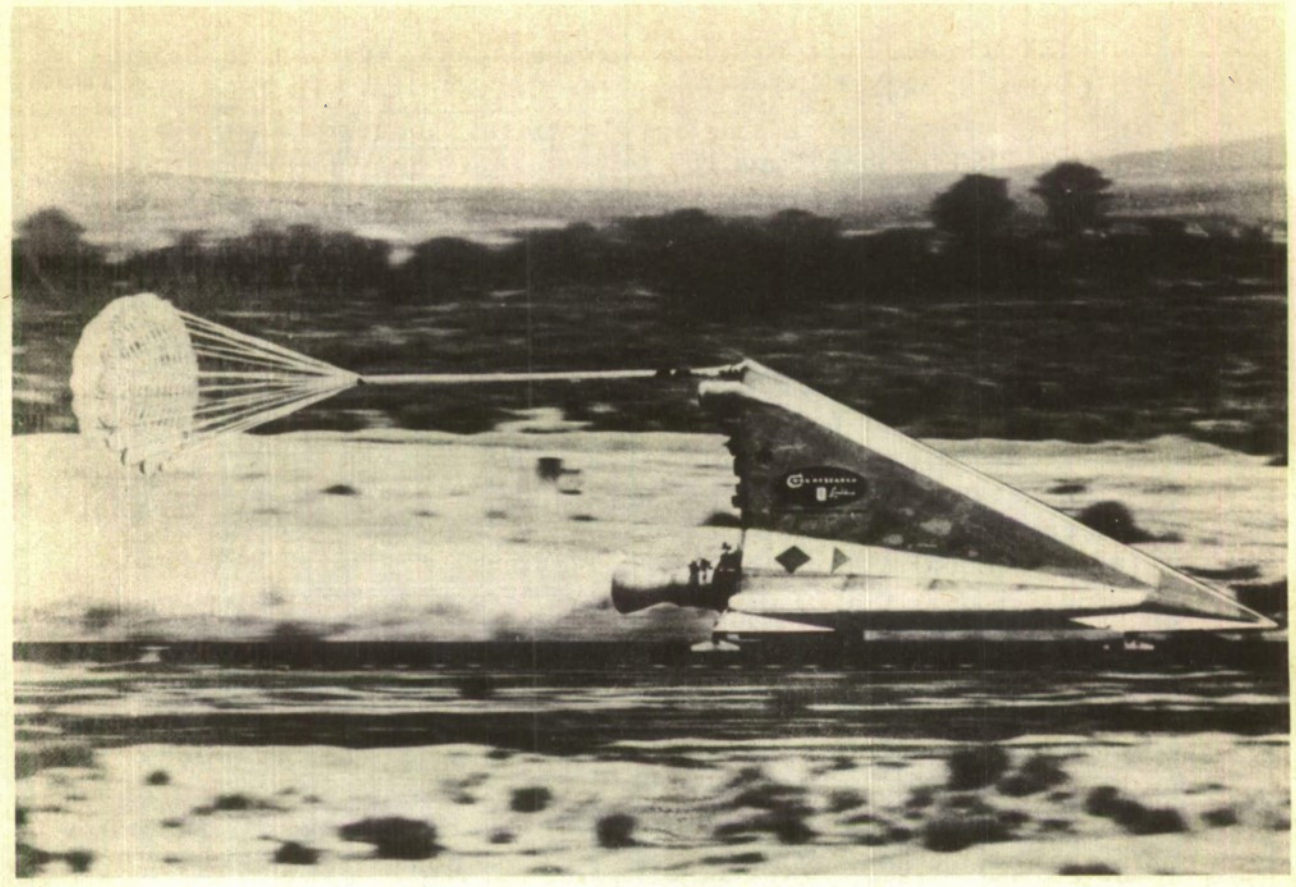

Figure 26 Typical FIST Ribbon Parachute in Operation on Test Vehicle

C. Parachute Performance

FIST Ribbon parachute performance data for the 12 parachute types considered in 33 test runs, are tabulated in Table 14 according to parachute type number and corresponding geometric porosity. Summary curves which give the important performance characteristics are graphically presented for each test and type number. For rapid and accurate comparison, multiple sets of performance curves have been placed on graphs common to any one configuration group. This serves to highlight erratic operation as well as indicate the average characteristics of the type being presented. Performance details of the 12 configuration groups are listed below in order of type number. This approximately coincides with the order of design and testing. Within each group the velocity increases closely parallel the increase in run number as each type was tested.

1. FIST Ribbon Type 107 (λ_g = 14.62%)

The FIST Ribbon Type 107 parachute tested in this program was a strengthened version of the Phase I, subsonic, Type 107 parachute. The heavy material required for the anticipated higher deployment velocities of Phase II tests, eliminated the porosity addition due to material permeability. This resulted in a significant decrease in the total porosity (λ_g now equal λ_t) of the high-speed design over that of the final Phase I design (from 17.6% to 14.6%).

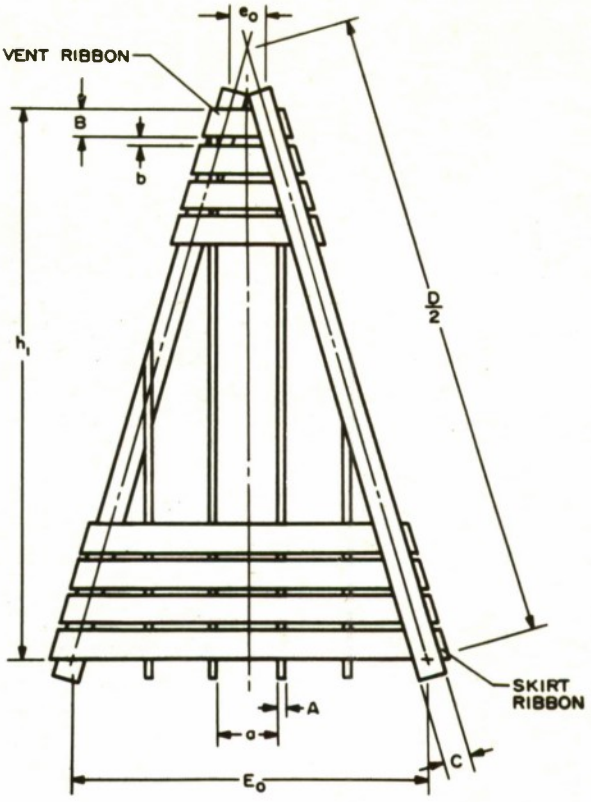

Figure 27 Panel Layout - FIST Ribbon Parachutes

A total of six tests, test run Nos. 7, 8, 10, 12, 13, and 18, was conducted with the 107 configuration. On two of the tests in this group insufficient information was obtained for complete analysis. On one of these tests, test run No. 8, it was observed that the parachute inflation appeared improper, with one section of the parachute remaining pushed in. On test run No. 10, an extremely low deployment velocity caused parachute to be damaged by dragging along the track. Good performance data were obtained on test run Nos. 7, 12, 13, and 18 at deployment velocities of 450, 577, 645, and 770 mph, respectively. Performance curves for these tests are plotted in Fig. 28. On test run No. 18, however, severe damage to parachute and lines, at a maximum force of 35,803 pounds, rendered the information useful only through the inflation process. In the three tests where steady state analysis was possible, the drag coefficient C_{D_o} averaged 0.57 and the opening shock factor (X) averaged 1.21. This opening shock factor appears to be of greater magnitude than would be expected when compared to over-all FIST Ribbon results. In this respect, it should be noted that one of the three tests from which the average was determined exhibited an unusually high opening shock factor, and contributed greatly to the high average result. If this test is eliminated from the average results, the drag coefficient would not be greatly affected but the average opening

TABLE 12

PHYSICAL DETAILS OF FIST RIBBON PARACHUTES

FIST TYPE	107	107-A	107-B	118	119	121	122	123	124	124	124	125	126
NOMONIAL DIAMETER D_o (ft)	8.6	8.06	8.33	6.57	8.62	8.32	8.51	8.51	8.6	6.6	8.6	8.15	8.92
CANOPY AREA S_o (ft^2)	56.6	49.5	53.14	33.05	56.9	53.78	55.46	55.46	56.6	56.6	56.6	50.94	60.90
GEOMETRIC POROSITY λ_g (%)	14.62	12.86	14.37	18.22	18.85	18.47	23.10	23.10	21.15	21.15	21.15	23.25	23.30
SPACING BETWEEN VERTICAL RIBBONS a (in.)	6.0	6.0	4.0	3.0	3.0	3.0	3.0	3.0	3.0	3.0	3.0	3.0	2.0
SPACING BETWEEN HORIZONTAL RIBBONS b (in.)	$\frac{9}{16}$	$\frac{9}{16}$	$\frac{5}{8}$	$\frac{13}{16}$	$\frac{15}{16}$	1.0	1.375	1.375	1.156	1.156	1.156	1.25	1.50
VENT LINE LENGTH (in.)	9.625	8.97	14.5	9.625	13.375	15.06	13.57	13.57	13.57	13.57	13.57	13.57	13.57
WIOTH OF GORE AT SKIRT E_o (in)	20.1	20.1	19.62	15.36	20.18	13.33	19.96	19.96	20.5	20.5	20.5	18.18	21.24
WIOTH OF GORE AT VENT e_o (in.)	2.25	2.25	3.4	2.25	3.4	2.53	3.4	3.4	3.4	3.4	3.4	3.4	3.74
LENGTH OF GORE h_1 (in.)	45.6	45.6	41.4	32.95	43.125	41.0	42.5	42.5	43.03	43.03	43.03	41.0	44.00
NUMBER OF HORIZONTAL RIBBONS	18	16	16	12	15	14	13	13	14	14	14	13	13
NUMBER OF VERTICAL RIBBONS	2	2	3	3	3	2	4	4	4	4	4	4	6
NUMBER OF GORES & SUSPENSION LINES	16	15	16	16	16	24	16	16	16	16	16	16	16
SUSPENSION LINE LENGTH	8.6	6.06	8.33	6.57	6.62	8.32	6.51 | 16.65	8.51 | 16.85	8.6	8.6	8.6	6.15	6.92
SUSPENSION LINE MATERIAL	1 x 6000	1 x 6000	1 x 6000	1 x 6000	1 x 12000	1 x 12000	1 x 12000	1 x 6000	1 x 6000	1 x 6000	1 x 6000	1 x 6000	1 x 6000
HORIZONTAL RIBBON MATERIAL	2 x 1000	2 x 1000	2 x 1000	2 x 1700	2 x 1700	2 x 1700	2 x 1700	2 x 1700	2 x 1700	2 x 1700	2 x 1000	2 x 1700	2 x 1700
VERTICAL RIBBON MATERIAL	$\frac{9}{16}$ x 500	$\frac{9}{16}$ x 500	$\frac{9}{16}$ x 500	$\frac{9}{16}$ x 500	$\frac{9}{16}$ x 500	$\frac{9}{16}$ x 500	$\frac{9}{16}$ x 500	$\frac{9}{16}$ x 500	$\frac{9}{16}$ x 500	$\frac{9}{16}$ x 500	$\frac{9}{16}$ x 500	$\frac{9}{16}$ x 500	$\frac{9}{16}$ x 500
RADIAL RIBBON MATERIAL	$1\frac{3}{4}$ x 3600	$1\frac{3}{4}$ x 3600	$1\frac{3}{4}$ x 3600	$1\frac{3}{4}$ x 3600	2 x 1700	2 x 1700	2 x 1700	2 x 1700	2 x 1700	$1\frac{3}{4}$ x 3600	2 x 1000	2 x 1700	2 x 1700
HORIZONTAL REINFORCING BAND MATERIAL	$1\frac{3}{4}$ x 3600	$1\frac{3}{4}$ x 3600	$1\frac{3}{4}$ x 3600	$1\frac{3}{4}$ x 3600	$1\frac{3}{4}$ x 3600	$1\frac{3}{4}$ x 3600	$1\frac{3}{4}$ x 3600	$1\frac{3}{4}$ x 3600	$1\frac{3}{4}$ x 3600	$1\frac{3}{4}$ x 3600	$1\frac{3}{4}$ x 3600	$1\frac{3}{4}$ x 3600	$1\frac{3}{4}$ x 3600
REINFORCING BAND ON RIBBON NUMBERS	4,7,10,13	4,7,10,13	4,8,12	3,6,9	4,7,10	4,7,10	4,7,10	4,7,10	4,7,10	4,7,10,13	4,7,10	4,7,10	4,7,10
WEIGHT (lbs)	20.2	18.9	17.6	~ 15	32.9	~ 42.0	28.4	21.0	21.5	20.1	19.5	20.0	22.0
BULK (ft^3)	0.95	0.86	0.76	0.6	1.52	1.63	1.30	0.98	1.00	1.06	0.92	0.96	1.04
USED ON RUN NUMBERS	7,8,10,12 13 & 18	14	22	16 & 21	25	23 & 24	27,26 29&34 | 36	33&35 | 37	36 & 42	41	46,53 & 59	43,44 & 50	46,47 &51

TABLE 13

MATERIALS USED IN FIST RIBBON PARACHUTES

PART	MATERIAL	SPECIFICATION	SIZE	MINIMUM TENSILE STRENGTH
HORIZONTAL RIBBONS	RIBBON; NYLON PARACHUTE	MIL-R-5608A	WIDTH = 2 in	1000 lbs
	TAPE; REINFORCING	MIL-T-5038	WIDTH = 2 in	1700 lbs
RADIAL RIBBONS	WEBBING; NYLON TAPE	MIL-W-4088	WIDTH = 1 3/4 in	3600 lbs
	NYLON REINFORCING	MIL-T-5038	WIDTH = 2 in	1700 lbs
	RIBBON; PARACHUTE	MIL-R-5608A	WIDTH = 2 in	1000 lbs
VERTICAL RIBBONS	TAPE; NYLON REINFORCING	MIL-T-5038	WIDTH = 9/16 in	500 lbs
HORIZONTAL REINFORCING WEBBING	WEBBING, NYLON	MIL-W-4088	WIDTH = 1 3/4 in	3600 lbs
VENT REINFORCING	WEBBING, NYLON	MIL-W-4088	WIDTH = 1 in	6000 lbs
SKIRT REINFORCING	WEBBING, NYLON	MIL-W-4088	WIDTH = 1 3/4 in	3600 lbs
	WEBBING, NYLON	MIL-W-4088	WIDTH = 1 3/4 in	6000 lbs
SUSPENSION LINES	WEBBING, NYLON	MIL-W-4088	WIDTH = 1 in	6000 lbs
	WEBBING, NYLON	NON-SPEC	WIDTH = 1 in	12000 lbs
POCKET BANDS	WEBBING, NYLON TUBULAR	MIL-W-5625	WIDTH = 1 in	3000 lbs
	WEBBING, NYLON	MIL-W-4088	WIDTH = 1 3/4 in	3600 lbs
THREAD	THREAD; NYLON	MIL-T-7807	SIZE F	11 lbs
			SIZE FF	14 lbs
			3 CORD	24 lbs
			5 CORD	40 lbs

TABLE 14
TEST RESULTS OF FIST RIBBON PARACHUTES

TYPE NO. (GEOMETRIC POROSITY)	RUN NO.	VELOCITY (FPS) V_s AT PEAK SNATCH	VELOCITY (FPS) V_o AT PEAK OPENING SHOCK	DYNAMIC PRESSURE (PSI) q_s AT PEAK SNATCH	DYNAMIC PRESSURE (PSI) q_o AT PEAK OPENING SHOCK	TIME INTERVAL (SEC) t_p DEPLOYMENT TO PEAK SNATCH	TIME INTERVAL (SEC) t_f SNATCH TO PRIMARY MAXIMUM INFLATION	TIME INTERVAL (SEC) t_{sd} SNATCH TO MAXIMUM LOAD	FORCE (LBS.) F_s SNATCH FORCE	FORCE (LBS.) F_o OPENING SHOCK	DIAMETER RATIO (PERCENT) $(D_f/D_o)_p$ MAXIMUM	DIAMETER RATIO (PERCENT) $(D_f/D_o)_p$ AVERAGE	STABILITY – ANGULAR DISPLACEMENT (DEGREES) (R) MEAN	STABILITY – ANGULAR DISPLACEMENT (DEGREES) (R) MAXIMUM	C_{D_o} AVERAGE DRAG COEFFICIENT	N OPENING SHOCK FACTOR	PARACHUTE DAMAGE	PARACHUTE OPERATION	INSTRUMENTATION OPERATION
107 (1.468)	7	661	651	483	466	.030	–	0.120	5,250	21,450	–	–	–	–	.084	1.45	NONE	SKIRT FLUTTER IN TWO PANELS	SLED CAMERA INOPERATIVE
	9	APPROX. 300 MPH	–	–	–	–	–	–	–	APPROX. 14,000	–	–	–	–	–	–	NONE	IMPROPER INFLATION–UNSTABLE	DEFECTIVE POWER SUPPLY
	10	175	–	–	–	–	–	–	–	–	–	–	–	–	–	–	TRACK DAMAGE FROM DRAGGING	NORMAL DEPLOYMENT / LOW VELOCITY / ENGINE VALVE MALFUNCTION	NO TIMING LIGHTS / SLED OR TRACKSIDE
	12	846	825	718	683	0.347	0.084	0.084	7,400	25,200	103.6	98.4	12.4	13.9	0.82	1.00	MINOR DAMAGE STRAINS & BURNS	NORMAL DEPLOYMENT SLIGHT SKIRT FLUTTER	NORMAL
	13	952	925	980	906	0.300	0.120	0.12	11,100	36,700	106.1	100.6	13.2	18.1	0.86	1.18	NONE	NORMAL	NORMAL
	19	1129	1113	1422	1398	0.246	0.075	0.082	8,150	36,800	96.2	–	–	–	–	–	MAJOR DAMAGE / SEVERE LINE DAMAGE	NORMAL DEPLOYMENT / FAILED DURING INFLATION	NORMAL
107 A (10.66)	14	924	911	889	863	0.296	0.116	0.116	6,300	27,850	116.8	–	–	–	–	–	NONE	NORMAL DEPLOYMENT / EARLY RELEASE	NORMAL / TEST VEHICLE DAMAGED
107 B (14.37)	22	1085	1036	1160	1167	0.297	–	0.117	10,400	27,200	–	–	–	–	–	–	PARACHUTE BURNED BY FLAME	NORMAL	NORMAL
119 (10.82)	18	782 MPH	–	–	–	–	–	–	–	–	–	–	–	–	–	–	–	NO DEPLOYMENT / PACK BRIDLE FAILURE	NORMAL
	21	1129	1068	1406	1280	0.277	–	–	10,700	28,400	MAX. 98.8 MIN. 78.4	93.0	–	–	MAX. 0.72 MIN. 0.34	–	MINOR / MAJOR LINE DAMAGE	NORMAL DEPLOYMENT / POINT FAILED LONG SEC. AFTER DEPLOYMENT	NORMAL
115 (10.82)	99	1214	1204	1589	1573	0.257	–	0.093	12,300	46,600	–	–	–	–	0.90	1.07	NONE / SLIGHT LINE DAMAGE AT KEEPER 4T TACH.	NORMAL DEPLOYMENT / INFLATION, DEFLATION, SLIGHT OSCILLATION FIRST SECOND	SLED CAMERA MALFUNCTION
		1210		1589		0.296		0.084	14,800							1.08		DOUBLE SNATCH FORCE	NO TIMING LIGHTS
191 (10.47)	23	APPROX. 300 M.P.H.	–	–	–	–	–	0.46	–	30,000	90.0	–	–	–	–	–	NONE	NORMAL DEPLOYMENT / FAULTY SEVERANCE DEVICE	NORMAL
	24	APPROX. 200 MPH	–	–	–	–	–	–	–	–	–	–	–	–	–	–	NONE	LOW VELOCITY / PANIC KNIFE SHUT DOWN	NORMAL
122 (23.10)	27	APPROX. 650 MPH	–	–	–	–	–	–	54,000	–	–	–	–	–	–	–	MINOR DAMAGE / 3 STEEL CABLE RISERS SEVERED	PREMATURE INFLATION PRIOR TO F_o	NORMAL
	28	1189	1181	1466	1400	0.328	0.088	0.088	42,850	36,000	96.0	96.3	2.3	4.0	0.47	X_o = 1.11 X_o = 0.98	NONE	PREMATURE INFLATION PRIOR TO F_o	NORMAL
	29	1193	1146	1484	1360	0.360	0.142	0.149	12,400	40,800	96.9	96.4	1.9	3.2	0.84	0.64	NONE	NORMAL DEPLOYMENT / SLIGHT BREATHING	NORMAL
	34	1110	1070	1279	1186	0.330	0.150	0.190	17,300	41,000	107.2	101.4	3.9	9.0	0.82	1.11	NONE	NORMAL	NORMAL
	36	1119	1098	1316	1258	0.367	0.103	0.086	19,700	46,850	110.9	106.3	4.2	7.3	0.64	1.00	NONE	NORMAL	NORMAL
123 (23.10)	35	APPROX 650 MPH	–	–	–	–	–	–	–	–	–	–	–	–	–	–	NONE	NO DEPLOYMENT / PILOT CHUT SEVERED	NORMAL
	36	1227	1180	1561	1444	0.290	0.140	0.140	12,800	43,900	108.0	105.0	5.0	6.3	0.48	1.08	MINOR / MINOR LINE DAMAGE	NORMAL	NORMAL
	37	1080	1060	1239	1194	0.340	0.078	0.078	15,450	41,600	112.9	107.6	4.9	7.2	0.86	1.08	NONE	NORMAL	NORMAL
124–17 (21.15)	38	1212	1183	1607	1551	0.246	–	0.134	11,000	46,250	–	–	–	–	0.84	0.93	NONE / MINOR LINE DAMAGE	NORMAL	SLED CAMERA MALFUNCTION
	41	1205	1172	1607	1525	0.280	0.90	0.08	12,300	46,000	108.4	–	–	–	0.81	0.98	NONE / MINOR LINE DAMAGE	NORMAL	NORMAL
	42	1216	1182	1664	1567	0.280	0.120	0.100	12,100	43,400	98.3	96.2	9.2	3.9	0.92	0.89	MINOR DAMAGE	NORMAL	NORMAL
124–10 (21.15)	48	APPROX 150 MPH	–	–	–	–	–	–	–	–	–	–	–	–	–	–	–	NO DEPLOYMENT / AUTOMATIC SHUT–DOWN	NORMAL
	53	1173	1086	1016	1331	0.150	0.210	0.180	16,900	38,900	107.0	101.5	3.7	7.9	0.35	0.60	NONE	NORMAL	NORMAL
	99	923	904	912	875	0.230	0.128	0.128	10,950	28,900	104.0	101.9	3.3	3.7	0.85	1.06	NONE	NORMAL	NORMAL
123 (23.25)	45	1211	1137	1646	1603	0.256	0.184	0.144	19,700	39,700	39.0	98.4	5.7	7.2	0.43	1.06	NONE / MINOR LINE DAMAGE	NORMAL	NORMAL
	44	APPROX 199	–	–	–	–	–	–	–	–	–	–	–	–	–	–	–	NO DEPLOYMENT / AUTOMATIC SHUT–DOWN	NORMAL
	50	1174	1119	1498	1348	0.202	0.138	0.168	18,380	38,100	104.9	102.0	4.0	3.9	0.81	0.99	MINOR DAMAGE TO TWO VENT RIBBONS	NORMAL	NORMAL
126 (23.30)	46	APPROX. 297	–	–	–	–	–	–	–	–	–	–	–	–	–	–	–	NO DEPLOYMENT / AUTOMATIC SHUT DOWN	NORMAL
	47	1067	1002	1241	1119	0.036	0.174	0.204	13,980	36,300	97.3	94.9	2.3	3.9	0.49	0.98	NONE	NORMAL	NORMAL
	51	1213	1144	1510	1432	–	0.187	0.187	17,300	40,360	97.3	39.0	1.9	3.3	0.41	0.87	MINOR DAMAGE TO SEVERAL VENT RIBBONS	NORMAL	NORMAL

shock factor would drop to 1.09, a value more consistent with the maximum range expected for this type of parachute. Table 15 shows the

TABLE 15

PERFORMANCE CHARACTERISTICS OF FIST TYPE 107 PARACHUTE

RUN NO.	V_S	t_f	C_D	X	D_{p_t} / D_p AVERAGE	R mean	R max.
7	661	—	0.54	1.45	—	—	—
12	846	0.084	0.62	1.00	99.4	12.4	13.9
13	952	0.12	0.56	1.19	100.6	13.2	15.1
AVERAGE		0.102	0.57	1.21	100.0	12.8	14.5

average performance characteristics of the Type 107 parachute as determined from these tests.

In considering the stability of these parachutes, it will be noticed that there was excessive angular displacement in the tests analyzed, with the magnitude of the mean value approaching that of the maximum value. This relationship of maximum and mean values is significant since it indicates that the instability of the parachute was primarily due to drift rather than large amplitude oscillation. It can be seen from Fig. 28, that if a mean displacement is considered the actual oscillatory instability is on the order of ± 2 degrees maximum. It is also evident that the displacement due to drift increases slightly as velocity decreases, but this is a normal function of the test attitude. The test parachutes on both test run Nos. 12 and 13 exhibited slight flutter in some skirt ribbons at the higher velocities and settled in a low position during steady state operation. In the same test the average diameter ratio was 100% and the maximum was 104.9%, which indicates that inflations were full and essentially constant throughout the tests.

Because of the poor stability and inconsistent inflation characteristics of parachutes of this porosity range (Types 107, 107A and 107B, λ_g = approximately 14%) it was decided to design and test parachutes of higher porosity with a much narrower spacing between vertical ribbons to provide better control over the opening process.

2. FIST Ribbon Type 107A (λ_g = 12.86%)

This parachute was a 15 panel version of the normal 16 panel Type 107 FIST Ribbon parachute. Removal of the one panel altered the configuration to a 20 degree conical parachute of slightly smaller diameter and removed the parachute from the flat circular design category normally associated with FIST types.

Only one test (No. 14) was conducted with this parachute, and useful test data were obtained for only 0.65 second of operation due to accidental detachment of the test parachute.

At time of maximum force the parachute had attained a maximum inflated diameter of approximately 116% of the design projected diameter. The steady state drag coefficient, though not determined throughout the normal time interval, was 0.59 at the high velocity end of the test. The dynamic pressure decreased 120 psf (from 868 to 748 psf) and the corresponding velocity decrease over the short time interval involved was approximately 65 fps. The opening shock factor, based on the limited steady state information available, was 1.07.

Performance summary data for the parachute tested are graphically illustrated in the diameter and force curves in Fig. 28.

It was intended that additional tests would be made with this parachute but results of tests of parachutes in the same relative porosity region indicated that the porosity of this parachute was too low for further consideration. Consequently, the parachute was dropped from the test program.

Later tests, conducted with a Type 125 Conical FIST Ribbon parachute, are reported in Section 9 of this appendix.

3. FIST Ribbon Type 107B (λ_g = 14.37%)

This parachute was a redesigned version of the original Type 107 parachute, in which the vent was enlarged so that 1% of the total geometric porosity could be maintained after the vent lines were installed across the vent. The original model had a 1% vent area before addition of the vent lines. In order to maintain approximately the original porosity in the new design, the parachute was made slightly smaller with fewer horizontal ribbons and greater horizontal ribbon spacing.

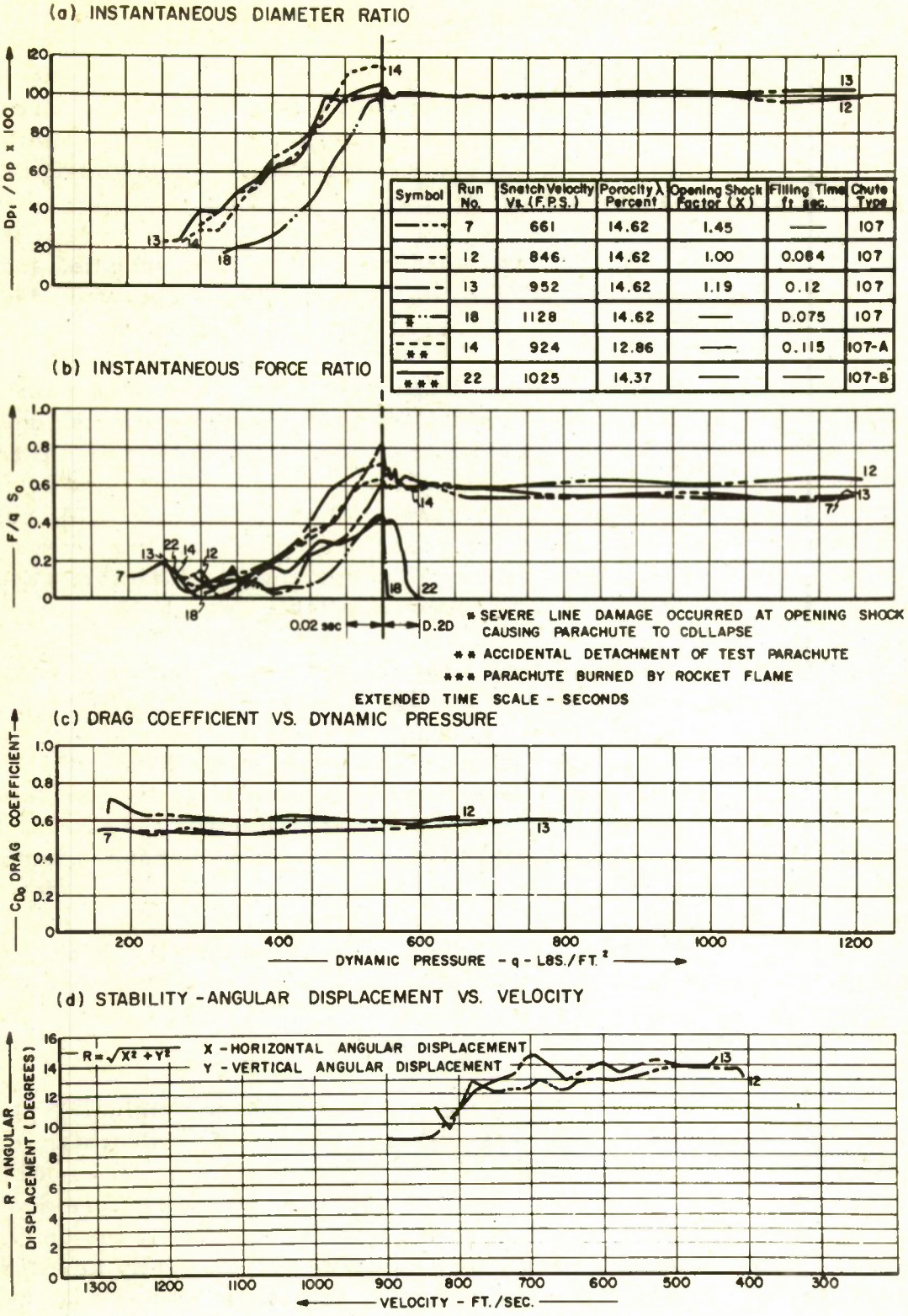

Symbol	Run No.	Snatch Velocity Vs (F.P.S.)	Porocity λ Percent	Opening Shock Factor (X)	Filling Time ft sec.	Chute Type
———	7	661	14.62	1.45	——	107
—— --	12	846	14.62	1.00	0.084	107
—— -	13	952	14.62	1.19	0.12	107
—·— *	18	1128	14.62	——	D.075	107
- - - - **	14	924	12.86	——	0.115	107-A
——— ***	22	1025	14.37	——	——	107-B

Figure 28 Summary Data - FIST Ribbon Parachute Type 107, 107A, and 107B

A normal deployment was accomplished at 700 mph, on test run No. 22, but due to a malfunction of the rocket engine main propellant valve, the injector and chamber burned through. Flame from the burned out engine reached the deployed parachute and lines and caused the parachute to collapse in rapid progression. The instantaneous force ratio during inflation is shown in Fig. 28. Since the cameras were damaged by flame on this test, inflation and stability data are not available.

Subsequent tests of other parachute types suggested that a higher porosity range was more desirable than that used on this parachute. Consequently, the FIST Ribbon Type 107B was dropped from the test program.

4. FIST Ribbon Type 118 (λ_g = 18.22%)

The Type 118 FIST Ribbon parachute was a 6.57 foot diameter special purpose design which originated as a first stage deceleration parachute for a supersonic missile. It was the only parachute tested in the program which did not approximate the 28 sq ft drag area classification of the other test parachutes. Since it was primarily important to proof-test the parachute structurally, only two tests were conducted, both at transonic velocities near Mach 1.0. On test run No. 16 the pack bridles connecting the pilot parachute to the pack were torn off when deployment was initiated at 762 mph. Consequently, no performance or structural data were obtained from this test. On test run No. 21, a successful deployment at 770 mph was initiated. Deployment and inflation were apparently normal with the inflation curve peaking 0.098 second after snatch force. The initial peak of the force curve followed this by 0.01 second. After this, however, a phenomena occurred which had not been observed in tests up to this time. A high amplitude force oscillation at a frequency of approximately 45 cps was initiated concurrent with a 20% diameter fluctuation at the same rate. High-speed photographic coverage shows that the riser and parachute line system was flexing, while the parachute itself was inflating and deflating at exactly the same cyclic rate, but out of phase with the load fluctuation. This situation continued for approximately 3/4 second of operation, after which seven suspension lines failed causing collapse of the parachute. At time of failure the primary load fluctuation had decreased to approximately 40 cps, but there was no apparent decrease in the average amplitude of the maximum and minimum force values.

Due to the nature of the masses of the independent parachute and line system, it is difficult to conduct an accurate frequency analysis.

The recorded data, however, did provide information which indicated that the interaction of the natural frequencies of the two systems would produce results similar to those encountered in this test. Similarly, it indicated that the ratio of the load fluctuation to that of the area fluctuation was such that the coincidence of the natural frequencies by the systems in this test was probable. If this is the case then, it follows that great care should be exercised in the design of a parachute system, to avoid incorporating a parachute having a breathing frequency equal to the elastic frequency of the lines in the velocity range where reliable operation is essential.

Performance curves illustrating the fluctuating force, drag and diameter relationships are shown in Fig. 29.

5. FIST Ribbon Type 119 (λ_g = 18.85%)

The FIST Ribbon Type 119 was the first parachute designed for testing in this program, which incorporated the heavy 2 inch x 1700 pound T.S. nylon horizontal ribbon material and 1 inch x 12,000 pound T.S. nylon suspension lines and risers.

Only one test (No. 25) was conducted with this parachute, and in that test two snatch forces were prevalent. The first occurred 0.257 second after deployment was initiated, and the second one occurred at 0.286 second. Deployment velocity, referred to the first snatch force, was 830 mph. The photographic sequence in Fig. 30 shows the deployment process of this parachute on test run No. 25.

Operational characteristics, similar to that observed for the Type 118, prevailed in the initial stages of the test. Immediately after deployment, a frequency of oscillation of approximately 40 cps combined with rapid inflation and deflation occurred. The combined oscilliatory motion rapidly decreased until it had completely damped out after approximately 1 second of operation. This indicates that the parachute design was borderline from the standpoint of separating the natural frequency of the breathing canopy from the natural frequency of the connecting lines, at the velocity at which it was operated. Obviously, the two frequencies were separated enough to allow damping, and transition into a steady state operation. If the deployment velocity had been higher, it is possible that the parachute would have destroyed itself before sufficient damping could take place.

The steady state drag coefficient averaged 0.50 and the opening

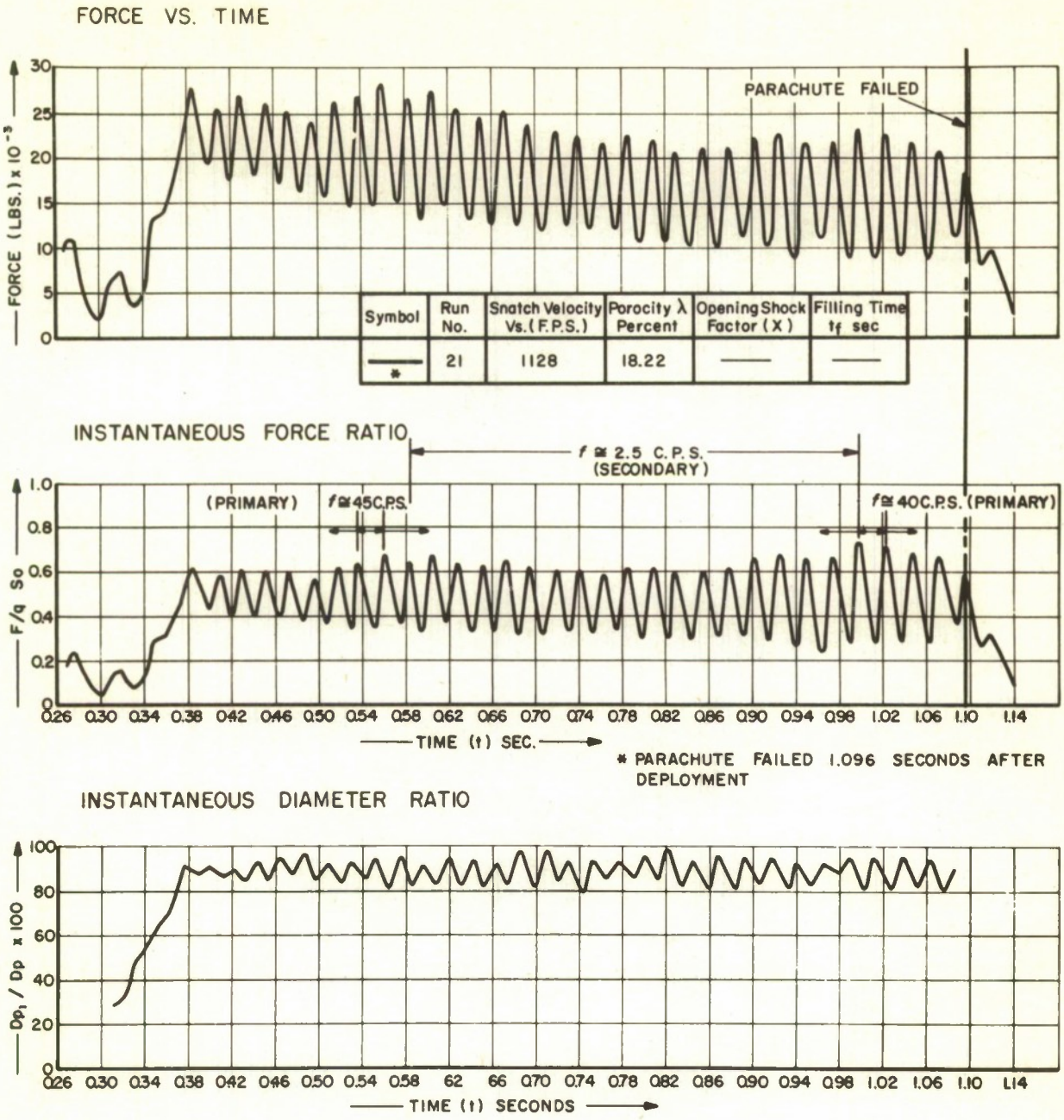

Figure 29 Summary Data - FIST Ribbon Parachute Type 118

shock factor was 1.07, referred to the velocity at the first snatch force. Curves showing the steady state drag force and the instantaneous force ratio are plotted in Fig. 31.

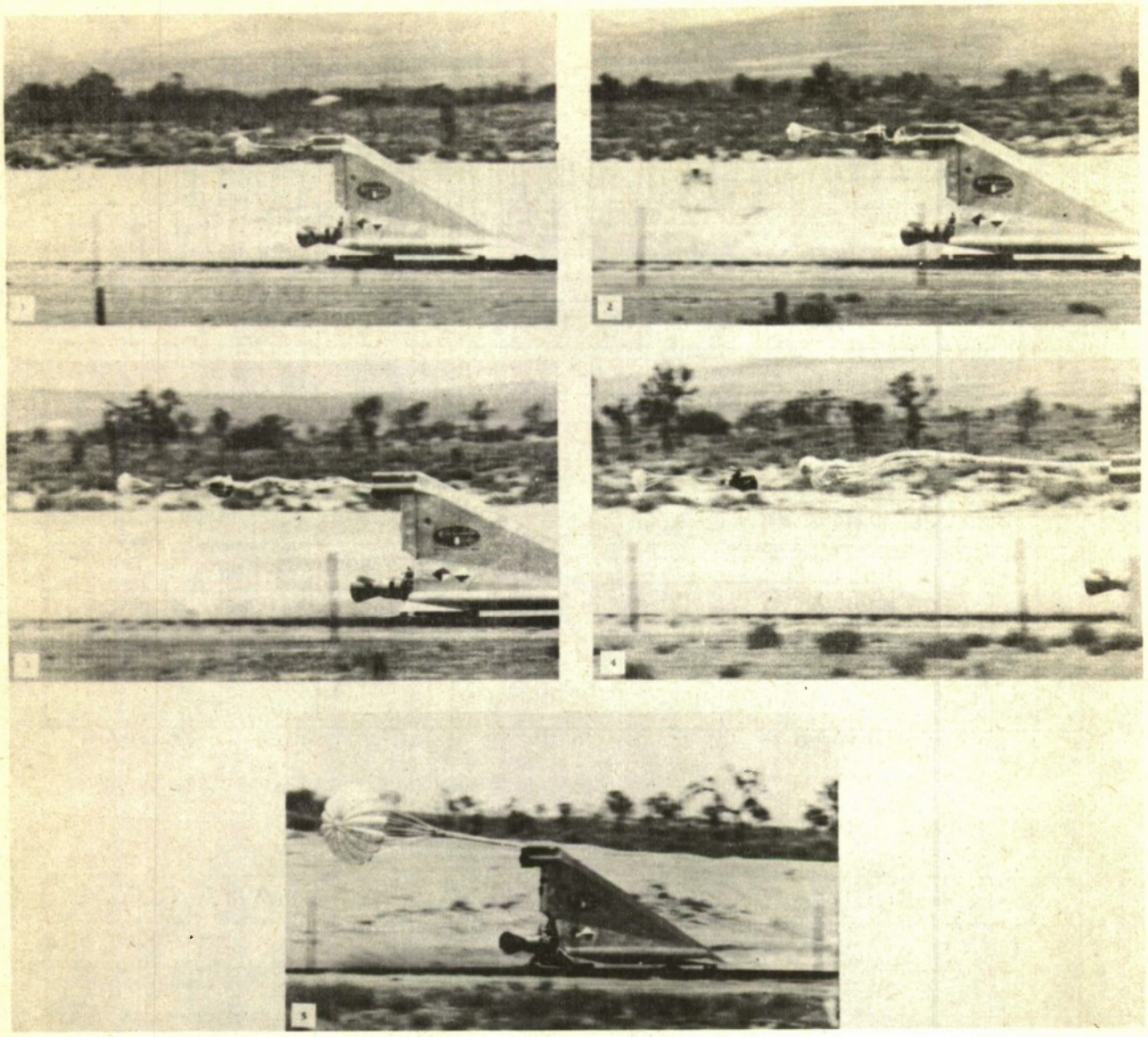

Figure 30 Deployment Sequence - FIST Ribbon Parachute Type 119

Due to the borderline operation of this parachute, no further tests were made with this type.

6. FIST Ribbon Type 121 (λ_g = 18.47%)

The FIST Ribbon Type 121 was originally designed as a first stage supersonic missile deceleration parachute. Since the 8.32 foot diameter of the parachute brought the size close to the approximate 28 sq ft

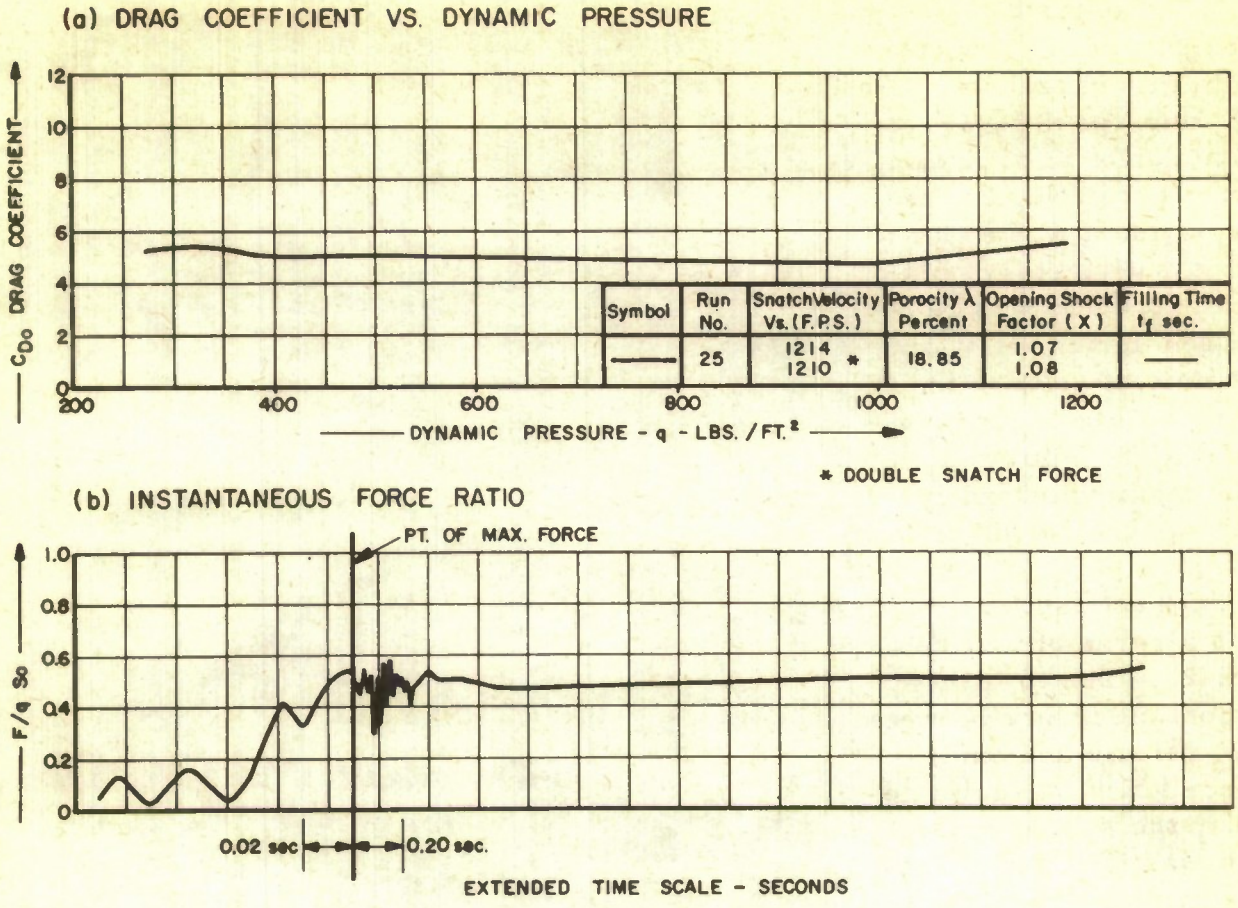

Figure 31 Summary Data - FIST Ribbon Parachute Type 119

drag area classification required for test parachutes in this program, the FIST Ribbon Type 121 was incorporated for structural and performance tests.

Due to the operational requirements of this parachute, extremely heavy construction was utilized in its design. In order to decrease the total load on individual components of the parachute, 24 panels were used instead of the usual 16 used on most test parachutes in the program. Ribbon material was the heavy duty 2 inch x 1700 pound nylon, and suspension lines were fabricated from 1 inch x 12,000 pound T.S. nylon webbing and were 17.0 feet long instead of the normal one diameter length.

Two tests, Nos. 23 and 24, were conducted with this parachute, both of them resulting in incomplete information. On test run No. 23 the deployment was apparently satisfactory, but the parachute was released during inflation. At time of release the parachute was approximately 80% inflated. The maximum load recorded was 30,000 pounds.

Test run No. 24 was a rerun of test run No. 23. Due to insufficient clearance between test vehicle and emergency track shutdown device, the shutdown circuit was initiated. This resulted in a maximum test vehicle velocity of only 200 mph. A normal deployment was initiated, but due to the extremely low velocity the resulting test information was not usable. The photograph in Fig. 32 shows the unusual configuration of the FIST Ribbon Type 121 in operation in test run No. 24.

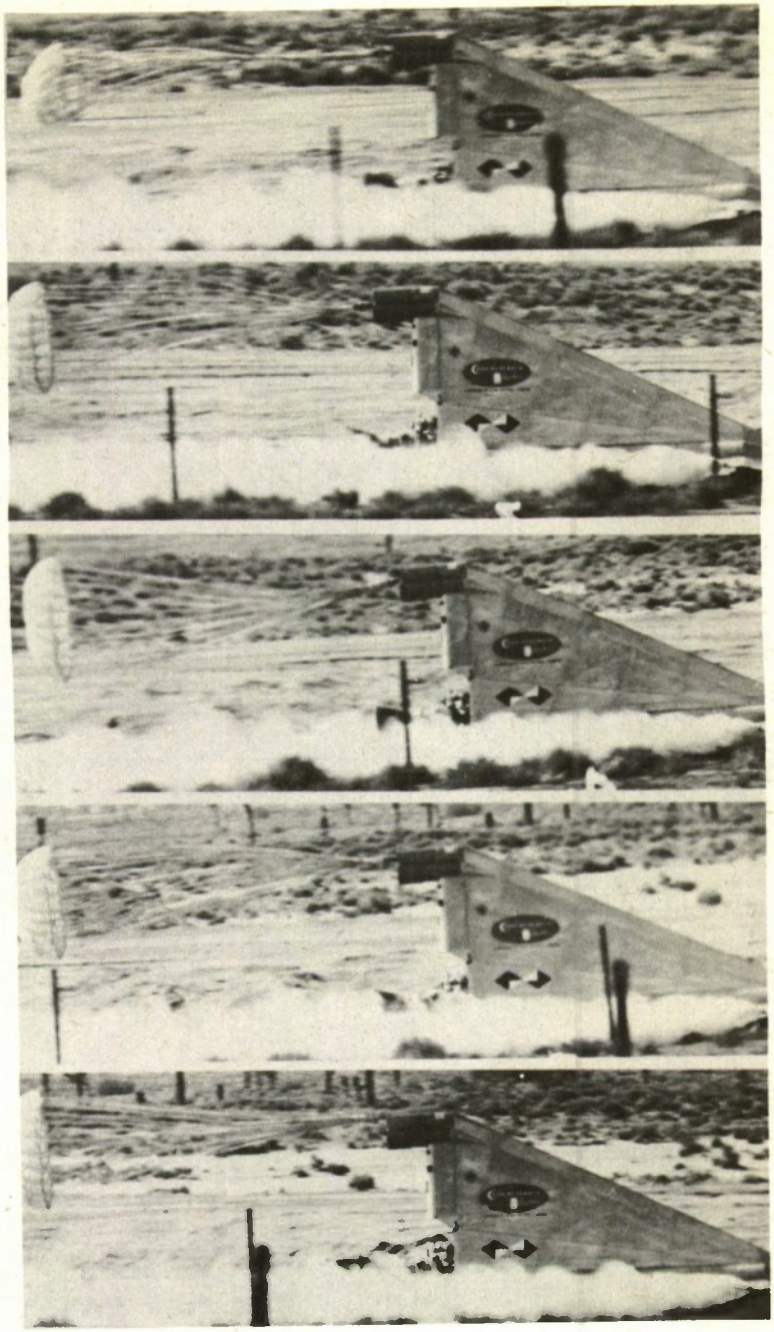

Figure 32 Deployment Sequence - FIST Ribbon Parachute Type 121

7. FIST Ribbon Type 122 and 123 (λ_g = 23.10%)

The only difference between the FIST Ribbon Type 122 and Type 123 was in the material used for suspension lines. The Type 122 was originally fabricated with 1 inch x 12,000 pound T.S. nylon suspension lines. When there was no indication, after several tests, that line damage would occur, a lighter 1 inch x 6000 pound T.S. nylon suspension line was substituted. The parachute types had identical geometric porosities of 23.10%, the highest that had been tested to date.

Since the parachutes are basically the same, they will be considered here in one group. Performance summary curves for the two types in the group are shown in Fig. 33.

Altogether eight tests were conducted; five (27, 28, 29, 34, 36) with the Type 122, and three (33, 35, 37) with the Type 123. Of the five tests conducted with the Type 122 parachute, four yielded complete data throughout the test period. One test, No. 27, which utilized eight steel cables as risers, severed all eight cables at snatch force when deployed at 830 mph. Partial inflation prior to snatch force resulted when mass of steel cables pulled the parachute out of the bag.

Of the three tests conducted with the Type 123 parachute, two of the tests yielded complete data throughout the recorded test period. The third test, No. 33, was invalid when severance of the pilot parachute caused test parachute to remain in the compartment instead of deploying.

Two of the tests which yielded complete performance data, Nos. 36 and 37, had extra long (16.85 foot) suspension lines. This is almost double the L_s/D ratio normally used for design of FIST Ribbon parachutes, and was done to compare the performance characteristics of the two line length configurations. A summary of the average characteristics of the two line length configuration groups of Type 122 and 123 parachutes is tabulated in Table 16. In the information shown in Table 16, the opening shock factor from test run No. 28 was not included in the average since premature inflation of the test parachute caused the snatch force to exceed the normal opening shock force.

Although average performance figures could be given for the entire series of tests, it would be misleading to imply that similar operational characteristics resulted in both line configuration groups. Distinct performance trends characterized each configuration, particularly

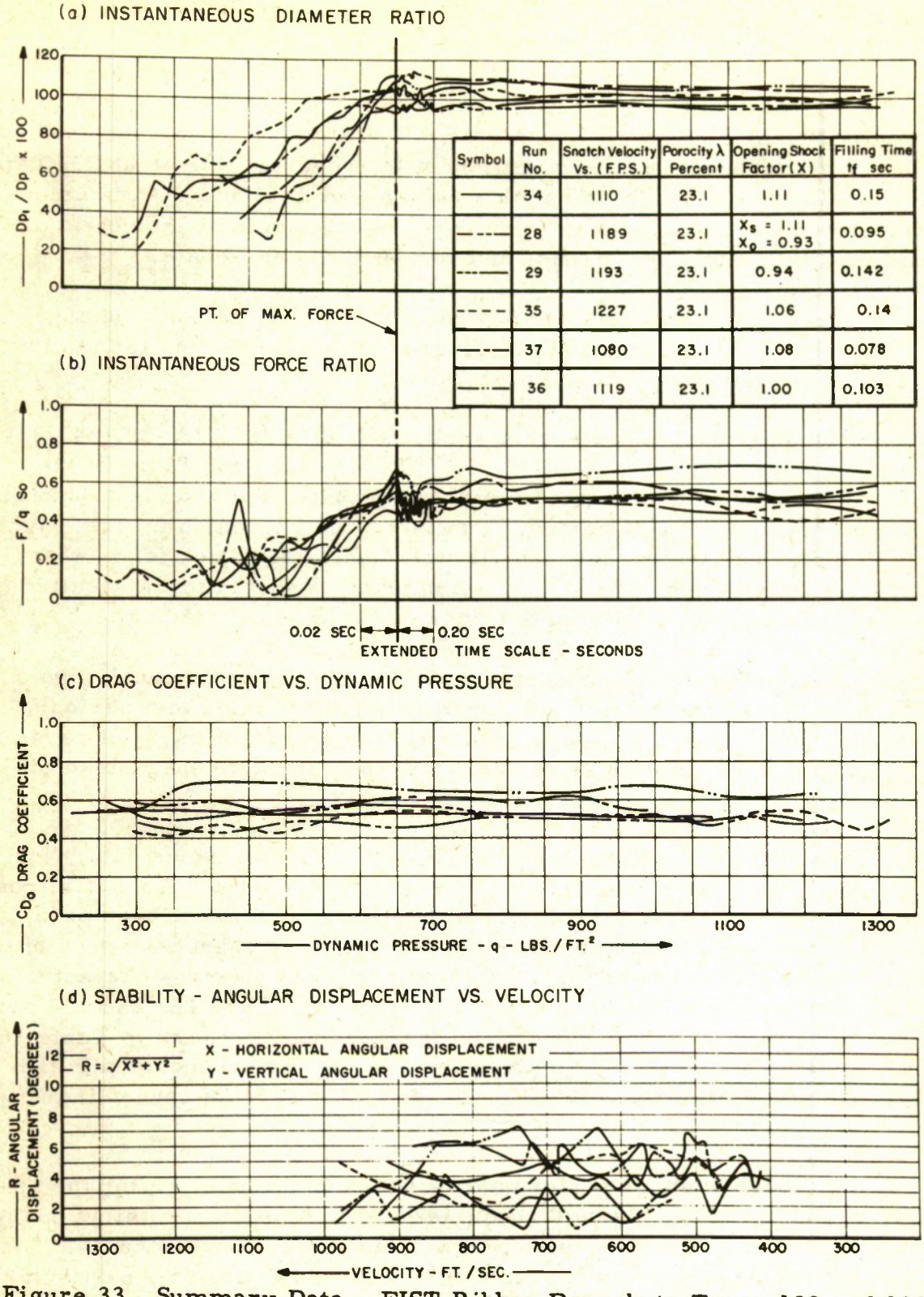

Symbol	Run No.	Snatch Velocity Vs. (F.P.S.)	Porocity λ Percent	Opening Shock Factor (X)	Filling Time tf sec
———	34	1110	23.1	1.11	0.15
– – –	28	1189	23.1	X_s = 1.11 X_o = 0.93	0.095
———	29	1193	23.1	0.94	0.142
– – – –	35	1227	23.1	1.06	0.14
—– —–	37	1080	23.1	1.08	0.078
—··—	36	1119	23.1	1.00	0.103

Figure 33 Summary Data - FIST Ribbon Parachute Types 122 and 123

TABLE 16

PERFORMANCE CHARACTERISTICS OF FIST TYPES
122 AND 123 PARACHUTES

$L_s/D = 1$

RUN NO.	V_S	t_f	C_D	X	D_{p_1}/D_p AVERAGE	$\bar{R}$ mean	max.
28	1189	0.095	0.47	—	96.78	2.26	4.0
29	1193	0.142	0.54	0.94	96.41	1.51	3.2
34	1110	0.150	0.52	1.11	1.39	3.52	4.96
35	1227	0.140	0.48	1.06	3.04	4.96	6.30
AVERAGE		0.132	0.50	1.04	99.4	3.1	4.6

$L_s/D = 2$

RUN NO.	V_S	t_f	C_D	X	D_{p_1}/D_p AVERAGE	$\bar{R}$ mean	max.
36	1119	0.103	0.64	1.00	6.76	4.22	7.28
37	1080	0.078	0.56	1.08	107.56	4.93	7.20
AVERAGE		0.090	0.60	1.04	107.2	4.6	7.20

AVERAGE-ALL TESTS TYPE 122-123 PARACHUTE	0.118	0.54	1.04	102.0	3.6	5.5

in the drag, inflation, and stability of the parachutes as a group.

As the table shows, the only parameter which was identical for both groups as well as for the average of all tests, was the opening shock factor (X) which averaged 1.04. The drag coefficient for the whole series averaged 0.54, but investigation by groups showed that the

short line group average 0.50 against 0.60 for the long line group. This is understandable when the inflation characteristics of the groups are analyzed. In steady state operation the short line group inflated to an average of 99.5% of the designed projected diameter, while the long line group inflated to an average of 107.2% of the designed projected diameter. Based on drag area this is an increase of approximately 16% for the long line parachute, and fairly consistent with the average rise in drag coefficient. The short line parachutes exhibited considerably less angular displacement than the parachutes with the longer lines. The mean angular displacement of the short line parachutes was 3.1 degrees while the corresponding displacement for the long line parachutes was 4.6 degrees. Maximum angular displacements were 4.6 degrees and 7.2, respectively. The difference here becomes more apparent when the average oscillatory variation from the mean is considered. It can be seen in the table that this variation is only ± 1.5 degrees for the short line parachutes while the corresponding average variation for the long line parachutes is ± 2.6 degrees.

The photographs in Fig. 34 and 35 show the deployment sequence and inflation process of the FIST Ribbon Type 123 parachute, which had an Ls/D ratio of one on test run No. 35. Figures 36 and 37 show the deployment sequence and inflation process of the FIST Ribbon Type 122 parachute, which had an Ls/D ratio of two, on test run No. 36.

8. FIST Ribbon Type 124 ($\lambda_g = 21.15\%$)

In the FIST Ribbon Type 124 parachute category, there were actually two distinct parachute types that were tested in the program. In order to identify them independently, a dash number signifying the modification, was added to the type number. The original parachute that was tested therefore became a 124-17 signifying a Type 124 parachute with 1700 pound T.S. horizontal ribbon material, while the later parachute was given No. 124-10 indicating a modification to 1000 pound T.S. horizontal ribbon material.

Six parachute test runs were conducted with the FIST Ribbon Type 124, three tests each with the 124-17 and 124-10. All three of the tests made with the Type 124-17 (38, 41, 42) were at deployment velocities above Mach 1 and produced quite consistent performance data. Of the three tests made with the Type 124-10, two of them, Nos. 53 and 59, yielded satisfactory, though varying data when deployed at 800 and 629 mph, respectively, In the remaining test in this group (No. 48), the test parachute was not deployed.

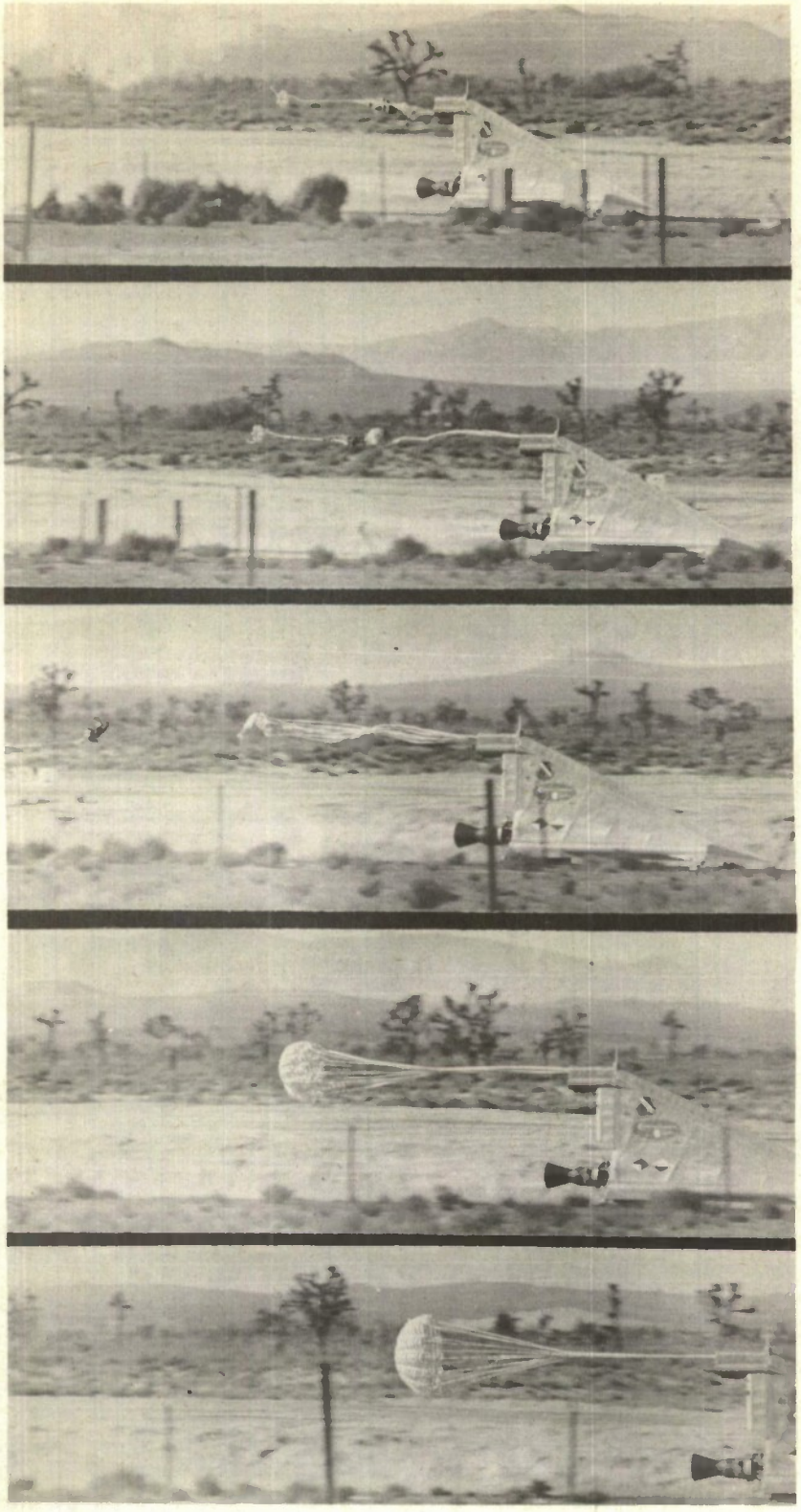

Figure 34 Deployment Sequence - FIST Ribbon Parachute Type 123 ($L_s/D_o = 1$)

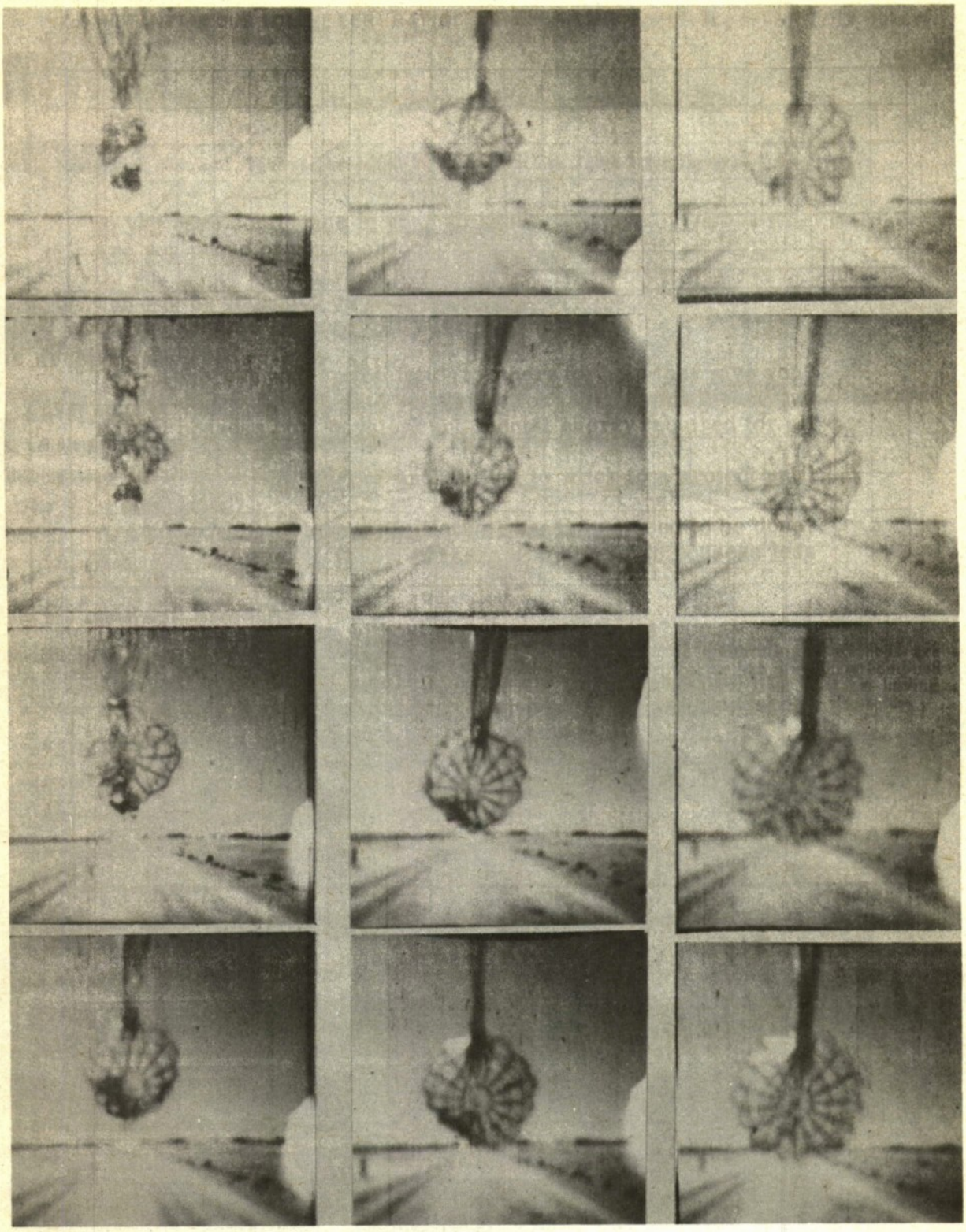

Figure 35 Inflation Sequence - FIST Ribbon Parachute Type 123 ($L_s/D_o = 1$)

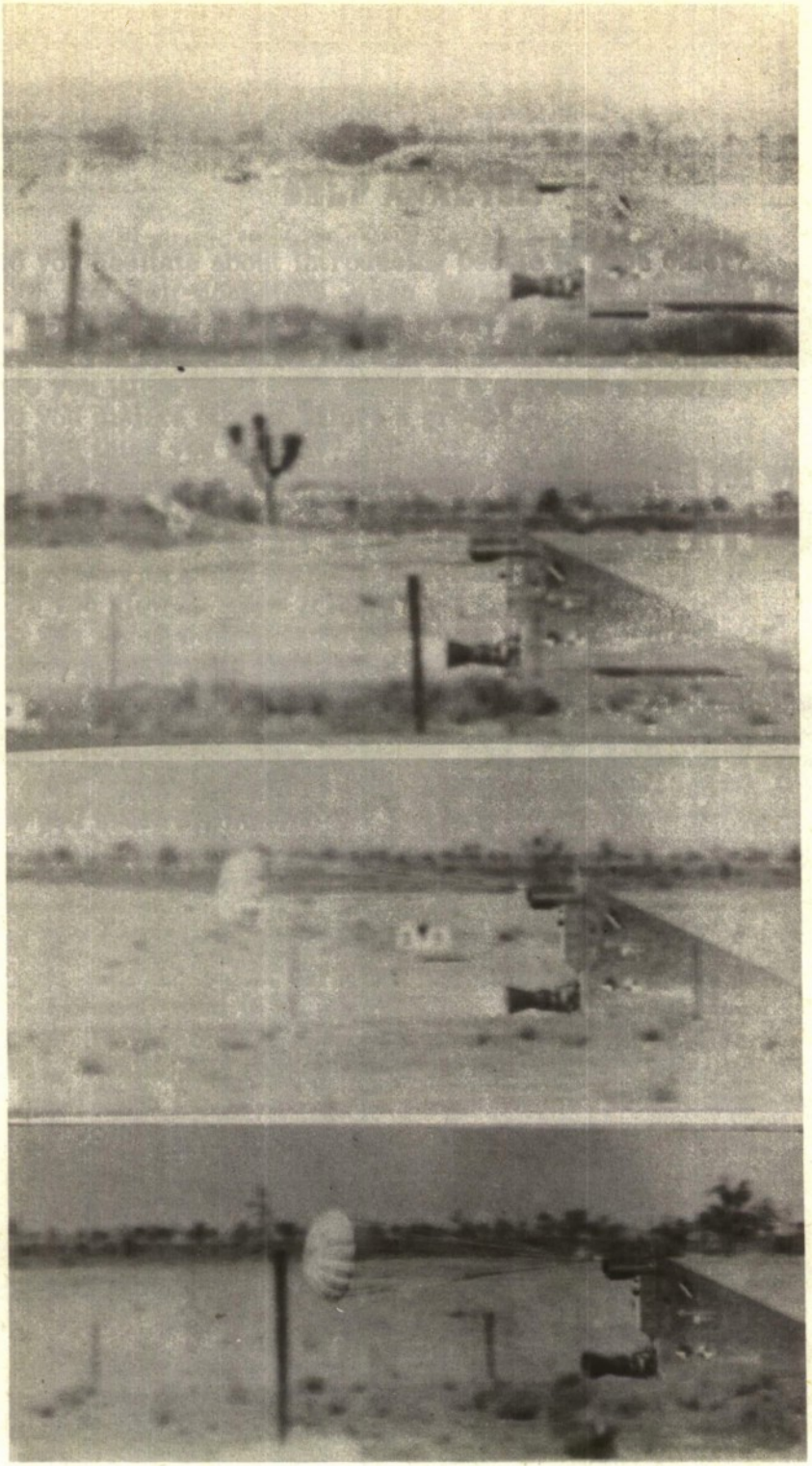

Figure 36 Deployment Sequence - FIST Ribbon Parachute Type 122 ($L_S/D_O = 2$)

Figure 37 Inflation Sequence - FIST Ribbon Parachute Type 122 ($L_s/D_o = 2$)

A summary of the performance characteristics of the two Type 124 configurations is graphically illustrated in the performance curves in Figs. 38 and 39. Average characteristics of the two configurations, are summarized in Table 17.

As the curves and table show, the drag coefficient was essentially constant for all test runs in the FIST Ribbon Type 124 category. The opening shock factor (X) was fairly consistent in the 124-17 group, but separated widely on the two tests made with the 124-10. With the exception of test run No. 53, the one test which had a significantly long filling time, the average opening shock factor of each group was within approximately 5% of the average of all tests made. The photographic series in Fig. 40, shows the opening process of the FIST Ribbon Type 124-10 in test run No. 53.

Three of the tests in both groups yielded information from which a stability analysis could be made. If these are assumed to be average, it indicates that the Type 124-17 parachute was approximately 2-1/2 times as stable as the Type 124-10, both in actual displacement from the reference axis and oscillation about the mean position assumed by the parachute in operation. It is possible that some of this stability difference can be attributed to the variation in cloth permeability of the respective ribbon materials used in the parachutes. If the matter of weight and bulk is not critical, the Type 124-17 has a slight advantage over the Type 124-10. Not only does the 124-17 show slightly better performance characteristics, it has been structurally designed and tested for considerably higher deployment velocities than the Type 124-10.

Overall, the Type 124 FIST Ribbon parachute generally exhibited the most favorable characteristics of all of the FIST Ribbon parachutes tested in this program.

9. FIST Ribbon Type 125 (λ_g = 23.25%)

The FIST Ribbon Type 125 was a 25 degree conical parachute designed for the higher porosity region of this series of tests. Unlike the original Type 107A conical parachute, which was a 15 panel version of a 16 panel parachute, the Type 125 was designed with 16 panels.

Three tests were conducted with the Type 125 parachute. Two of the tests, Nos. 43 and 50, yielded complete performance data throughout the test. In test run No. 44, deployment was not initiated, consequently no data were acquired.

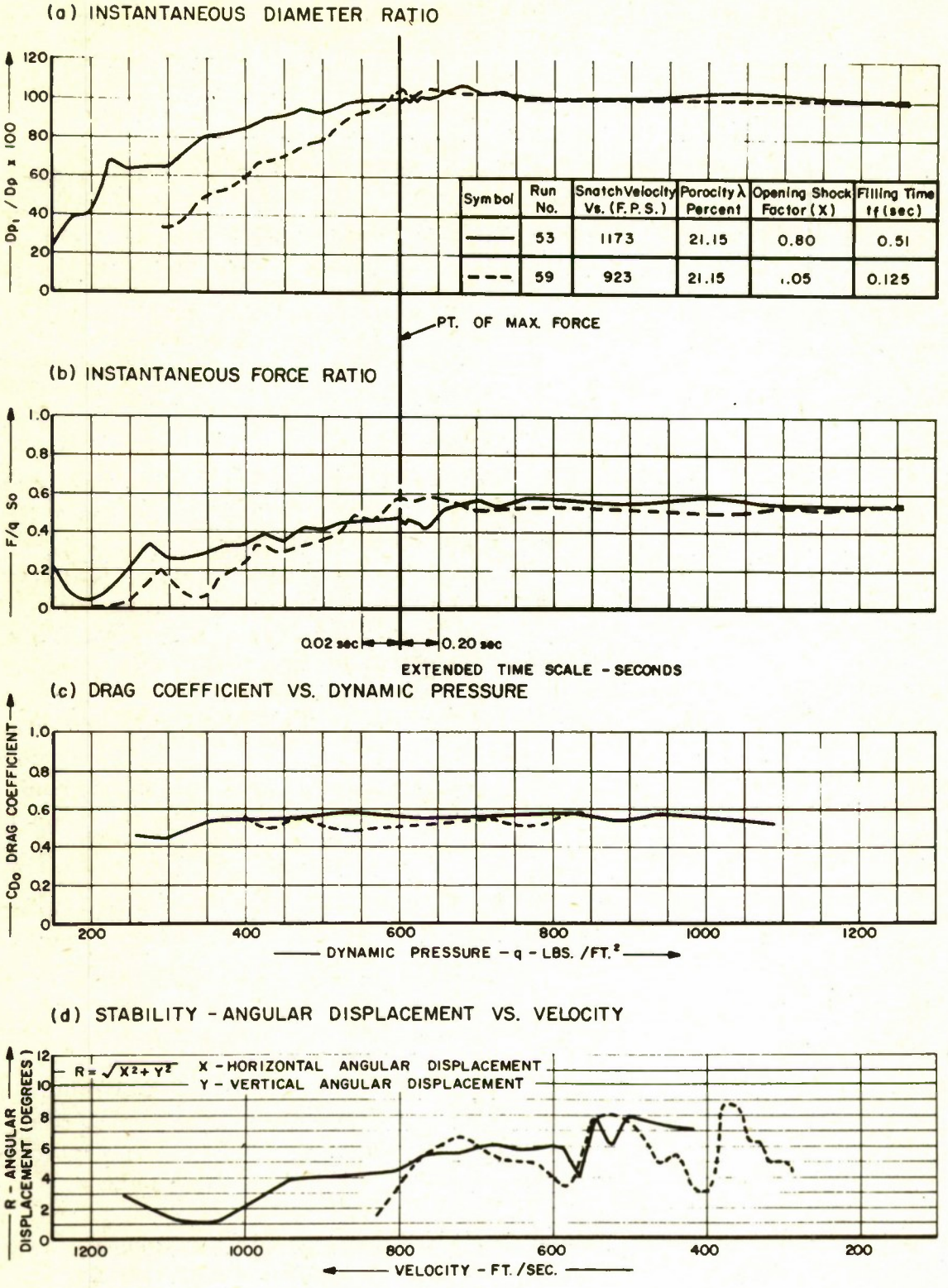

Figure 38 Summary Data - FIST Ribbon Parachute Type 124-10

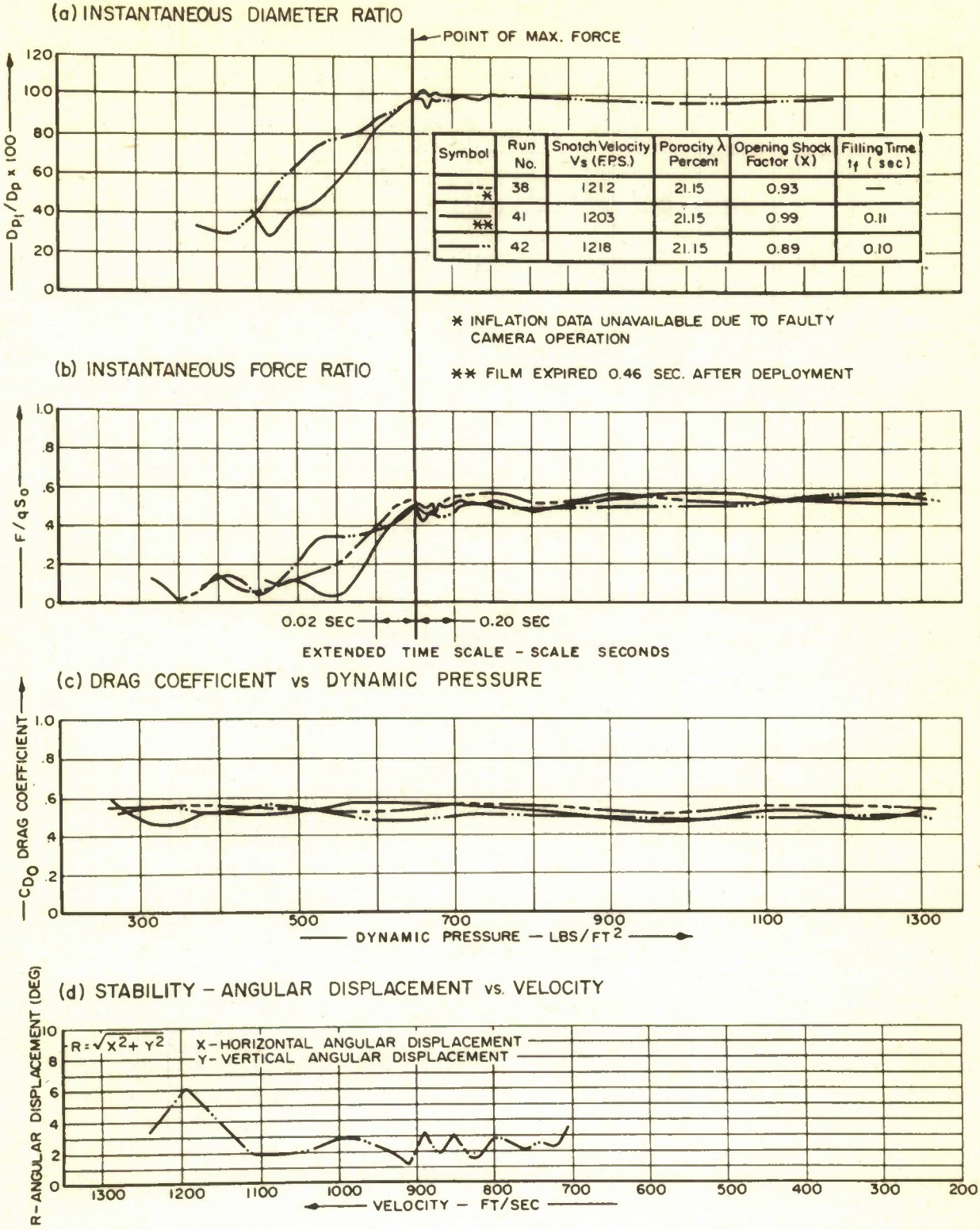

Figure 39 Summary Data - FIST Ribbon Parachute Type 124-17

TABLE 17

PERFORMANCE CHARACTERISTICS OF FIST TYPE 124 PARACHUTE

124-17

RUN NO.	V_S	t_f	C_D	X	D_{p_1}/D_p AVERAGE	R mean	R max.
41	1203	0.11	0.51	0.99	—	—	—
38	1212	—	0.54	0.93	—	—	—
42	1218	0.12	0.52	0.59	98.2	2.20	3.20
AVERAGE		—	0.52	0.94	98.2	2.20	3.20

124-10

59	923	0.125	0.53	1.05	101.9	5.66	7.80
53	1173	0.51*	0.53	0.80*	101.5	5.50	8.70
AVERAGE		—	0.53	1.05	101.7	5.58	8.25

AVERAGE - ALL TESTS TYPE 124 PARACHUTE	0.53	1.00	100.0	3.89	5.72

* NOT INCLUDED IN AVERAGE

The two tests, from which complete data were received, were made in approximately the same velocity region. Test run No. 43 was deployed at 826 mph and test run No. 50 was made at a deployment velocity of 801 mph. Performance curves for these two tests are shown in the graphs in Fig. 41. The average performance characteristics of the FIST Ribbon Type 125 parachute, as tested in this program, is given in Table 18.

The average drag coefficient of 0.48 was slightly below the general average for FIST Ribbon parachutes tested in this program.

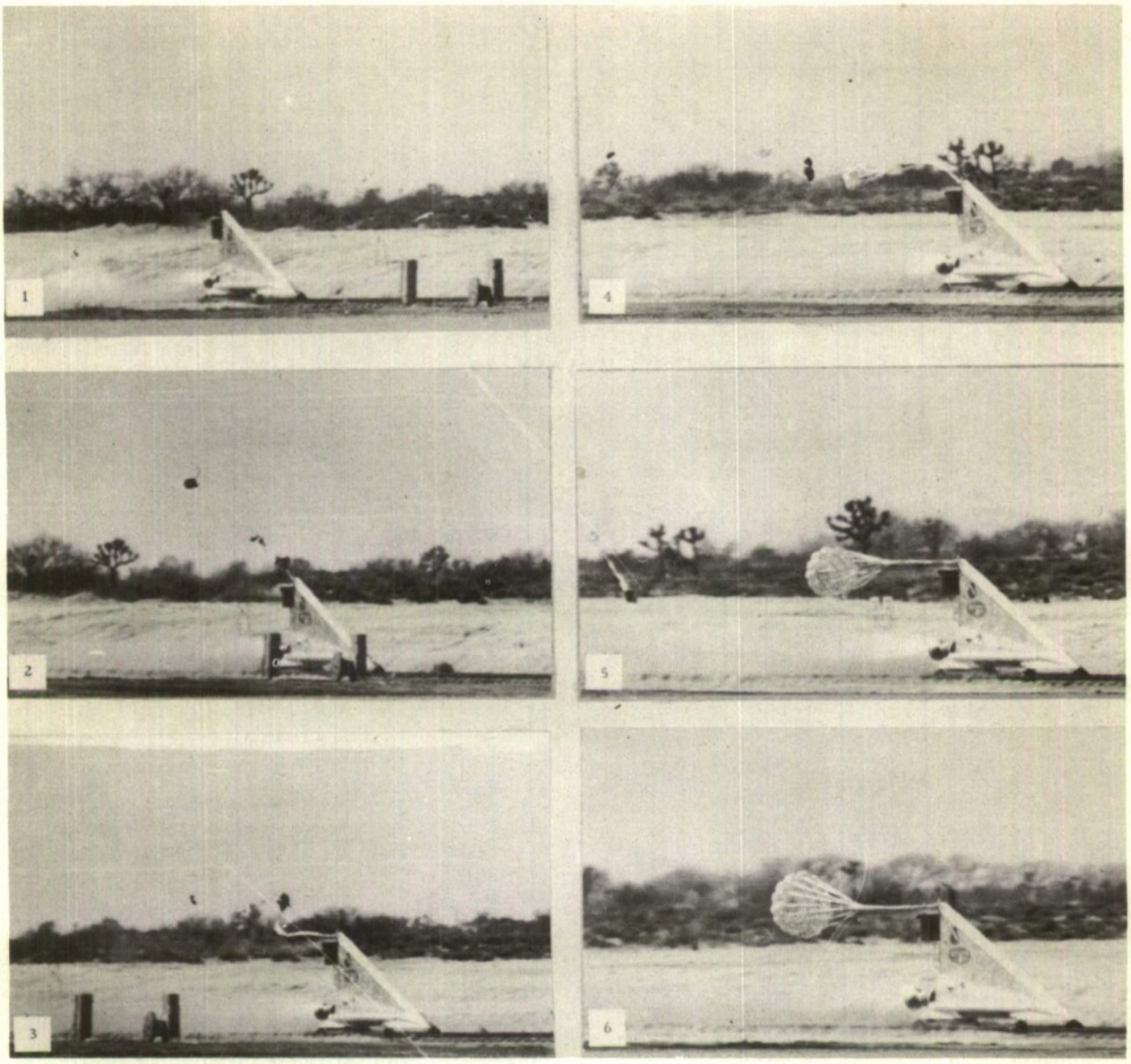

Figure 40 Deployment Sequence - FIST Ribbon Parachute Type 124-10

Inasmuch as the Conical FIST Ribbon Type 125 is a formed parachute and not a true FIST type, such comparison may not be entirely valid. However, since the program is of a comparative nature the difference in the basic parachute type should be taken into consideration in analyzing the results with respect to other types.

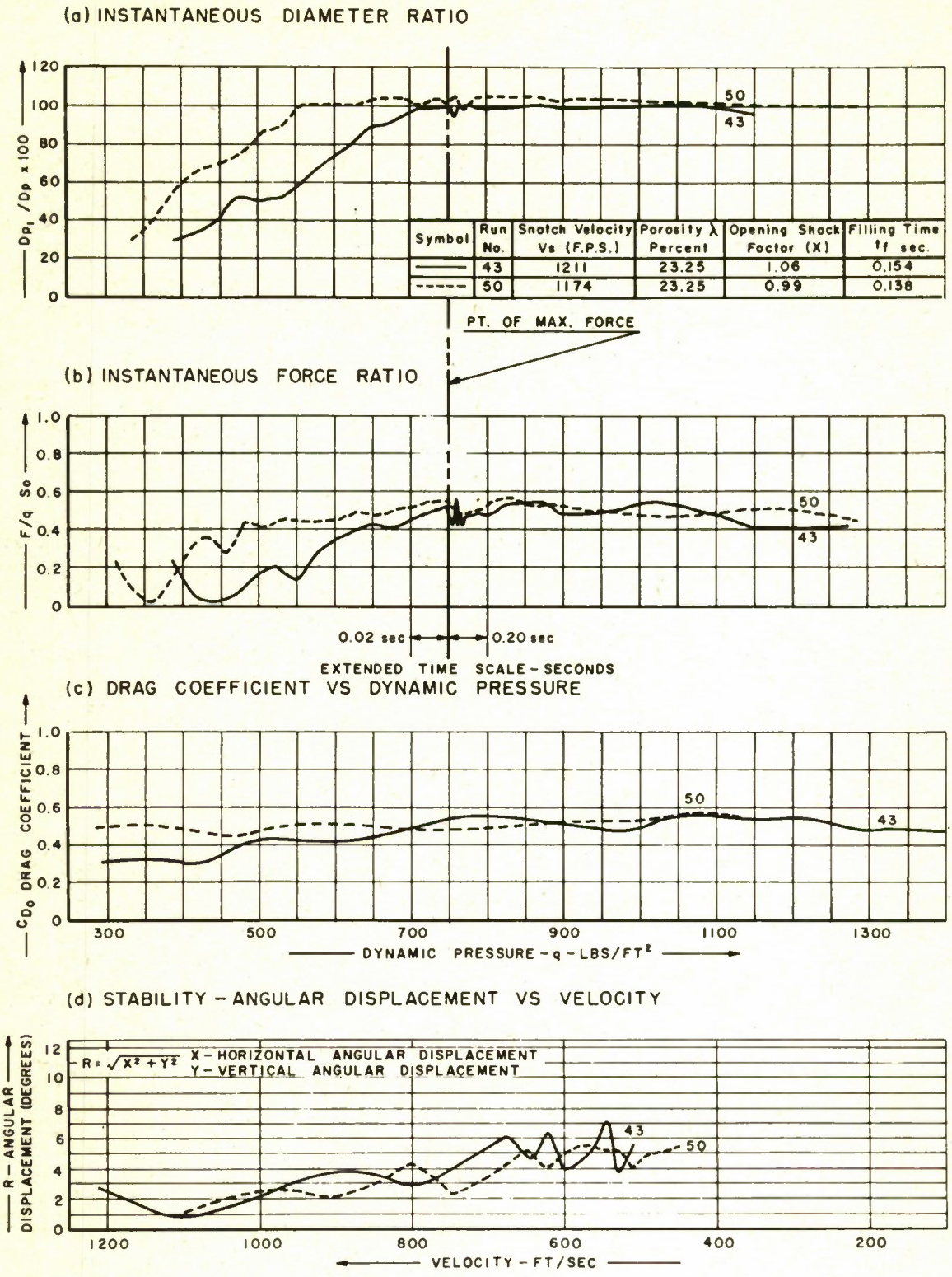

Figure 41 Summary Data - FIST Ribbon Parachute Type 125

TABLE 18

PERFORMANCE CHARACTERISTICS OF FIST TYPE 125 PARACHUTE

RUN NO.	V_S	t_f	C_D	X	D_{p_1} / D_p AVERAGE	R mean	R max.
50	1174	0.138	0.51	0.99	101.97	3.98	5.55
43	121	1.54	0.45	1.06	99.36	3.70	7.20
AVERAGE		0.146	0.48	1.03	100.66	3.84	6.38

There seemed to be a slight drift in the drag coefficient curves, the highest drag coefficients being realized at the high velocity end of the test. Concurrent with this there was a decrease in stability with the mean displacement drifting from approximately 2 degrees at the high velocity end to approximately 5 degrees at the low velocity end. Oscillatory stability was also noted to decrease at low velocity. There was little evidence in the inflation data which would indicate an appreciable difference in the parachute inflation at varying velocities. Throughout both tests, the parachutes inflated to approximately 100%. Further tests would have to be made with parachutes of this type to determine whether the above results are characteristic of this type of parachute or merely a function of the geometric configuration of this particular Ribbon Type 125 parachute.

10. FIST Ribbon Type 126 (λ_g = 23.30%)

The FIST Ribbon Type 126 was the largest (8.92 foot diameter) parachute tested in the program and had the highest porosity of any parachute tested.

A total of three tests was made with the FIST Ribbon Type 126 parachute. Two of the tests, Nos. 47 and 51, yielded complete performance data throughout the recorded test period. Respective deployment velocities were 721 and 827 mph.

The average performance characteristics of the parachutes tested on the two successful runs are tabulated in Table 19. Summary curves illustrating the performance are graphically shown in Fig. 42.

TABLE 19

PERFORMANCE CHARACTERISTICS OF FIST TYPE 126 PARACHUTE

RUN NO.	V_S	t_f	C_D	X	D_{p_1} / D_p AVERAGE	R mean	R max.
47	1057	0.174	0.49	0.95	94.76	2.50	3.94
51	1213	0.167	0.47	0.87	98.97	1.85	3.26
AVERAGE		0.170	0.48	0.91	96.87	2.16	3.60

Since the data were fairly consistent on both tests, it is quite significant to note that the averages for this parachute type are lower for all parameters than for any other FIST Ribbon parachute configuration tested in the program. The drag coefficient and the opening shock factor were both considerably lower than corresponding factors in other groups, with the possible exception of the Conical Ribbon Type 125 which also had a drag coefficient of 0.48. The opening shock factor (X) of 0.91 was the average of relatively close factors on each test. The stability of the parachute, which had an average mean displacement of only 2.16 degrees and an average maximum displacement of only 3.60 degrees, was significantly better than that of the other FIST types tested. The maximum displacement at any time during the test was under 4.0 degrees. Inflation times in the two tests varied less than 0.01 second, with an average value of 0.170 second. The average steady state inflation of the parachute was 96.87%, and only in rare instances did the maximum inflation reach 100%.

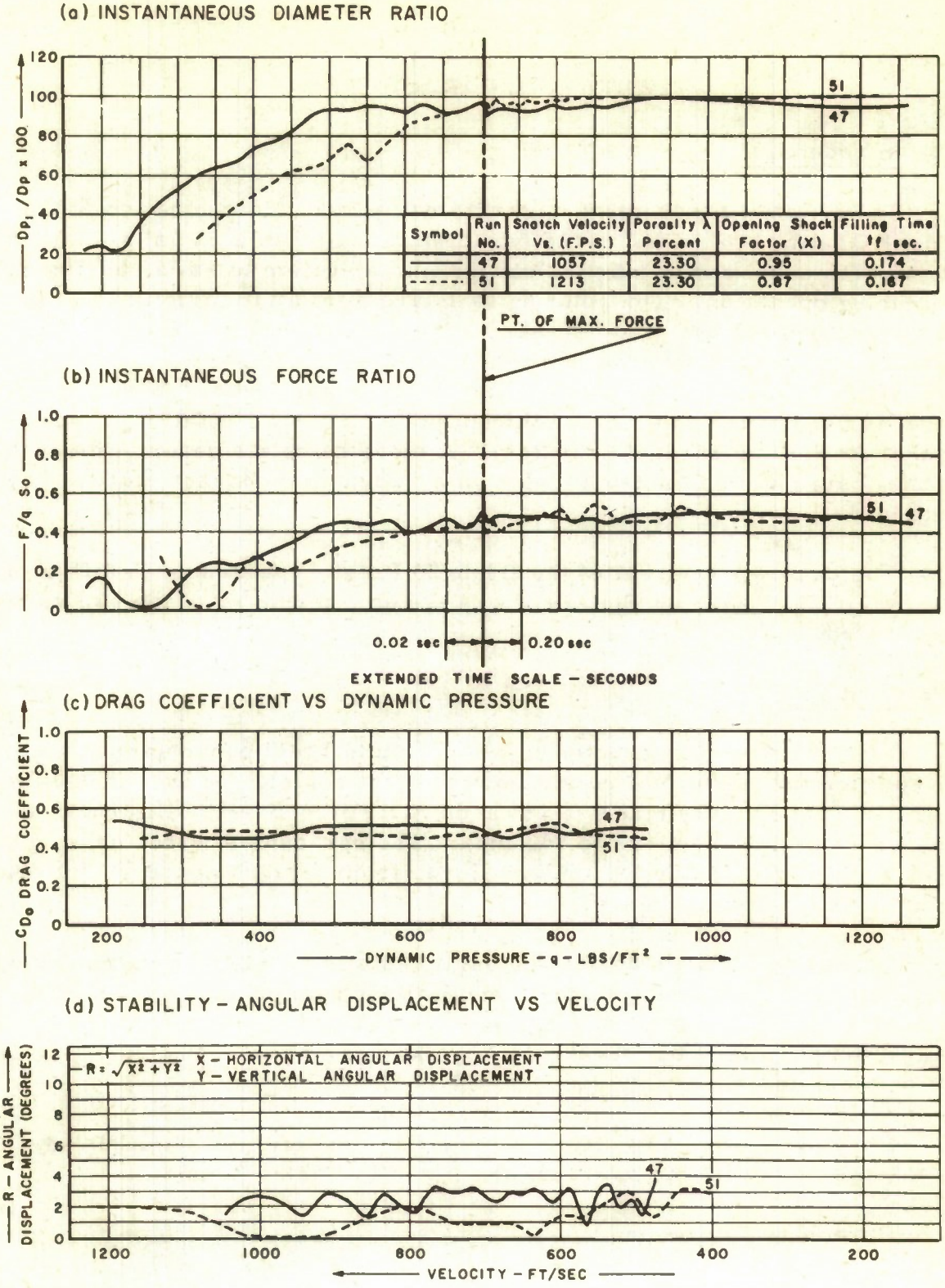

Figure 42 Summary Data - FIST Ribbon Parachute Type 126

APPENDIX D

ROTAFOIL PARACHUTES

A. Introduction

The Rotafoil parachute derives its name from a combination of the terms ROTating Air FOIL. This type of parachute has a radial slot on one side of each panel converting the canopy into a system of sails causing rotation during operation. The rotating sails are similar to airfoils and may provide a lift force acting in the same direction as the drag force of the parachute. The centrifugal force due to the rotation of the parachute increases its projected area and therefore enhances total drag force. A low friction swivel is used at the vehicle attachment point to permit rotation without twisting the lines in the parachute system. A more complete description of the Rotafoil parachute geometry and design aerodynamic characteristics may be found in Ref. 16.

The basic gore layout of the B7-8-20 Rotafoil parachute in this program is shown in Fig. 43, and Fig. 44 shows the sail geometry of the two variations tested.

B. Test Program

Five tests were conducted in which Rotafoil test parachutes were deployed from the liquid fuel rocket powered test vehicle, on the 10,000 foot Free Air Test Facility track at Edwards Air Force Base, California, at velocities ranging from 622 to 853 mph. The parachutes tested on the program were fabricated by Radioplane Corp. from designs approved for testing by the contracting agency.

Parachute failures during the early tests of this type dictated change requirements in suspension line strength, vent reinforcing, and confluence point assemblies. The later version of the parachute was tested with these changes incorporated but severe canopy damage was incurred during inflation on these tests.

Physical details and material specifications of the Rotafoil B7-8-20 parachutes tested in this program are listed in Tables 20 and 21.

C. Parachute Performance

Successful operation of a Rotafoil parachute was not attained in this series of high-speed tests. Suspension line and keeper failures occurred on

the two tests made with the original B7-8-20 configuration. Redesign of this parachute eliminated the structural weakness in the line system but tests with this modified version resulted in severe canopy damage. Available performance data of the tests made are tabulated in Table 22.

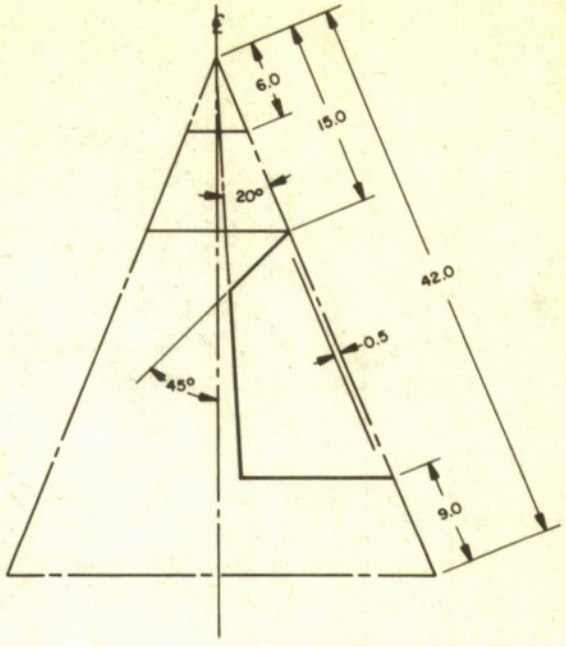

Figure 43 Basic Gore Layout - Rotafoil Parachute

On parachute test run No. 26, all suspension lines severed at inflation, approximately halfway between the keeper and the swivel coupling at the sled attachment end. Although the parachute was released prematurely and did not inflate immediately the test clearly indicated a structural weakness in the suspension line-riser system. This system was fabricated of two-ply-3000 pound T. S. nylon webbing with a two-ply wrap around keeper stitched to the lines at the confluence point. Again on test run No. 32 this weakenss was evident. At time of maximum load the keeper failed, allowing the suspension line-riser combination to separate. As the parachute rotated the centrifugal force caused the lines to assume an ogival shape and cut themselves on the edge of the parachute compartment. Progressive failure, illustrated in the photo sequence in Fig. 45, led to collapse and total destruction of the parachute. The force and diameter ratio measurements obtained on this test are shown in Fig. 46.

The modified version of the Rotafoil type B7-8-20 parachute, tested on test run Nos. 55, 56, and 57 incorporated suspension lines and risers of 1 inch - 12,000 pound T. S. nylon webbing with an improved keeper of the through-line circular type at the confluence point of the suspension line-riser system. This keeper is described further in Appendix E. The vent reinforcing band was also structurally strengthened on the latter parachutes.

Major canopy damage occurred when these parachutes were deployed at 853 and 698 mph. The force and diameter ratio measurements during the inflation process are shown in Fig. 47, and the damaged parachutes from the two test run Nos. 56 and 57 are shown in Figs. 48 and 49.

As discussed in Ref. 16 the number of panels in a Rotafoil parachute has a pronounced effect on performance. Parachutes with relatively few

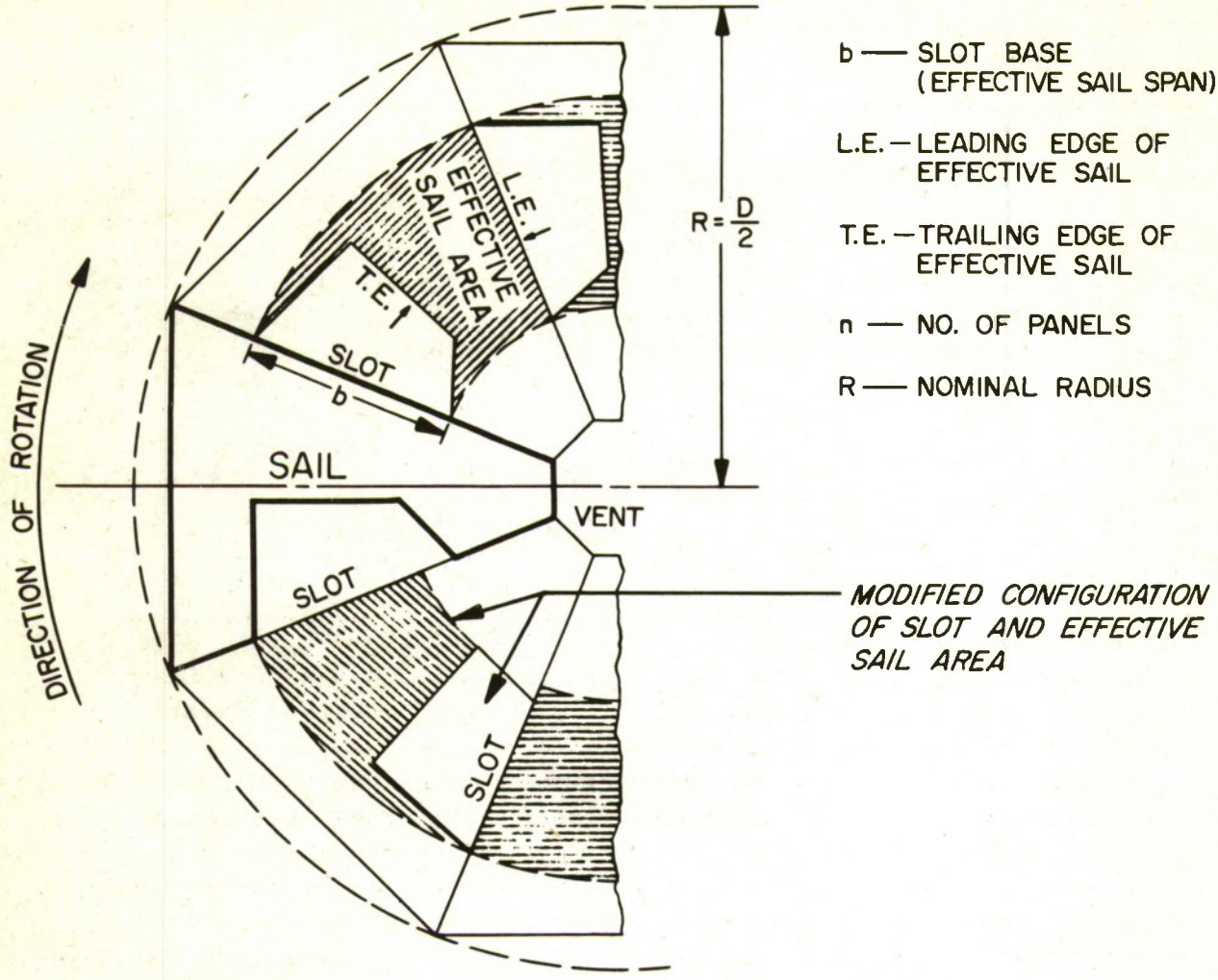

Figure 44 Elements and Geometry - Rotafoil Parachute

panels normally have higher drag coefficients than those with a greater number of gores. Stability, however, must be slightly sacrificed to maintain the higher gain in drag efficiency. This was illustrated in the Phase I tests of the Rotafoil parachute, (Ref. 14, Part I). Unfortunately, as the number of panels in a parachute is decreased the canopy stresses in the individual panels are increased. This ultimately leads to a point where either the parachute geometry must be changed or stronger structural material substituted. Since none of the Rotafoil parachutes tested in this program operated in the steady-state condition, aerodynamic parameters cannot be compared within this series of tests or with the lower velocity tests reported in Ref. 14.

TABLE 20
PHYSICAL DETAILS OF ROTAFOIL TYPE B7-8-20 PARACHUTE

TYPE OF ROTAFOIL PARACHUTE	B7-8-20	B7-8-20 MODIFIED
NUMBER OF PANELS, n	8	8
NOMINAL DIAMETER, D (ft)	7.0	7.0
SUSPENSION LINE LENGTH (ft)	7.0	7.0
GEOMETRIC POROSITY, λ (%)	20.1	15.8
CANOPY POLYGON AREA, S_0 (ft^2)	34.64	34.64
VENT AREA (ft^2)	0.41	0.41
TOTAL SLOT AREA (ft^2)	6.63	5.06
TOTAL SLOT & VENT AREA (ft^2)	7.04	5.47
SLOT BASE, b (ft)	1.50	1.0
SLOT ASPECT RATIO = $\frac{b^2}{\text{SLOT AREA}}$	2.71	1.58
EFFECTIVE SAIL AREA (ft^2)	12.21	8.82
SAIL ASPECT RATIO = $\frac{b^2}{\text{SAIL AREA}}$	1.474	0.91
SAIL SPAN (ft^2)	1.50	1.0
SAIL RATIO = $\frac{b}{R} = \frac{2b}{D}$	0.428	0.286
SOLIDITY RATIO = $\frac{\text{TOTAL EFFECTIVE SAIL AREA}}{\text{POLYGON AREA OF CANOPY}}$	0.352	0.255
CANOPY MATERIAL	TYPE III – 600 LB	TYPE III – 600 LB
SUSPENSION LINE MATERIAL	I x 3000 DOUBLE PLY	I x 12,000
VENT BAND REINFORCING	I x 3000	I x 6000
THREAD SIZE (CANOPY, SEAMS, & LINE ATTACHMENT)	3 CORD 5 CORD	3 CORD 5 CORD
USED ON RUN NUMBERS	26 & 32	55, 56 & 57

TABLE 21
MATERIALS USED IN ROTAFOIL TYPE B7-8-20 PARACHUTE

PART	MATERIAL	SPECIFICATION	SIZE	TENSILE STRENGTH
CANOPY MATERIAL	CLOTH - NYLON DRAG PARACHUTE	MIL-C-8021A	14.0 oz./sq. yd.	600 lbs
SUSPENSION LINES	WEBBING; NYLON TUBULAR	MIL-W-5625	WIDTH = 1 in	3000 lbs (2 PLY)
	WEBBING; NYLON	NON-SPECIFICATION	WIDTH = 1 in	12,000 lbs
THREAD	THREAD; NYLON	MIL-T-7807	3 CORD 5 CORD	24 lbs 40 lbs
REINFORCING TAPE	WEBBING; NYLON TUBULAR	MIL-W-5625	WIDTH = 1 in	3000 lbs
	WEBBING; NYLON	MIL-W-4088	WIDTH = 1 in	6000 lbs

TABLE 22

PERFORMANCE CHARACTERISTICS OF ROTAFOIL TYPE B7-8-20 PARACHUTE

	RUN NUMBER	26	32	55	56	57
VELOCITY F.P.S.	V_s AT PEAK SNATCH	APPROX. 1231	912	APPROX. 440	1251	1024
	V_o AT PEAK OPENING SHOCK	—	878	—	1240	1002
DYNAMIC PRESSURE P.S.I.	q_s AT PEAK SNATCH	—	855	—	1695	1120
	q_o AT PEAK OPENING SHOCK.	APPROX. 28,000	792	—	1665	1072
TIME INTERVAL SECONDS	t_s DEPLOYMENT TO PEAK SNATCH	—	0.366	—	0.192	0.215
	t_f SNATCH TO PRIMARY MAXIMUM INFLATION	—	0.154	—	0.098	0.112
	t_{ml} SNATCH TO MAXIMUM LOAD	—	0.194	—	0.048	0.112
FORCE LBS	F_s SNATCH FORCE	—	9,405	—	16,794	11,732
	F_o OPENING SHOCK	—	35,358	—	26,144	30,765
DIAMETER RATIO PERCENT	$\left(\frac{Dp_1}{Dp}\right)_m$ MAXIMUM	—	84.29	—	71.76	90.22
	$\left(\frac{Dp_1}{Dp}\right)_a$ AVERAGE	—	—	—	—	—
STABILITY DEGREES	MEAN RADIUS OF DISPLACEMENT	—	—	—	—	—
	MAXIMUM RADIUS OF DISPLACEMENT	—	—	—	—	—
C_{D_o} AVERAGE DRAG COEFFICIENT		—	—	—	—	—
X OPENING SHOCK FACTOR		—	—	—	—	—
PARACHUTE DAMAGE		MINOR CANOPY DAMAGE / ALL LINES BROKEN	SEVERE DAMAGE THROUGHOUT / KEEPER SPLIT, LINES CUT	NONE	SEVERE DAMAGE	SEVERE DAMAGE
PARACHUTE OPERATION		PILOT PCHT. OUT STA. 0 / TEST PCHT. OUT STA. 1400 / INFLATION STA. 3000	NORMAL DEPLOYMENT	LOW VELOCITY / EARLY SHUTDOWN	NORMAL DEPLOYMENT / FAILED DURING INFLATION	NORMAL DEPLOYMENT / FAILED 0.112 SEC. AFTER F_s
INSTRUMENTATION PERFORMANCE		NORMAL	NORMAL	NORMAL	NORMAL	NORMAL

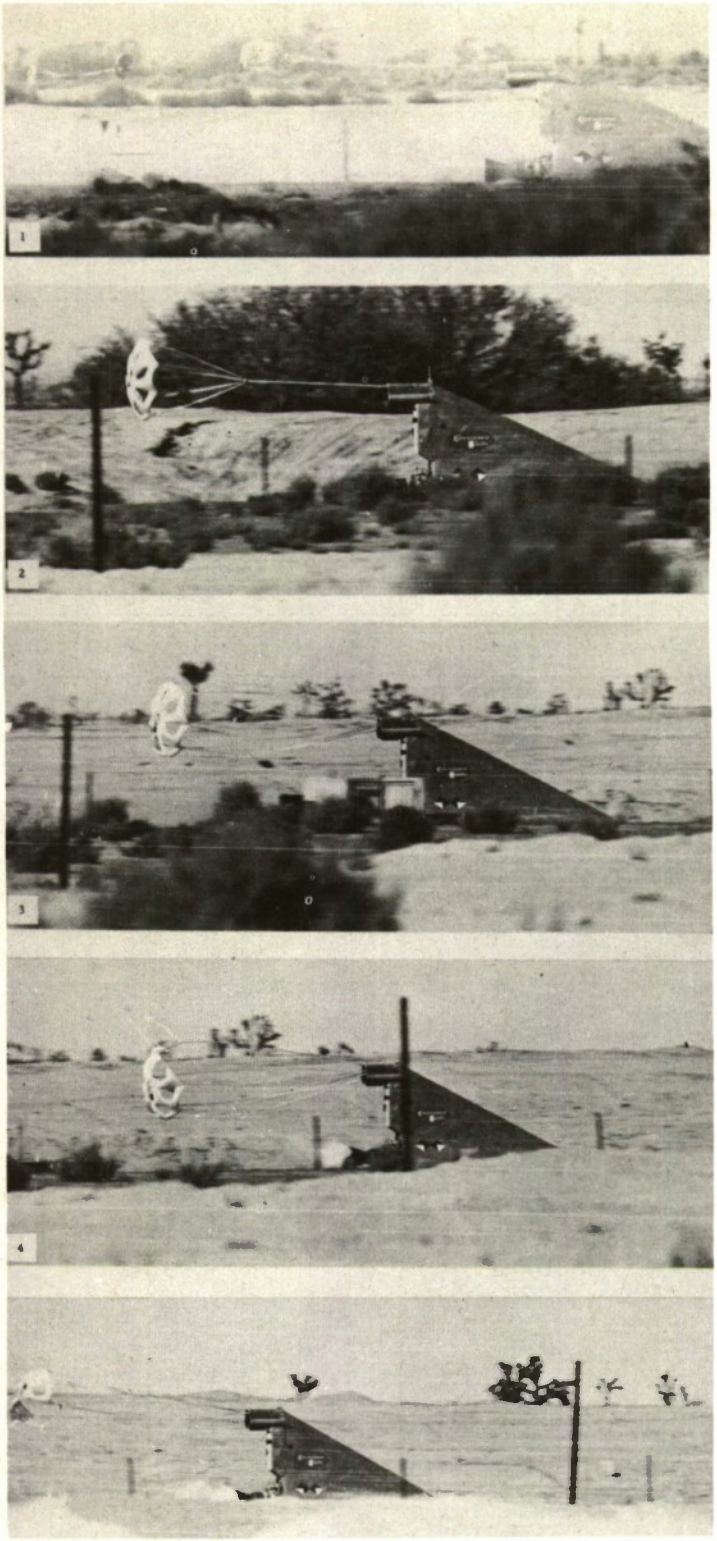

Figure 45 Deployment Sequence - Rotafoil Parachute Type B7-8-20 (Test Run No. 32)

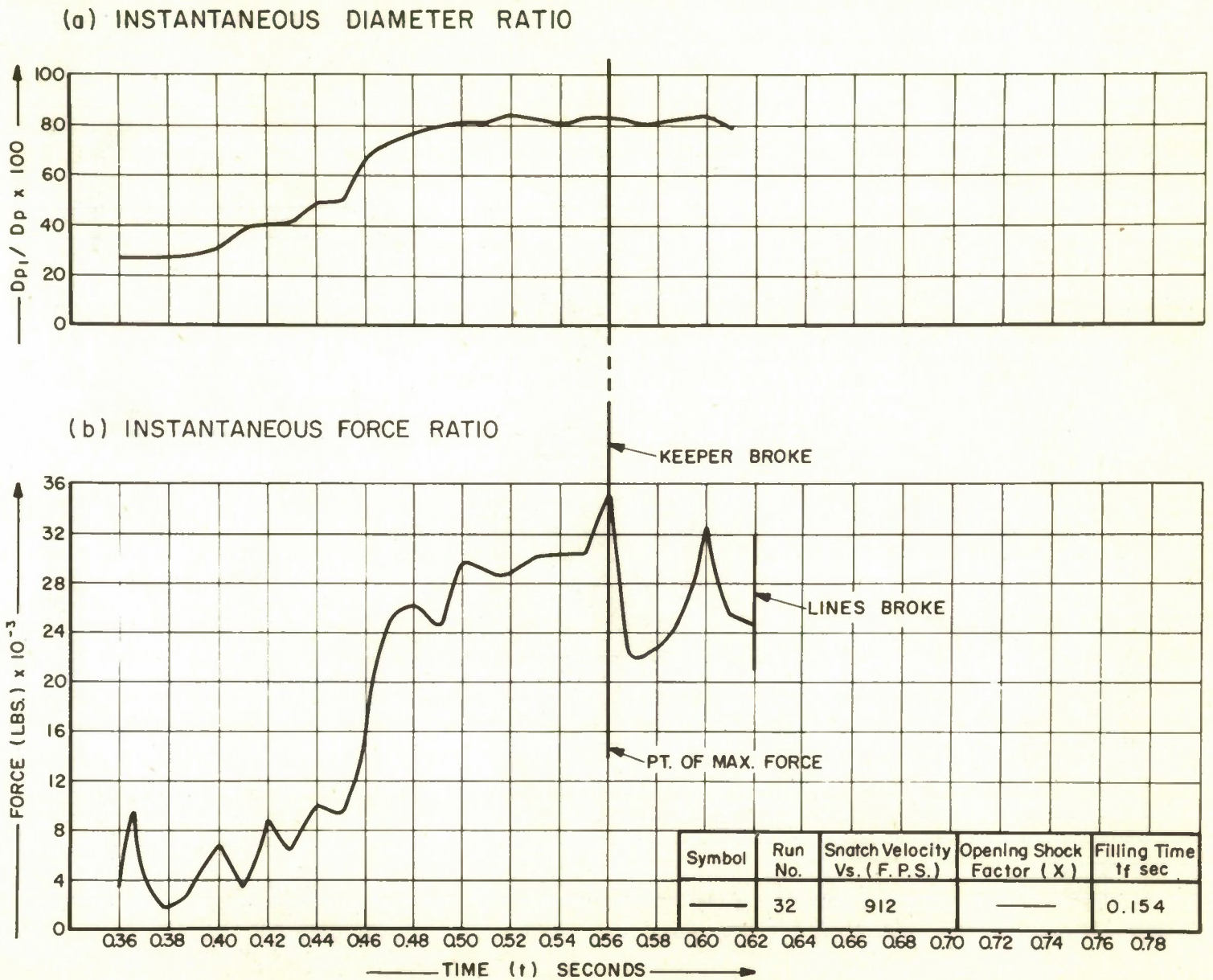

Figure 46 Force and Diameter Curves - Rotafoil Parachute, Type B7-8-20(Test Run No. 32)

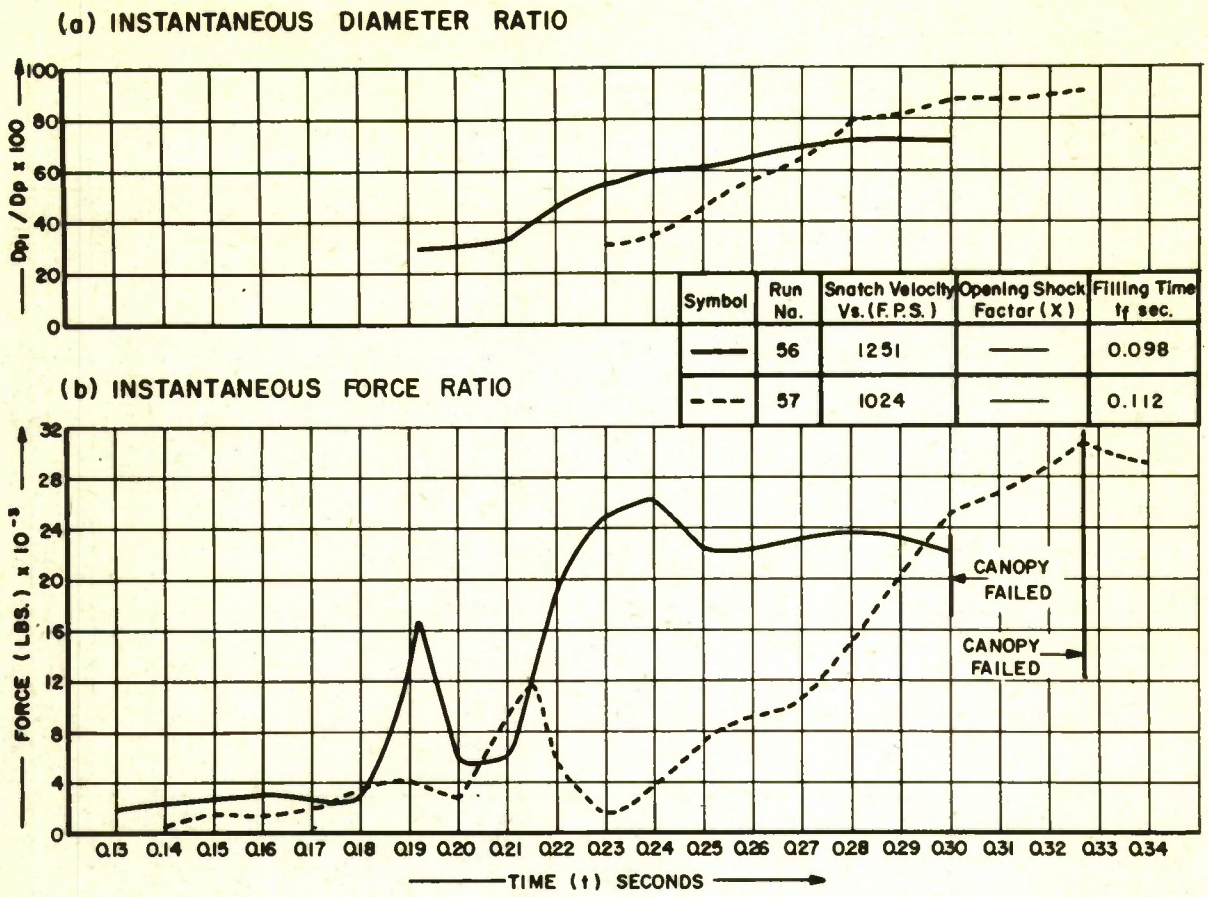

Figure 47 Force and Diameter Curves - Rotafoil Parachute, Type B7-8-20 (Test Run Nos. 56 and 57)

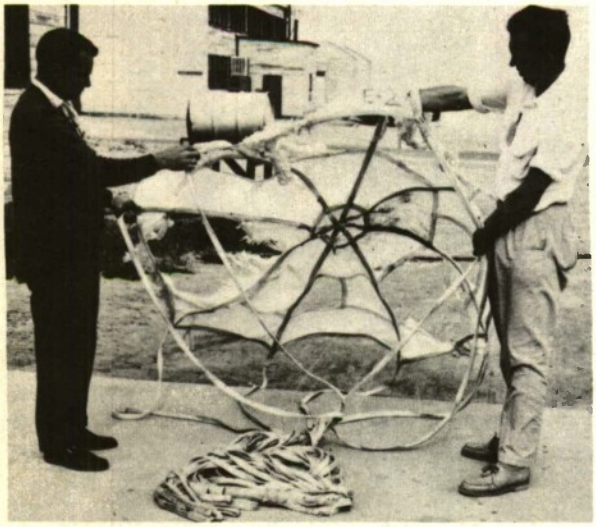

Figure 48 Damaged B7-8-20 (Modified) Rotafoil Parachute after Test Run No. 56

Figure 49 Damaged B7-8-20 (Modified) Rotafoil Parachute after Test Run No. 57

APPENDIX E

DEPLOYMENT SYSTEMS, HARNESS AND HARDWARE

A. General

Since the basic contract under which this program was conducted was a research and development program for recovery systems for missiles and target aircraft, the deployment systems, as well as the parachutes being tested, were given prime consideration. Experience indicated that failures in high-speed parachute operation were as frequently caused by inadequate deployment means as by parachute canopy design. With this in mind, several points are stressed as applicable design criteria for the development of a suitable deployment system:

(1) A snug fitting deployment bag for housing the canopy and lines is essential to obtain an orderly, controlled deployment and parachute inflation.

(2) Forceful expulsion of the pack containing parachute and lines, by utilization of such means as blast bags, powder charges, springs, etc., is believed to be more reliable than other means, such as pilot parachute extraction.

(3) A pilot parachute is desirable to prevent excessive bag tumbling during deployment.

(4) Aerodynamic forces acting on a pack and pilot parachute combination are generally of considerable magnitude. Without careful pack design, premature canopy and/or suspension line extraction may occur. This often leads to failure, due to the development of an excessive snatch force or the super-imposition of snatch force on opening shock force.

(5) Nylon parachute assemblies should be designed so that no relative motion can occur between adjacent parachute components carrying significant loads. Abrasion and friction heating is generated almost instantaneously in adjacent nylon assemblies under severe dynamic conditions. This causes crystallization of the nylon fibers and frequently initiates local failure of the component and subsequent failure of the system.

(6) Retention of the parachute pack in its compartment can become a major problem. Aerodynamic loads and/or inertia forces on the compartment cover and parachute pack may produce a premature deployment

and result in an over-all system failure.

Three basic methods of parachute deployment were employed on the series of high-speed sled tests in the program. They were as follows:

(1) Forceful Expulsion - Rearward

Rearward ejection of the parachute pack from a cylindrical compartment, with the energy supplied by the explosion of a powder charge acting directly on parachute deployment bag.

(2) Projectile and Pilot Deployment Rearward

Deployment gun fired a projectile which removed the compartment cover and pulled the pilot parachute into the airstream. The pilot parachute in turn pulled the main pack from the compartment.

(3) Forceful Expulsion - Perpendicular to Airstream

Vertical ejection of parachute pack and pilot parachute by means of powder charge and blast bag.

In all cases, the test parachute was packed in a deployment bag to obtain an orderly, controlled deployment and inflation.

A tabulation of the deployment method, type of container and powder charge for each test conducted in this series is shown in Table 23.

Early in the program, test results indicated the desirability of making the suspension lines and risers continuous from the parachute canopy to the test vehicle attachment point, eliminating the structurally weak assembly where suspension lines and riser lines normally were spliced. This arrangement also permitted a considerably greater latitude for the design and fabrication of the line keeper at the confluence point of the assembly.

Three types of line keepers were used on the parachutes tested in the program. They are explained in detail in paragraphs C.1, C.2 and C.3 of this appendix and were known as:

(1) Four-line keeper

(2) 'Octopus' keeper

(3) Fixed-line circular keeper.

TABLE 23

DEPLOYMENT SYSTEMS USED ON TEST PROGRAM

RUN NO.	DATE	DEPLOY-MENT SYSTEM	CHARGE (GRAMS)	TYPE OF POWER
7	5-8-53	RF1	30	B
8	7-7-53	RF1	30	B
9	7-9-53	RF1	30	B
10	7-17-53	RF1	30	B
11	7-21-53	RF1	30	B
12	7-23-53	RF1	30	B
13	8-5-53	RF1	30	B
14	8-6-53	RF1	40	B
15	12-7-53	RF1	40	B
16	12-10-53	GP2	4	S
17	12-15-53	RF1	40	B
18	12-29-53	RF1	40	B
19	12-29-53	RF1	40	B
20	12-30-53	RF1	40	B
21	1-18-54	GP2	4	S
22	3-19-54	GP2	4	S
23	6-4-54	GP3	2	S
24	6-7-54	GP3	2	S
25	6-9-54	GP3	2	S
26	7-7-54	GP3	2	S
27	8-25-54	GP3	2	S
28	9-10-54	GP3	2	S
29	9-13-54	GP3	2	S
30	9-15-54	GP3	2	S
31	9-17-54	GP3	2	S
32	9-20-54	GP3	2	S
33	9-21-54	GP3	2	S
34	10-14-54	GP3	2	S
35	10-15-54	GP3	2	S
36	10-19-54	GP3	2	S
37	10-23-54	GP3	2	S
38	11-10-54	GP3	2	S
39	11-16-54	GP3	2	S
40	11-24-54	GP3	2	S
41	11-29-54	GP3	2	S
42	12-17-54	GP3	2	S
43	12-10-54	GP3	2	S
44	12-14-54	GP3	2	S
45	1-21-55	GP3	2	S
46	1-28-55	GP3	2	S
47	2-1-55	GP3	2	S
48	2-11-55	GP3	2	S
49	3-9-55	VF4	55	B
50	3-14-55	VF4	55	B
51	3-16-55	VF4	70	B
52	3-18-55	VF4	70	B
53	3-21-55	VF4	70	B
54	3-28-55	VF4	70	B
55	3-30-55	VF4	55	B
56	4-5-55	VF4	55	B
57	4-7-55	VF4	55	B
58	4-13-55	VF4	70	B
59	6-2-55	VF4	70	B
60	6-9-55	VF4	70	B
61	6-10-55	VF4	70	B
62	7-15-55	VF4	70	B
63	7-21-55	VF4	70	B

DEPLOYMENT SYSTEM

R - REARWARD EJECTION
V - VERTICAL EJECTION
F - FORCEFUL EXPULSION (POWDER CHARGE)
GP - GUN & PILOT PARACHUTE

1 - CYLINDRICAL COMPARTMENT
2 - RECTANGULAR COMPARTMENT
3 - MODIFIED RECTANGULAR
4 - VERTICAL COMPARTMENT
B - BLACK POWDER
S - BULK SMOKELESS

The parachute attachment and severance device used on the entire series of Part III tests was designed and developed by Cook Research Laboratories for use on the subject contract. The unit, capable of withstanding parachute shock loads in excess of 100,000 pounds, is described and illustrated in Part D of this appendix.

B. Deployment Systems

1. Rearward Ejection

On test run Nos. 7 through 15 and 17 through 20 the parachutes were ejected rearward from a cylindrical compartment on the sled by the explosion of a charge of black powder acting directly on the base of the deployment bag.

The system operated satisfactorily with charges of 30 to 40 grams of FFFg black powder ignited by Dupont electric fireworks squibs. A diagram of the operation of this deployment system is shown in Fig. 50. The parachute compartment shown in the photograph in Fig. 51 was 18 inches long and 12 inches in diameter. It was fabricated of 5/16 inch 24ST aluminum and had a hemispherical cover of 0.032 inch thick aluminum. The cover was held in place by four 8-32 screws which sheared the cover material as the force of the explosion ejected the parachute.

The parachute deployment bag used with this system was a canvas cylinder approximately 12 inches in diameter with a double ply cover sewed in the closed end. The packing procedure and bag closure method is shown in Fig. 52. No pilot parachute was employed with this deployment system.

Figure 53 shows the system in operation on run No. 15, approximately at the instant of peak snatch force. The suspension lines and riser have been stretched taut and the bag is shown just leaving the canopy. The canopy had not started to inflate so that complete separation of snatch and opening shock forces was accomplished. It may be noted that because of the height of the parachute attachment point above the rocket engine, parachute deployment could be initiated during afterburning of the engine.

2. Deployment Gun and Pilot Parachute

On test run Nos. 16 and 21 through 48, a projectile and pilot chute deployment system was employed. The gun fired a two pound projectile aft from the sled. The kinetic energy of the projectile, acting through wire rope and/or nylon webbing, removed the compartment cover, and pulled the pilot parachute into the airstream behind the sled. The pilot parachute, attached to the pack of the test parachute with a bridle of heavy webbing and to the vent lines of the test parachute with a nylon break line, pulled the test parachute pack from the compartment and aft from the vehicle. Figure 54 diagrams the operation of the system, and Fig. 55 is a sequence showing the system in operation.

Several variations in compartment size and cover arrangement were employed with the gun and pilot parachute deployment system.

The compartment used on test run No. 16 was roughly rectangular with dimensions 8 by 20 by 24 inches. The compartment is shown after

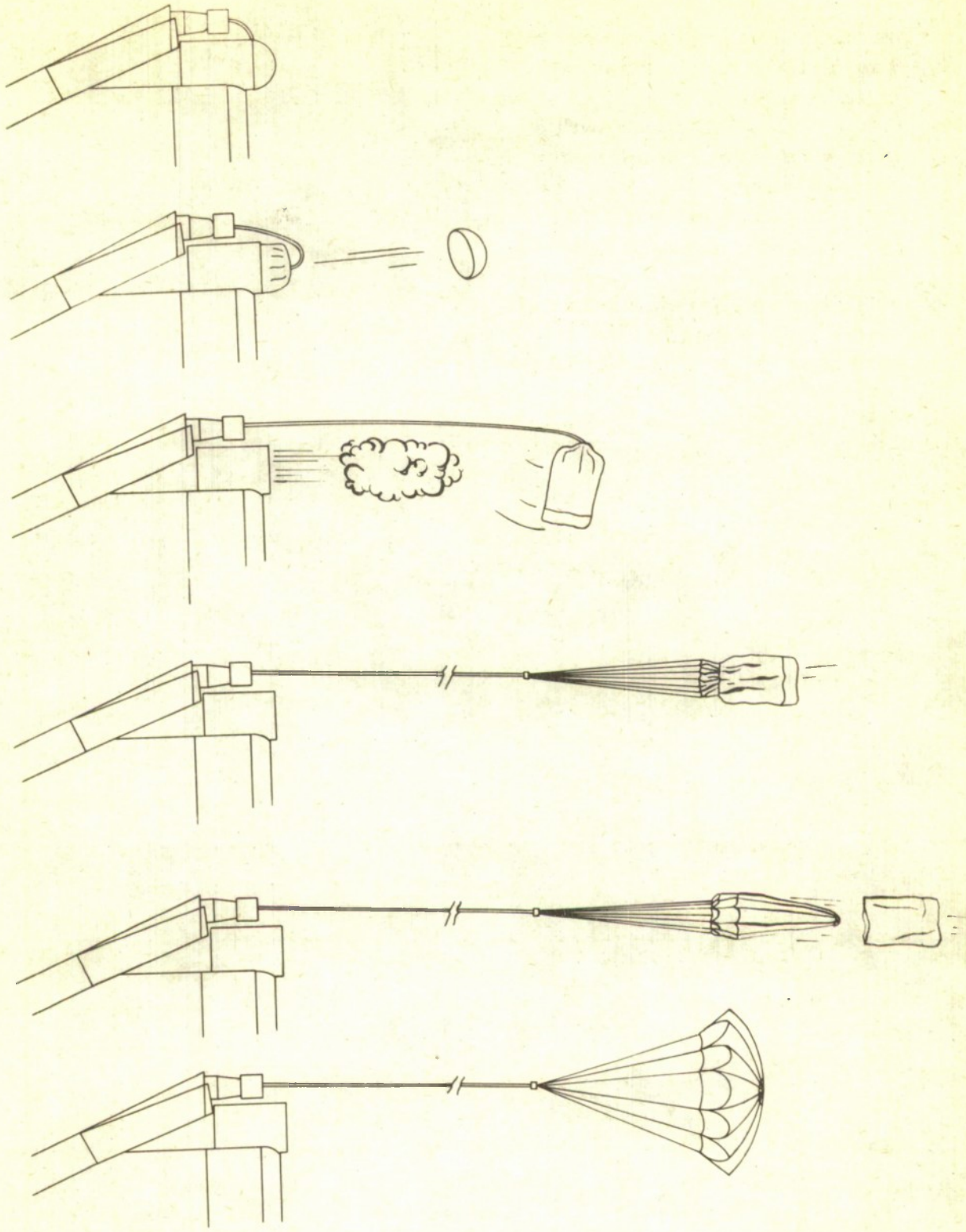

Figure 50 Ejection Sequence from Cylindrical Compartment

the test in Fig. 56. The compartment cover was canvas and was fastened in position with metal snaps. The projectile was connected to the cover with 3/16 inch wire rope. In operation the kinetic energy of the projectile tore the cover around its circumference rather than unfastening the snaps. The pilot parachute was deployed normally, but the bridles to the bag of the test parachute failed. The bridle

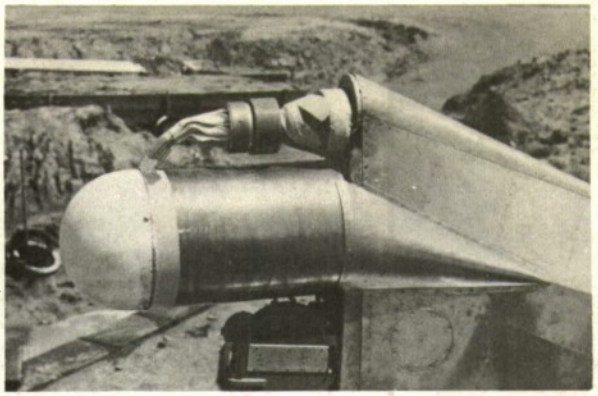

Figure 51 Cylindrical Parachute Compartment

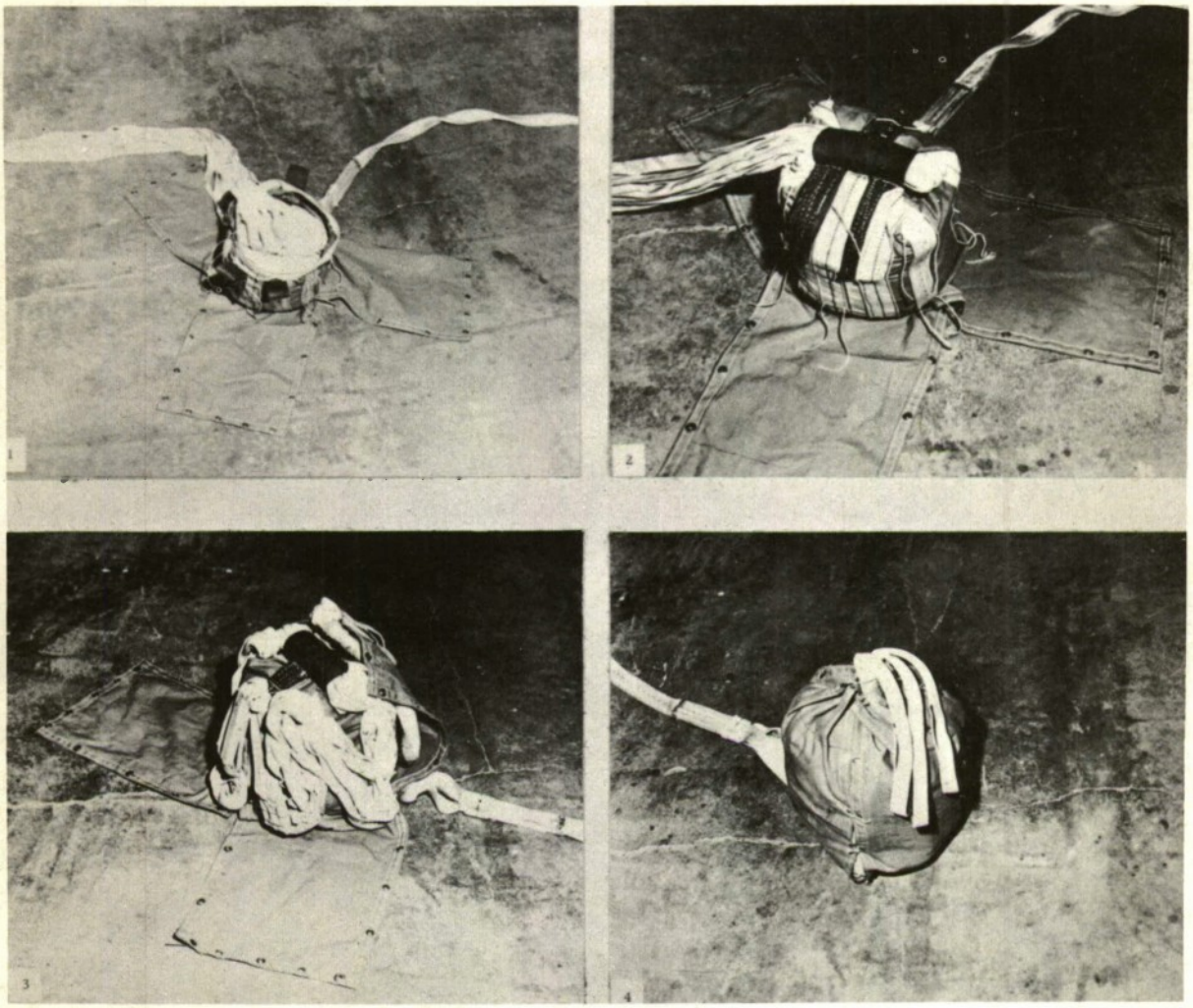

Figure 52 Cylindrical Bag-Packing Procedure and Closure Method

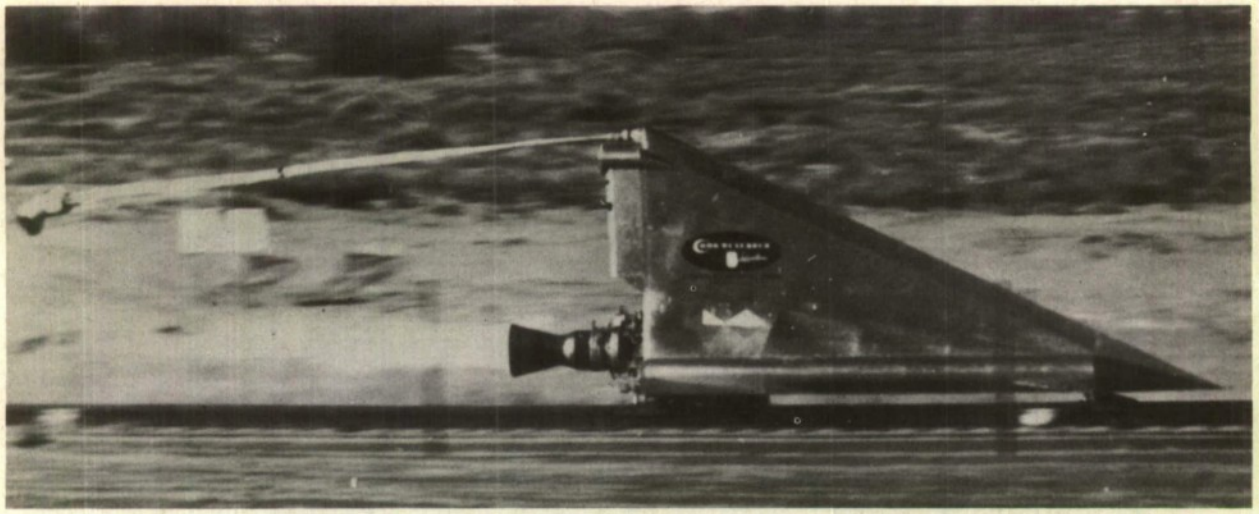

Figure 53 Typical Deployment from Cylindrical Compartment

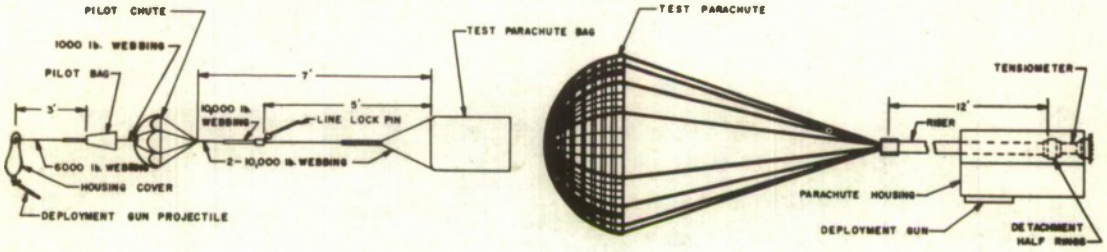

Figure 54 Diagram of Projectile and Pilot Chute Deployment System

was fabricated from four strands of 2400 pound cotton webbing.

The compartment used on test run Nos. 21 and 22 was the same one as was used on run No. 16, but different cover attachment methods were employed. The cover was metal and was held in place by a pair of locking levers, as shown in Fig. 57. The kinetic energy of the projectile released the levers and the remainder of the deployment system was similar to that of test run No. 16. A diagrammatic illustration of the lever release systems used on run Nos. 21 and 22 is shown in Figs. 58a and 58b, respectively.

The pilot parachute riser consisted of two strands of 10,000 pound nylon webbing and the bridle to the test parachute pack was fabricated of the same material. In addition, a deployment bag, as shown in Fig. 59, was employed with the pilot parachute to separate snatch and opening shock forces of the pilot parachute. The vent of the pilot parachute

was attached to the bag with 1000 pound nylon and bag closure was accomplished with two ties of 3 cord nylon thread. This system operated satisfactorily.

The parachute compartment employed on test run Nos. 23 through 48 was operationally similar to the one used on test run Nos. 21 and 22 but was appreciably larger to accommodate more bulky test parachutes.

The method of cover attachment employed on test run Nos. 23 through 26 is shown in Fig. 60 and diagrammatically illustrated in Fig. 58c. The vertical bar on the cover fits in a slotted strap at the top of the compartment and is held at the bottom with a 10-32 machine screw in shear. In addition the lock pin and strap arrangement shown in Fig. 61 was employed inside the compartment. The riser of the pilot parachute was connected to the locking pin so that the parachute pack could not leave the compartment until the pilot parachute developed considerable drag force. This arrangement performed satisfactorily except on test run No. 26 on which the cover was released prematurely.

The arrangement shown in Fig. 62 was installed for run No. 27 and was used on all tests through test run No. 48. An internal locking arrangement similar to the one shown in Fig. 61 was employed. Performance of the

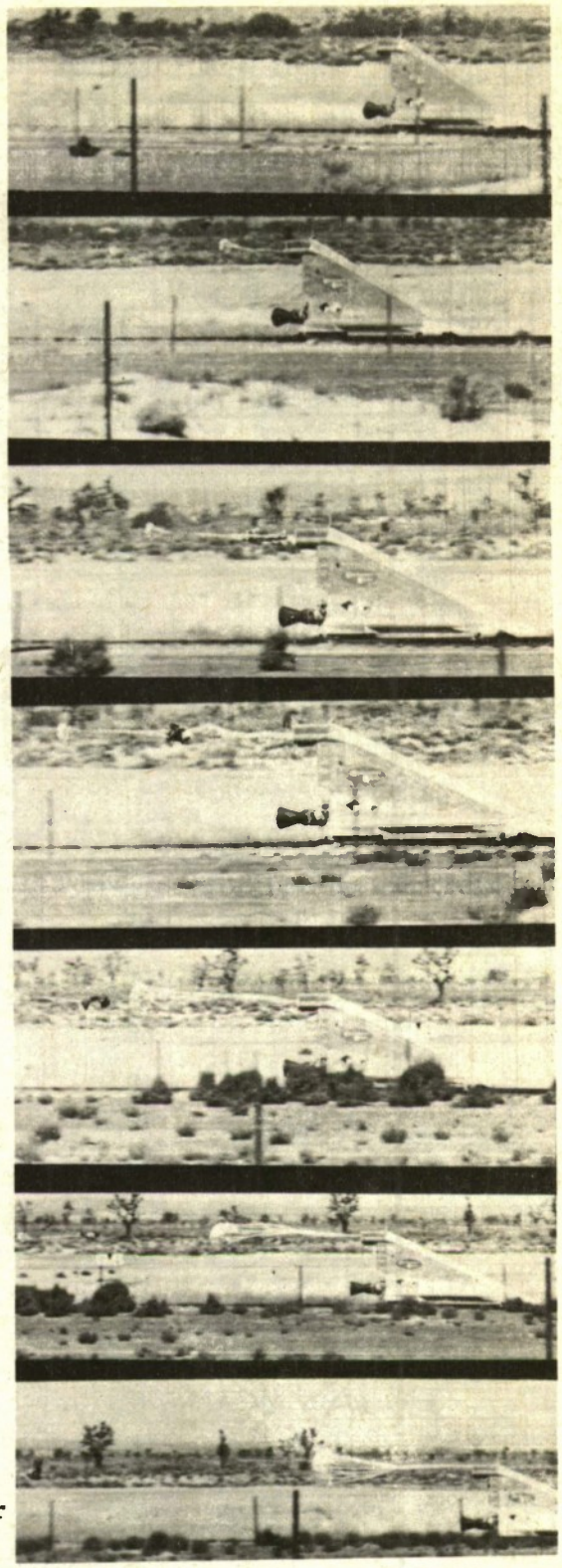

Figure 55 Deployment Sequence - Projectile and Pilot Chute System

system was satisfactory on all tests.

The arrangement of a typical test parachute deployment pack for the gun and pilot parachute system is shown in Fig. 63. The suspension lines and risers are tied to the long flap with break ties of 100 pound nylon cord. The canopy is contained in the closed part of the bag by means of closure stows until the suspension lines and riser have been stretched taut. Thus, the possibility of snatch force and opening shock force occurring simultaneously is eliminated.

Figure 56 Small Rectangular Compartment after Test Run No. 16

This type of deployment pack was employed for all test runs on which a pilot parachute was employed. There were minor variations in size and constructional details, but Fig. 64 gives representative details. The performance of this type of bag was very satisfactory throughout the test program.

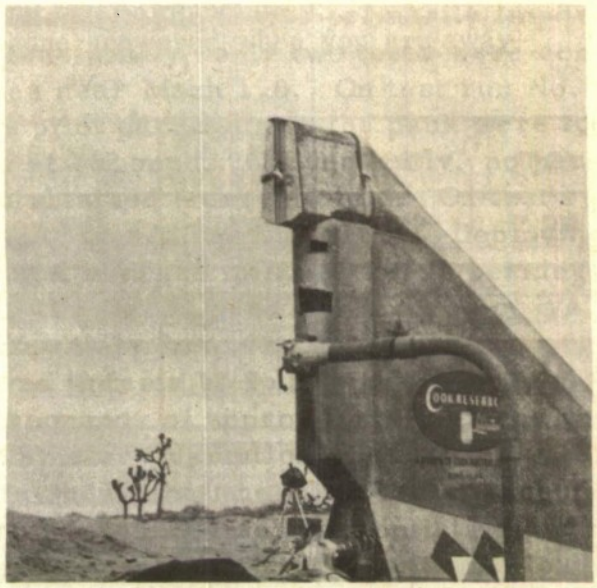

Figure 57 Locking Lever System on Small Rectangular Compartment

In the first three tests in which the deployment gun system was utilized, a charge of four grams of bulk smokeless powder was used in the gun. The remainder of the tests used a charge of two grams of bulk smokeless powder. In all cases the charge was initiated by electric fireworks squibs. Pertinent details of the gun used to initiate the deployment system are given in Fig. 65.

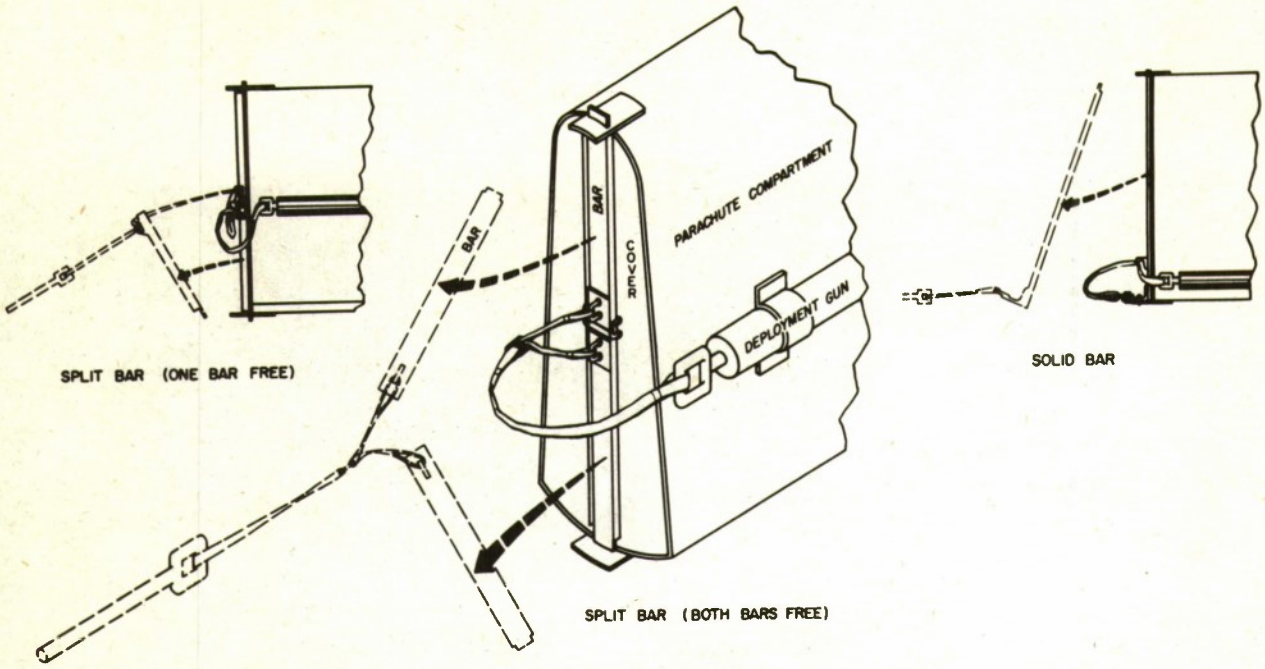

Figure 58 Compartment Cover Release Assemblies

3. Forceful Expulsion - Perpendicular to Airstream

On run Nos. 49 through 63 the compartment shown in Fig. 66 was employed to provide a parachute pack ejection normal to the direction of sled motion. A typical series of sequence photographs of such a deployment is shown in Fig. 67.

A theoretical study was made of the trajectory of a parachute pack with this type of ejection system. Figures 68 and 69 show the theoretical trajectories for variations on pack weight and ejection velocity with an assumed vehicle velocity of 1200 fps. Results of static tests indicated that it would be most desirable to conduct the sled tests with pack ejection velocities between 50 and 150 fps.

This series of static tests was conducted with a compartment identical to the one installed on the test vehicle. The compartment was fabricated of 3/16 inch 24ST aluminum plate, was rectangular in shape, except for the rounded trailing edge, and had dimensions of 12 by 24 by 24 inches.

It was found necessary to employ a blast bag, or bladder, to confine the explosion in order to obtain the desired ejection velocities without serious burn damage to the simulated parachute pack. Blast bags

Figure 59 Typical Pilot Chute Deployment Bag

of several different materials such as nylon cloth and canvas of various weights were tested in the dummy compartment. The final configuration of blast bag chosen from the static tests is shown with the test compartment in Fig. 70. Charges of 55 to 70 grams of FFFg black powder, ignited by electric fireworks squibs, were employed to eject the test parachutes on the test runs made with this system. Figure 71 shows the variations of ejection velocities for various charges of FFFg black powder with a pack weight of 25 pounds as obtained from tests with a compartment mockup.

C. Line Keepers

The necessity and advantages of utilizing a line keeper in an

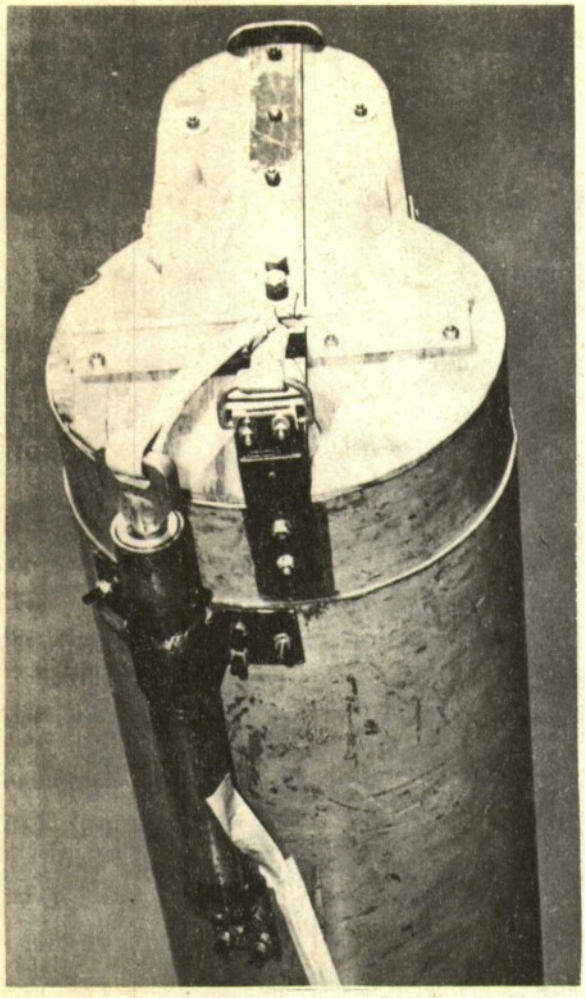

Figure 60 Solid Bar Locking Lever System

Figure 61 Lock Pin and Stowage Strap Arrangement

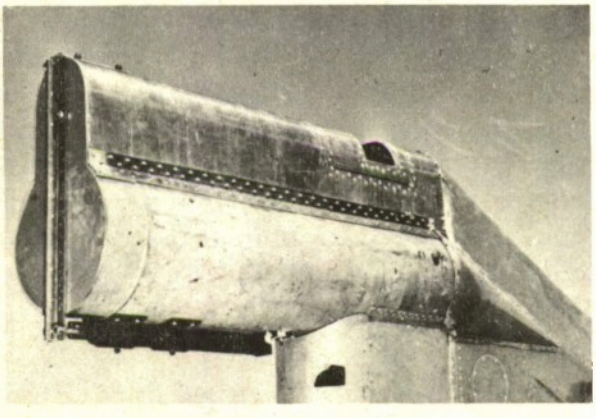

Figure 62 Revised Solid Bar Locking Lever System

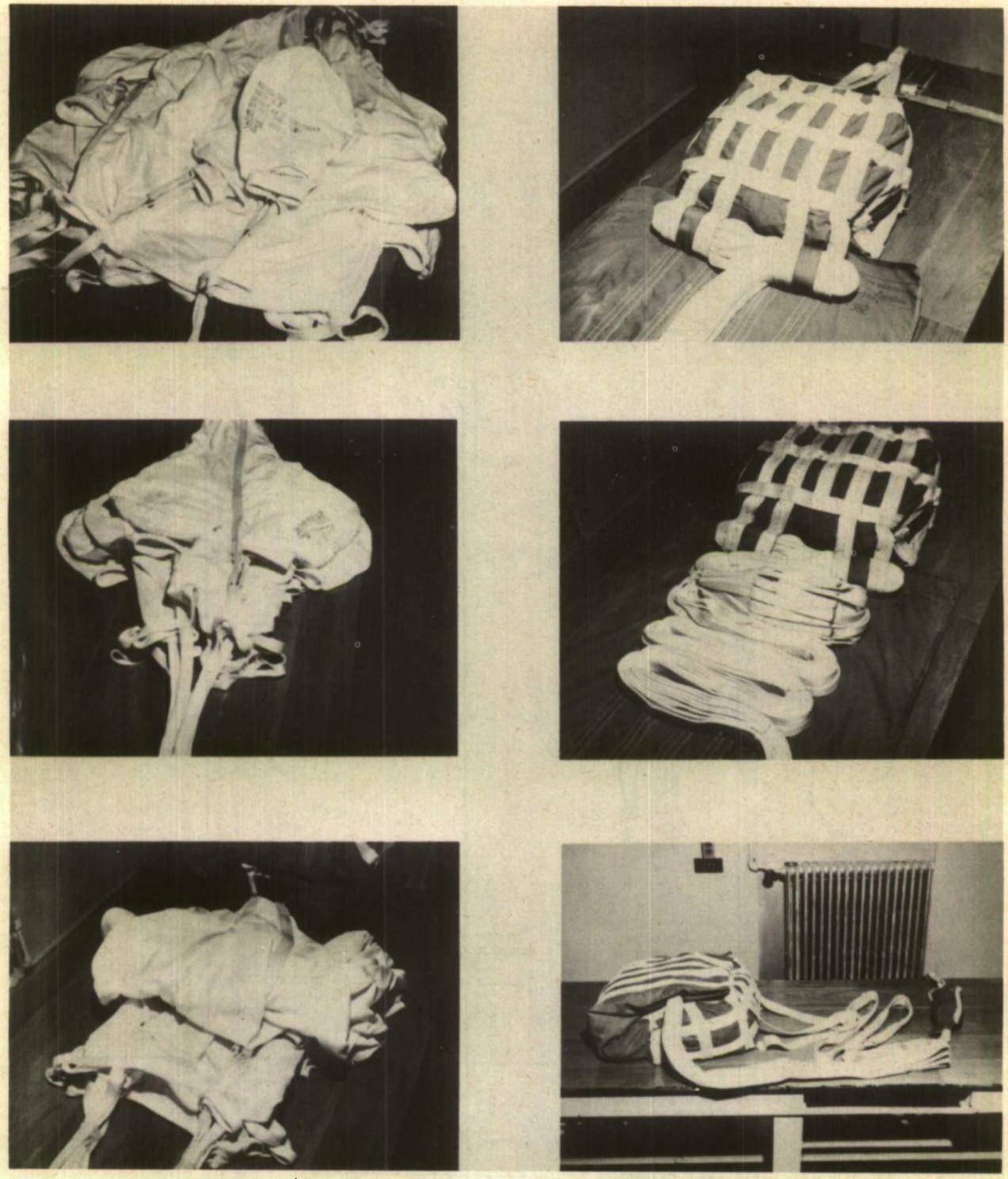

Figure 63 Test Parachute Deployment Pack and Packing Procedure

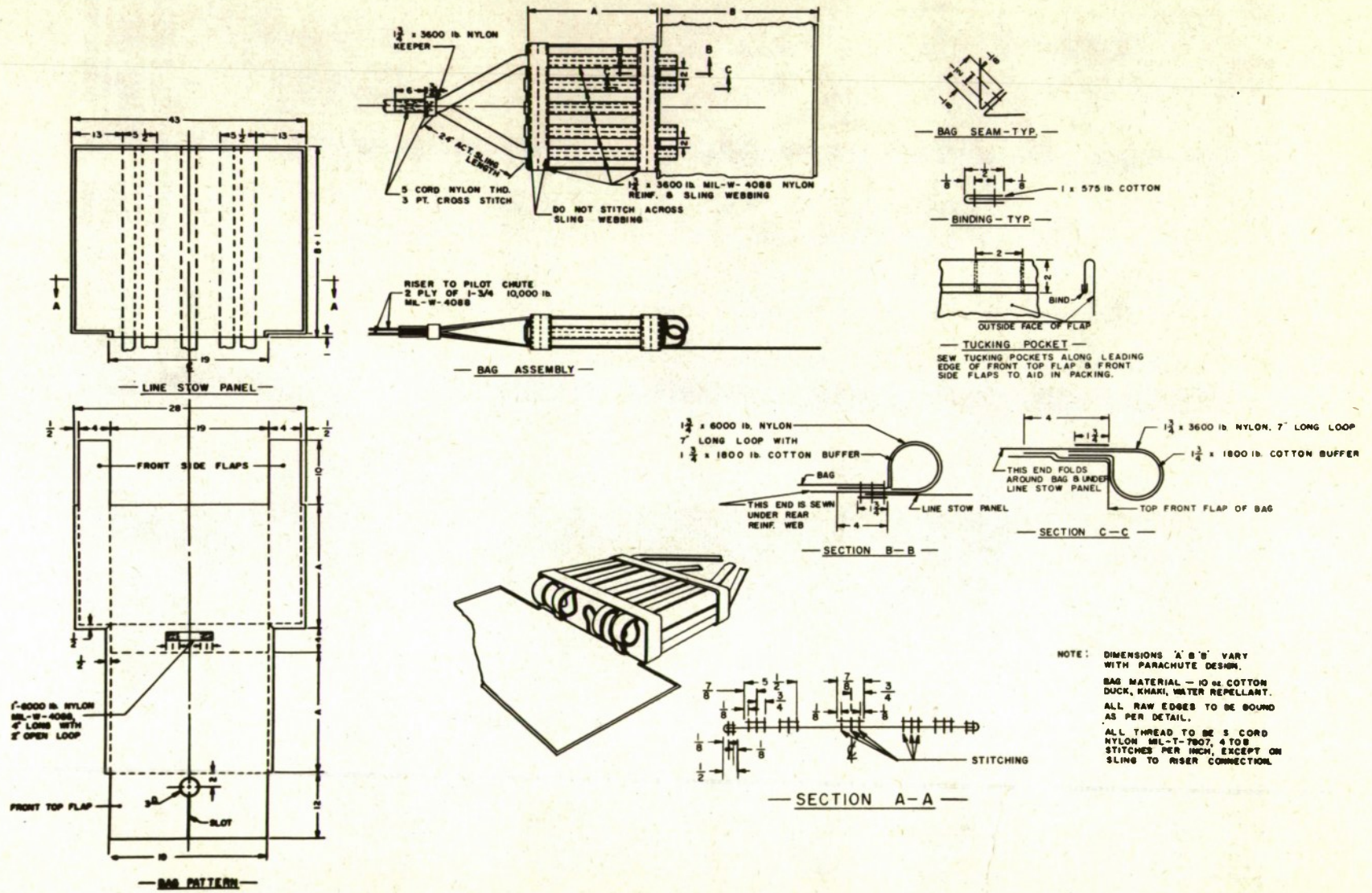

Figure 64 Flat Rectangular Deployment Pack

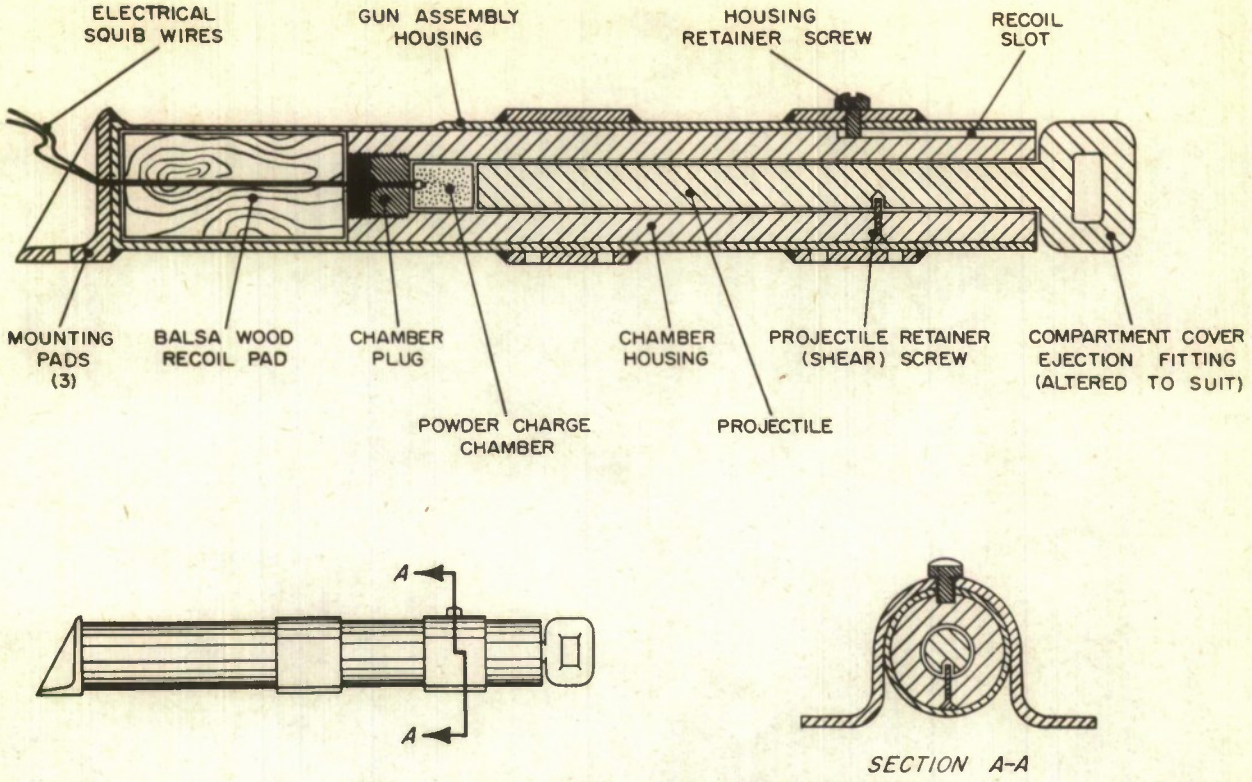

Figure 65 Deployment Gun Details

optimum location in the suspension line system was illustrated in several of the FIST Ribbon parachute tests presented in a previous section of the report. Primarily, these units are required in the system to maintain the desired suspension line length to diameter (L_s/D) ratio for optimum parachute performance and to reinforce the confluence point assembly.

Three types of keeper were developed during the program, each one eliminating apparent faults of the preceding one as test velocities were increased.

1. Four-Line Webbing Keeper

The original webbing keeper, as shown in Fig. 72, was fabricated from a double ring of 1-3/4 inch - 10,000 pound T. S. nylon webbing. Four of the suspension lines were attached to the keeper to prevent it from sliding along the lines. Parachute failures occurring with this type of installation indicated that this method of attachment often contributed to line failure due to unequal line load distribution or material crystallization caused by friction heating due to relative motion in the

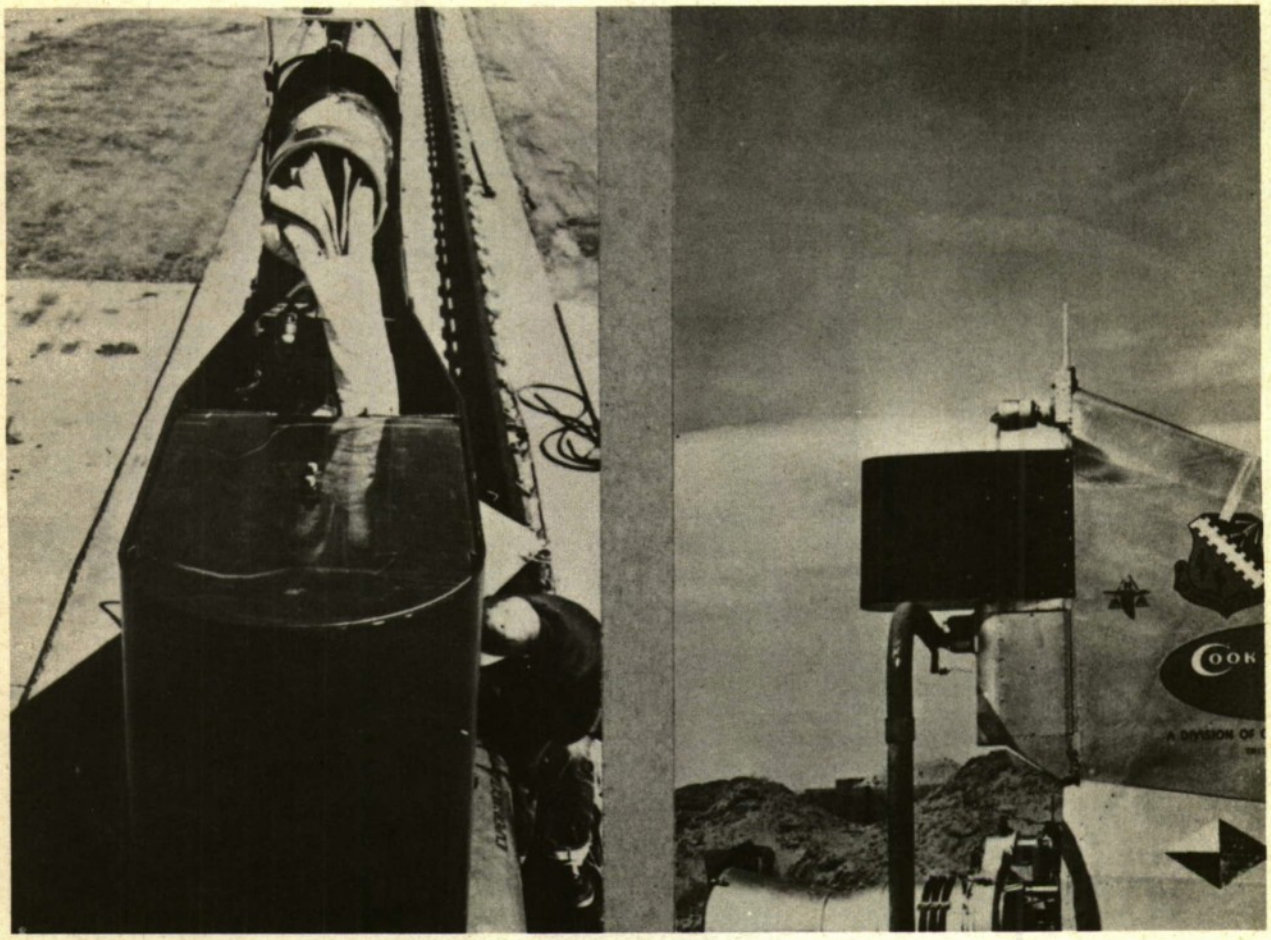

Figure 66 Vertical Deployment Compartment

keeper assembly. Consequently, this keeper was replaced on test run No. 28 with the configuration known as the 'octopus' type.

2. Octopus Keeper

The octopus keeper was used on all parachute assemblies tested in the program on test run Nos. 28 through 41, except for the early model Rotafoil B7-8-20 parachute tested on test run No. 32. This keeper consisted of a double thickness ring of 1-3/4 inch - 10,000 pound T.S. nylon webbing with an equal number of lines of the same material as the parachute suspension lines looped over the ring, equally spaced and alternately faced in opposite directions. The suspension lines are passed through the ring and attached to these keeper tentacles. A typical keeper of the octopus type is shown in the photographs in Fig. 73, before and after installation in the parachute line

assembly.

3. Fixed Line Circular Keeper

The fixed line circular keeper was the final keeper configuration designed for the parachutes in this test program.

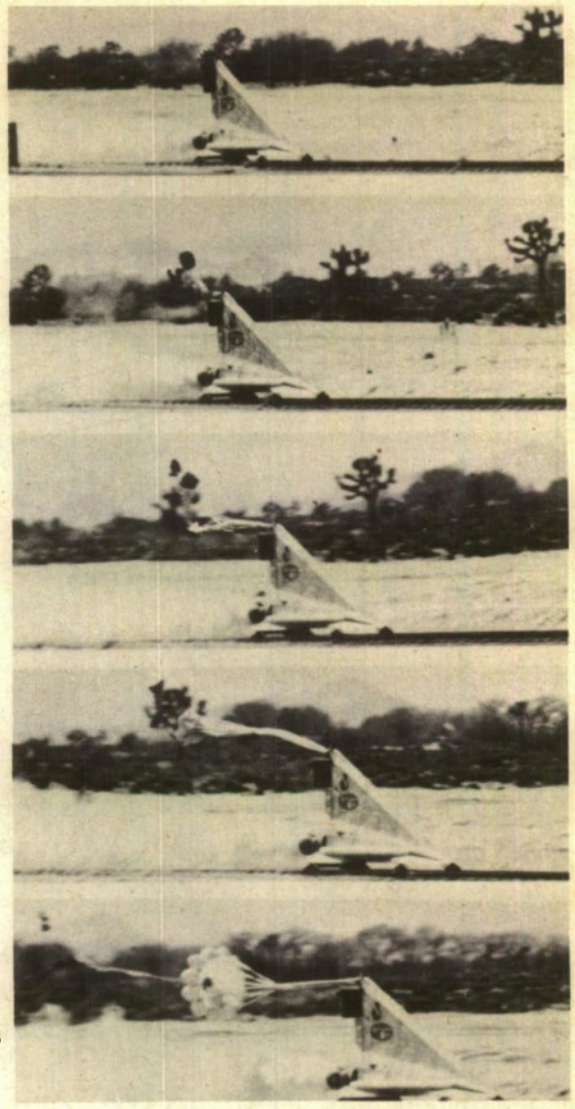

Figure 67 Sequence Photographs - Vertical Deployment System

All test parachutes after test run No. 41, with the exception of the Rotafoil parachutes, were fabricated with this type of keeper installed. All of the advantages of the octopus type are retained with the added advantages of simpler fabrication and installation. The basic ring is the same as the previous type but instead of the alternately faced loops of the octopus type, the keeper lines are fixed to the outer circumference of the ring and attached to each suspension line fore and aft of the keeper, and on the keeper itself. A photograph of the installed keeper is shown in Fig. 74. This arrangement of keeper and lines provides for a generally equalized distribution of the loads being transferred from the parachute through the lines and minimizes elongation differences due to unsymmetrical parachute loading. Most significant perhaps is the total elimination of relative motion between keeper and lines, which has often been found to be the initial cause of line failure due to subsequent friction heating and material crystallization.

4. Rotafoil Keepers

The Rotafoil parachute keeper used on the early B7-8-20 Rotafoil parachute was similar to the four-line keeper, except that the retainers

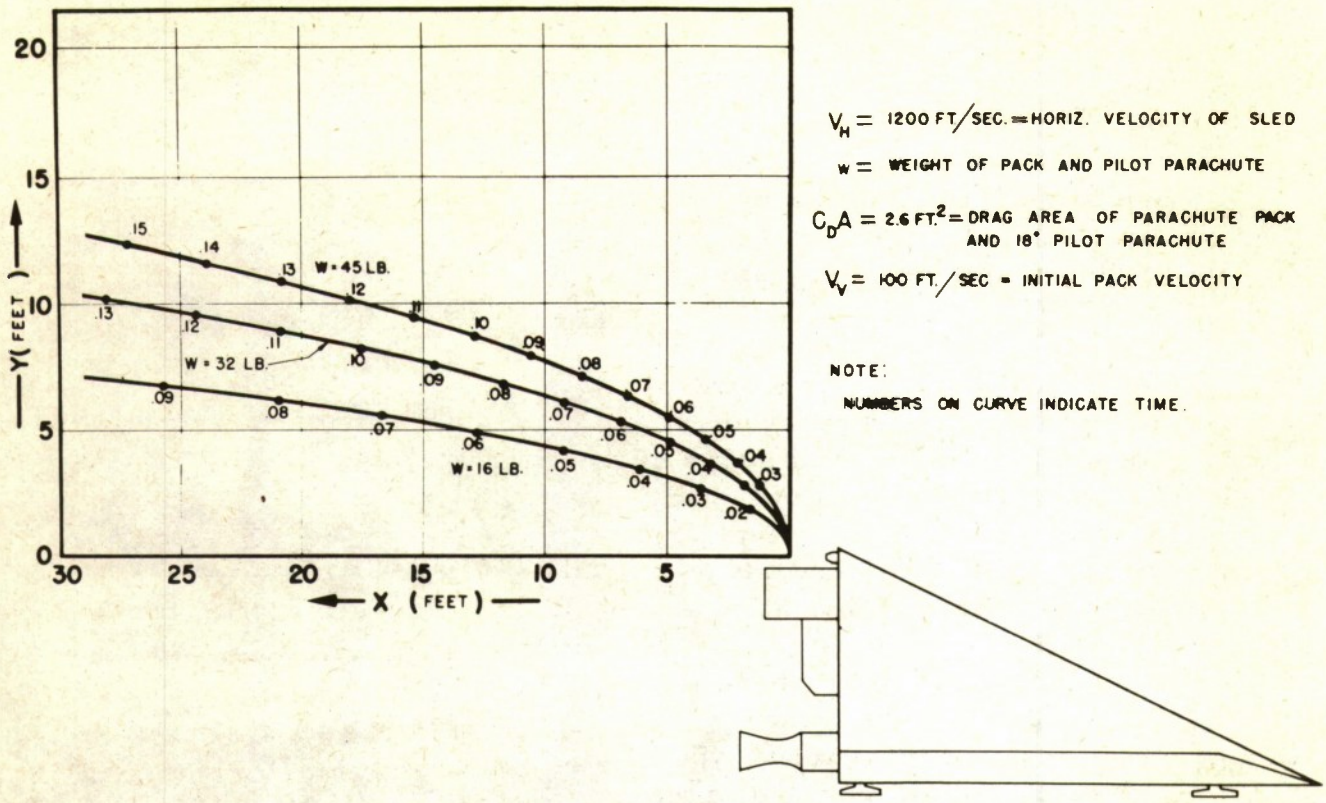

Figure 68 Theoretical Trajectory of Parachute Pack Ejected Upward from Sled for Various Pack Weights

on the keeper ring were attached to two adjacent suspension lines instead of one. This made a connection to all of the suspension lines although there was no restriction to the movement between keepers and lines.

The later model Rotafoil parachute, the modified B7-8-20, was fabricated with a keeper nearly identical to the fixed line circular keeper, described in paragraph 3 above. Identified as the through line circular keeper this unit had keeper lines fixed to the outer circumference of the ring, and attached to each suspension line on each side of the keeper. No attachment was made directly to the keeper; consequently some movement of adjacent components was allowed. In the tests made with this unit installed there was no apparent damage to the keeper or lines in the vicinity of the keeper.

D. Half-Ring Attachment and Separating Device

This type of attachment and separating device was originally designed

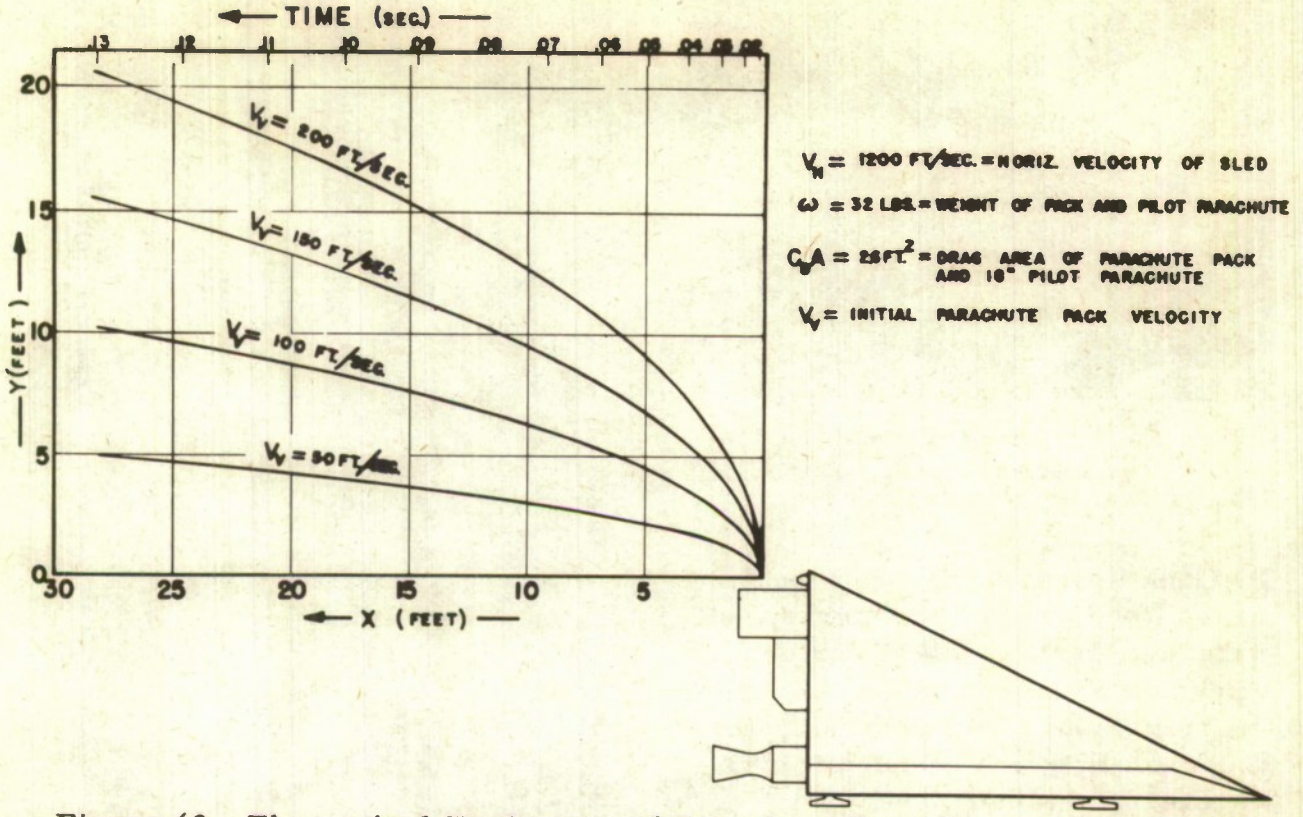

Figure 69 Theoretical Trajectory of Parachute Pack Ejected Upward from Sled for Various Ejection Velocities

Figure 70 Blast Bag and Test Compartment

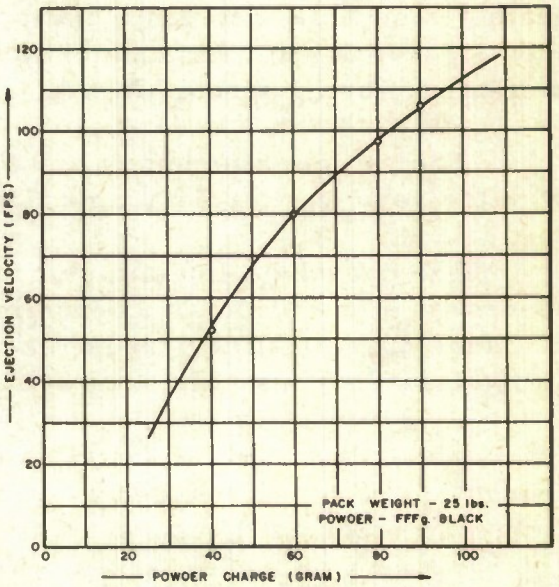

Figure 71 Curve of Pack Ejection Velocity for Various Powder Charges

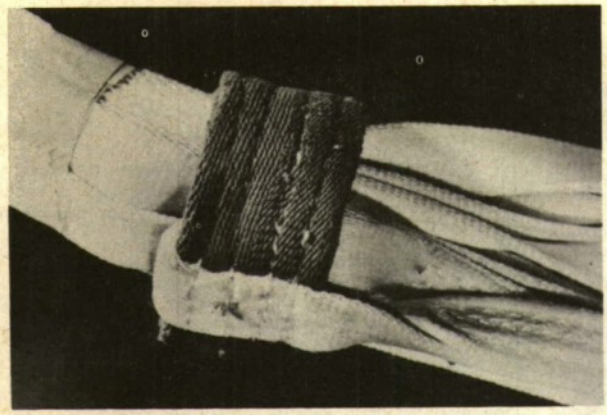

Figure 72 Four-Line Webbing Keeper

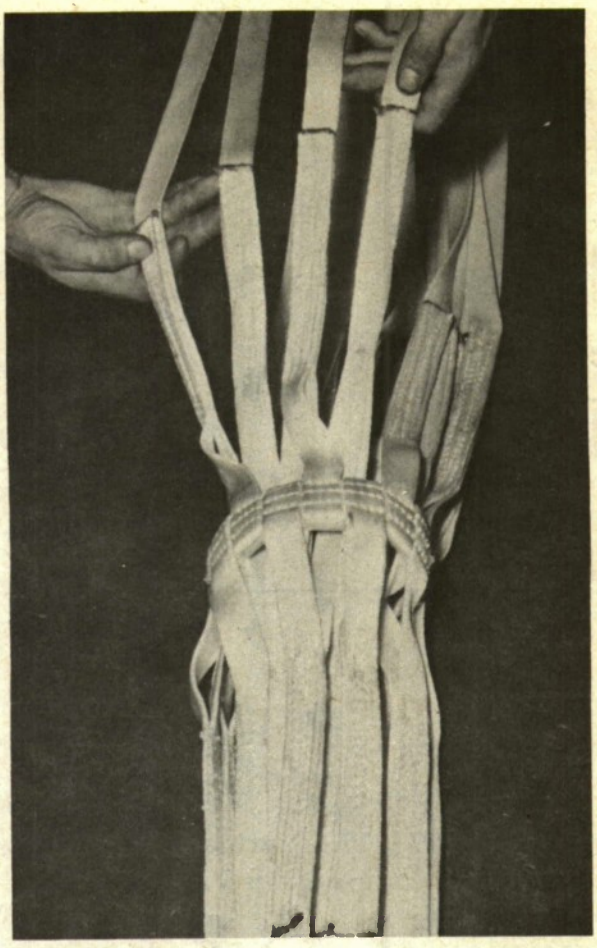

Figure 73 "Octopus" Keeper

by Cook Research Laboratories engineers to be used on the high-speed parachute test vehicle described in Appendix F and has since been successfully applied to missile systems incorporating high-speed parachute recovery systems.

The basic unit consists of three main components, the vehicle attachment, parachute line attachment and half-rings, as illustrated in Fig. 75.

The vehicle attachment end ties into the vehicle structure and remains with the vehicle after detachment is initiated in the unit.

The parachute line attachment end is a mating part to the vehicle attachment with a provision for connecting and securing the parachute line ends. The face of the mating part is recessed on opposite sides to accept standard No. 6 blasting caps which are used as the separating force.

The half-rings are installed over the blasting caps and mating attachment ends, and are secured by small shear screws which hold the assembly firmly together until separation is initiated.

Separation is accomplished by energizing the blasting caps which exert sufficient force to shear the screws and blow the half-rings from the assembly. This leaves the two attachment ends free to separate.

A number of these tests were conducted in which the half-rings were contained inside the stowage compartment after the separating blast. Results indicated that repeated tests could be made without damaging the interior of the compartment, at the same time eliminating all danger of the half-rings flying into congested areas.

Figure 74 Fixed Line Circular Keeper

Operation of these units has been consistent, and functional reliability excellent throughout the test program. Designed for shock forces up to 100,000 pounds, the unit has been subjected to frequent tests where shock forces exceeding 60,000 pounds were applied, with no apparent detrimental effects to the unit or its subsequent function.

The swivel assembly used with the Rotafoil parachutes is shown in Fig. 76. The assembly, including riser attachment fitting, weighed 26.5 pounds. The unit was statically tested to a load in excess of 100,000 pounds, at which time webbing failure occurred.

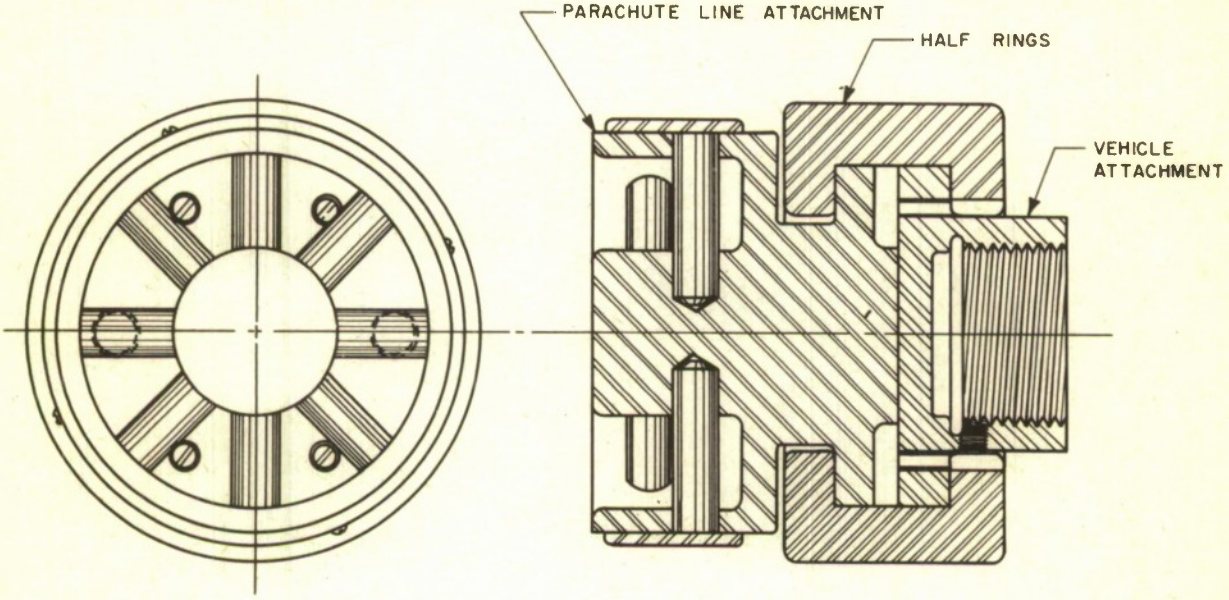

Figure 75 Parachute Attachment and Severance Device

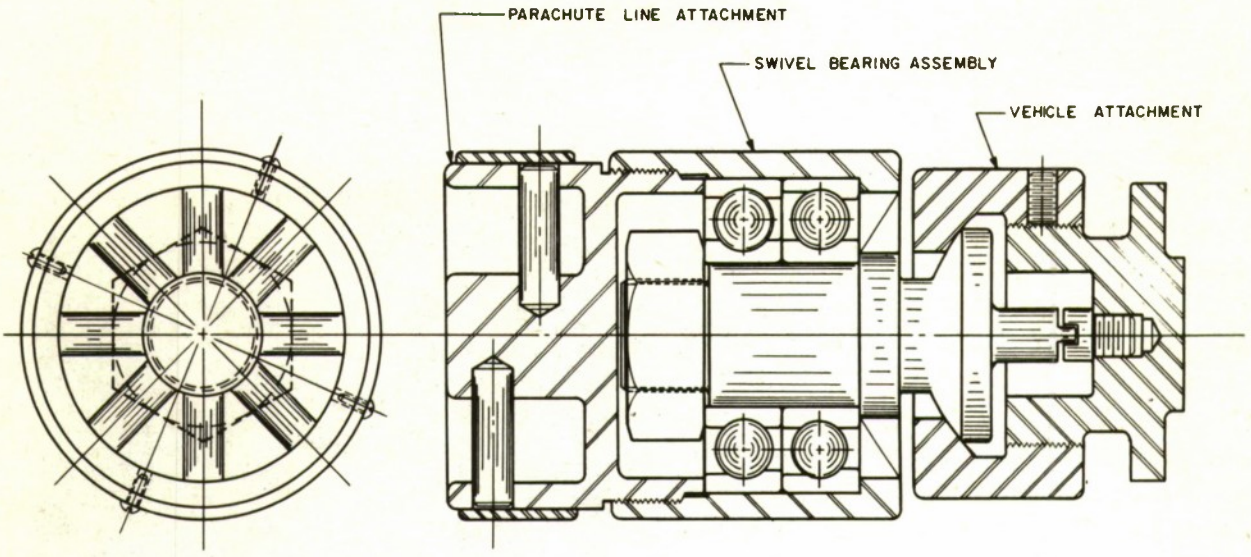

Figure 76 Rotafoil Parachute Swivel Assembly

APPENDIX F

DESCRIPTION OF TEST VEHICLE

The test vehicle for this phase of the project was a ground-operated Liquid Propellant rocket sled designed specifically to be operated on the 10,000 foot Free Air Test Facility Track at Edwards Air Force Base, California, for transonic parachute deployment tests. Figure 77 shows the complete vehicle at track station '0' during test program, and Fig. 78 is a three-view drawing showing basic vehicle dimensions.

Figure 77 Test Vehicle at Track Station '0'

The power plant, a gas pressurized, liquid propellant rocket engine was developed and manufactured for the project by the North American Aviation Corporation. Maximum design capability of the engine and propellant system was a thrust of 50,000 pounds for a duration of 4.5 seconds. This was actually exceeded on several tests. The maximum attained was 4.64 seconds of operation providing a corresponding velocity of 872 mph, or a Mach number of 1.11, with an expended-fuel sled weight of 4000 pounds. All tests at lower velocities were conducted by shortening the duration of maximum thrust. Propellants consisted of a fuel mixture of 75% ethyl-alcohol (ALC) and 25% water, and an oxidizer of liquid oxygen (LOX). Total propellant consumption at a mixture ratio of 1.3 LOX/ALC was 222 lb/sec. The fuel feed system was the pressurized type with gaseous nitrogen used as the main pressurizing gas and helium used as a precharge LOX stabilizing agent. This helium precharge was done to avoid excessive absorption and condensation of nitrogen in the LOX tank during the starting and early burning phases.

The cylindrical thrust chamber was of conventional design with a convergent-divergent nozzle section having a 3.65 to 1 expansion ratio and the chamber-to-throat area ratio of 2 to 1. Except for film cooling in the combustion chamber no added cooling provisions were made. The injector assembly, located at the front of the combustion chamber, was of the triplet impinging type with two alcohol jets impinging upon one central oxygen jet. Initial propellant ignition was obtained with two integral alcohol-oxygen igniters fired by Aircraft type spark plugs.

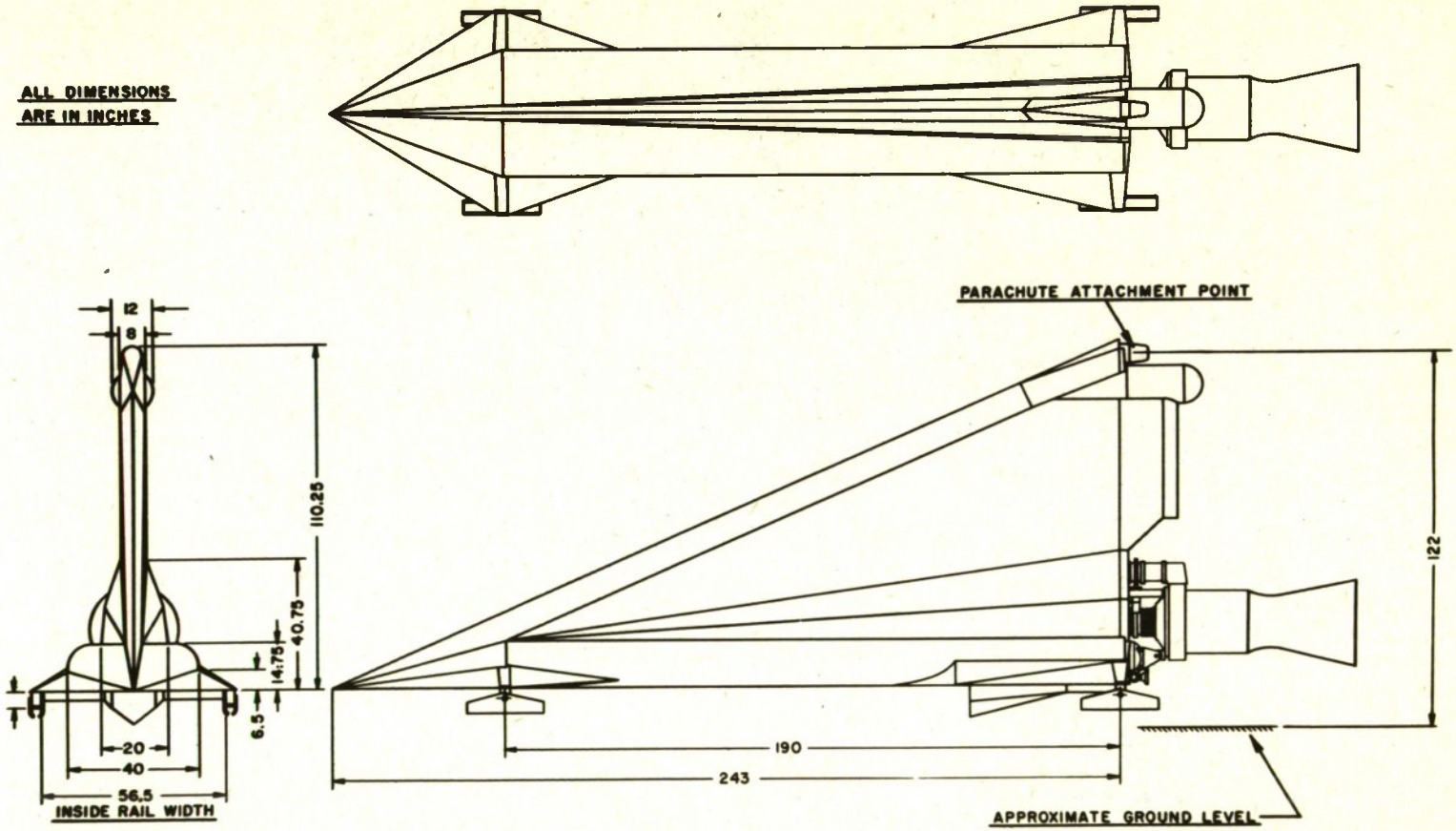

Figure 78 . Vehicle Outline Drawing Showing Basic Dimensions

A pneumatic control box, located just forward of the rocket engine, contained solenoid control valves through which 750 psig nitrogen gas was supplied to all pneumatically operated engine control valves. For this purpose, nitrogen was drawn from an auxiliary nitrogen tank which was isolated from the main tank by a check valve. The solenoid valves were actuated by a 24 volt battery carried on the sled.

The propellant feed pressure system was used to expel the propellants from their tanks. The heart of this system was the feed pressure regulator which was set to regulate the rate of propellant flow and hence the delivered thrust of the rocket engine. The regulator was located at the forward end of the main nitrogen tank and reduces the 3000 psig main tank pressure to a nominal operating pressure varying between 400 and 600 psig. The system was doubly protected from over pressurization by a 1100 psig burst-diaphragm set in the regulator, and by relief features of the vent valve system.

The main propellant valves and actuator assemblies were pneumatically operated, double-blade type shutoff valves, which were located in the piping immediately between the propellant tanks and the injector assembly on the rocket engine. The valve controlled the flow of liquid oxygen and alcohol to the thrust chamber.

Figure 79 shows the basic structure of the vehicle before aerodynamic fairing was installed. The main longitudinal member, a 10 inch diameter tube of 1/4 inch SAE 4130 heat treated steel, formed the backbone of the sled and served as the reservoir for the pressurizing gas of the fuel system. The cross members, welded to each end of the center tank, were box structures of SAE 4130 steel. The upright at the rear of the sled, also of SAE 4130 steel, was a weld-fabricated I-beam section. The top of this upright served as the attachment point for the parachutes to be tested. To support the rear upright and to complete the structural rigidity of the sled, a tubular diagonal member was attached between the top of the rear upright and the front of the main nitrogen tank. This strut also served as the auxiliary nitrogen tank for all pneumatically operated engine control valves. The structure was designed to withstand parachute opening shock loads of 100,000 pounds applied at the attachment point at the top of the upright.

The fuel and oxydizer tanks were 12 inch diameter tubes of 1/4 inch 61 ST aluminum designed for working pressures of 600 psig. They were attached to either side of the nitrogen tank with fixed supports at the rear and front supports which permitted longitudinal movement due to expansion or contraction.

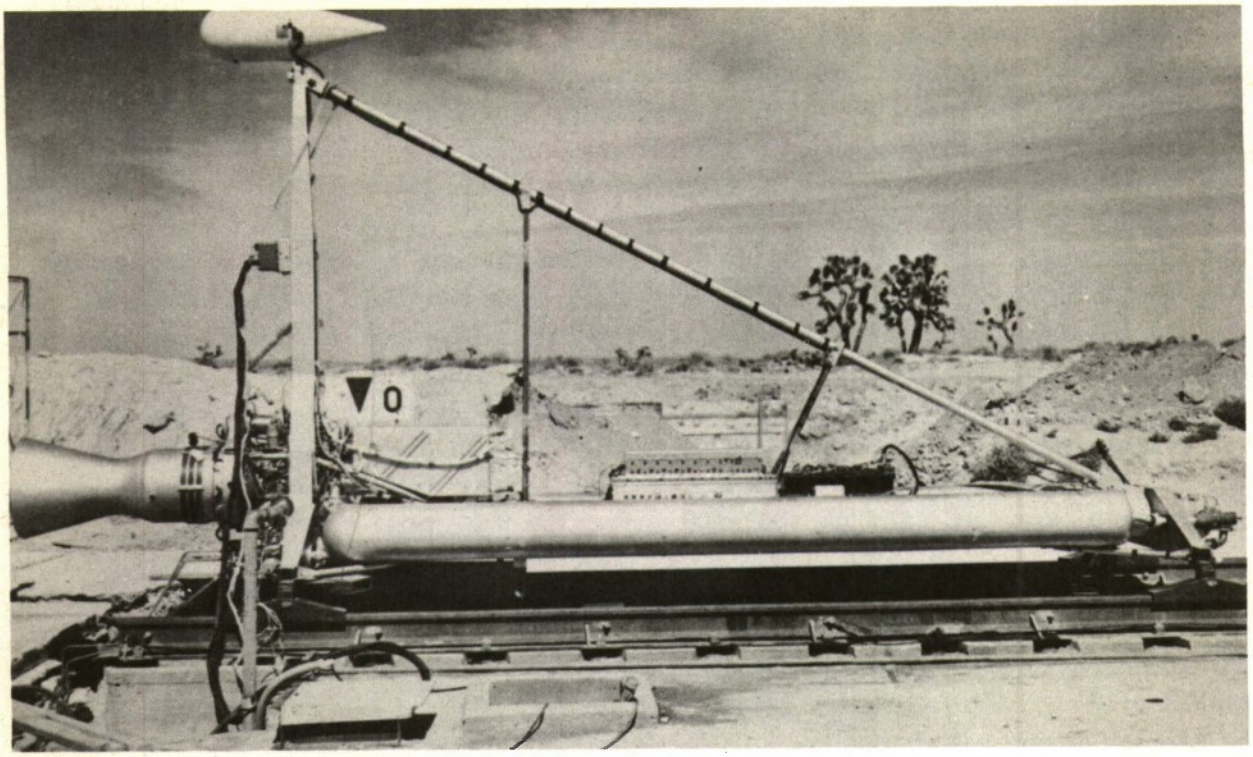

Figure 79 Basic Structure of Test Vehicle

After initial dynamic tests with the basic structure, an aerodynamic fairing was fabricated around the structure to minimize drag and reduce turbulence behind the sled. Since aerodynamic calculations, confirmed by wind tunnel data obtained in the transonic tunnel at WPAFB, had predicted comparatively small loads on the fin section of the proposed design, a multi-spar, semistressed-skin type of construction was used. Large, hinged access doors were provided to the instrumentation and control compartments of the fins and nose section assemblies. A camera compartment housing high-speed motion picture cameras was fabricated on the rear of the vertical upright over the rocket engine.

One of the series of Schlieren photos obtained from the tests performed in the transonic wind tunnel at WPAFB is shown in Fig. 80.

The slippers on which the sled traveled were designed by Cook Research Laboratories' Engineers and were typical of the type used at the Free Air Test Facility at EAFB. They were fabricated of heavy heat-treated steel with sectional stellite pads welded to the inner surfaces to reduce frictional wear. The slippers were designed to grip the rail in such a manner that upward as well as downward loads could be transmitted to the rails. No lubrication was provided.

A water brake, developed by the Cook Research Laboratories, (PR3-7; Ref. 15) and a water trough installed between the rails of the last 2000 foot of track at the test facility, served as the braking method for stopping the test vehicle after each test run. As the sled entered this portion of the track, which slopes approximately 6 inches over its length, the scoop, mounted on the aft-under side of the vehicle, picked up water and discharged it on both sides of the vehicle with a relative velocity forward. The energy thus imparted to the water provided a braking force as a reaction on the test vehicle. The intake shape was designed with respect to the track profile (slope) so that a constant braking force would be realized as the vehicle was decelerated.

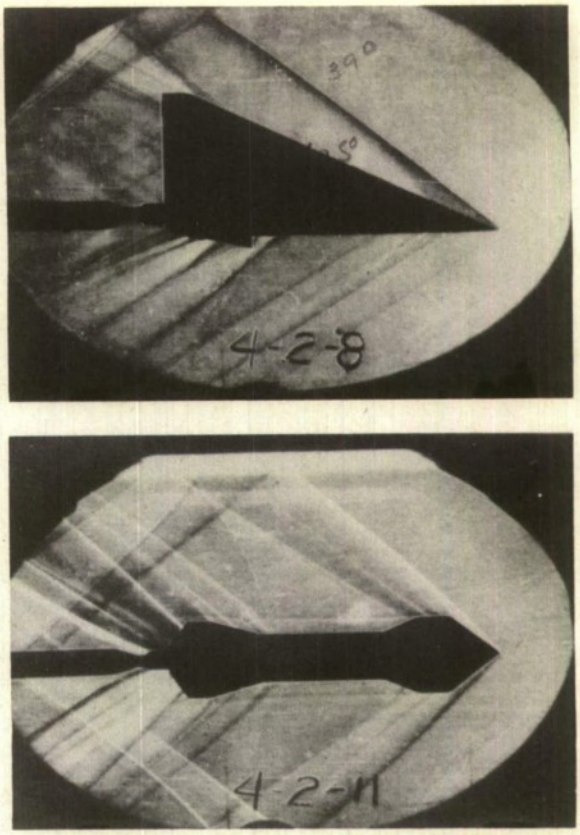

Figure 80 Schlieren Photographs of Wind Tunnel Test Model

The effective drag area of the faired sled with slippers and projecting water scoop was approximately 6 sq ft in the subsonic region and 13 sq ft in the transonic region.

Instrumentation was carried in the test vehicle to record all parameters essential in obtaining complete performance data for the vehicle as well as for the parachutes being tested. A complete description of the sled-borne and associated instrumentation utilized in the test program is presented in Appendix G.

APPENDIX G

INSTRUMENTATION

The primary data recording instrumentation used on the test vehicle was a magnetic tape recording system designed and developed by Cook Research Laboratories, Chicago, Illinois. In the early part of the program two eight channel tape drive mechanisms and associated signal converter units were used to record rocket engine performance parameters as well as parachute and sled performance. When rocket engine performance characteristics had become fairly well established the tape recording system was changed to include one eight channel recorder with associated signal converter units and a dual power supply unit.

The outputs of resistance type sensing elements such as strain gage tensiometers, pressure gages, accelerometers, etc., were converted to a frequency modulated signal which was amplified and recorded on magnetic tape. The signal frequency was adjusted to vary from 12 kc at no signal to approximately 16 kc at full scale. A constant 10 kc signal was also recorded and served as a reference time base during playback of the record. A block diagram of the instrumentation utilized to record parachute and sled performance parameters on a typical sled test is shown in Fig. 81, and Fig. 82 shows a typical oscillograph record of some of the quantities measured. Figure 83 shows the instrumentation compartments in the test vehicle with the dual-recorder instrumentation mounted in place. The playback equipment is diagrammed in Fig. 84 and the photographs in Fig. 85 show the front and rear views of the playback equipment consoles.

The important quantities measured for analysis of parachute performance data and the sensing elements for the measurements are shown in Table 24. Various other gages were employed during the program to measure items such as tank pressures, chamber pressure, valve positions, and other engine performance parameters.

In addition to the 10 kc reference time base from the reference frequency oscillator, a 100 cycle signal was recorded on both the magnetic tape and on the 16 mm film in the sledborne cameras. This provided positive synchronization between the photographic record and the tape recorded information.

An exact record of the space-time history of the vehicle on each test run was obtained by recording impulses from sled mounted inductive pickup coils as they passed stationary, permanent magnets equally spaced in 50

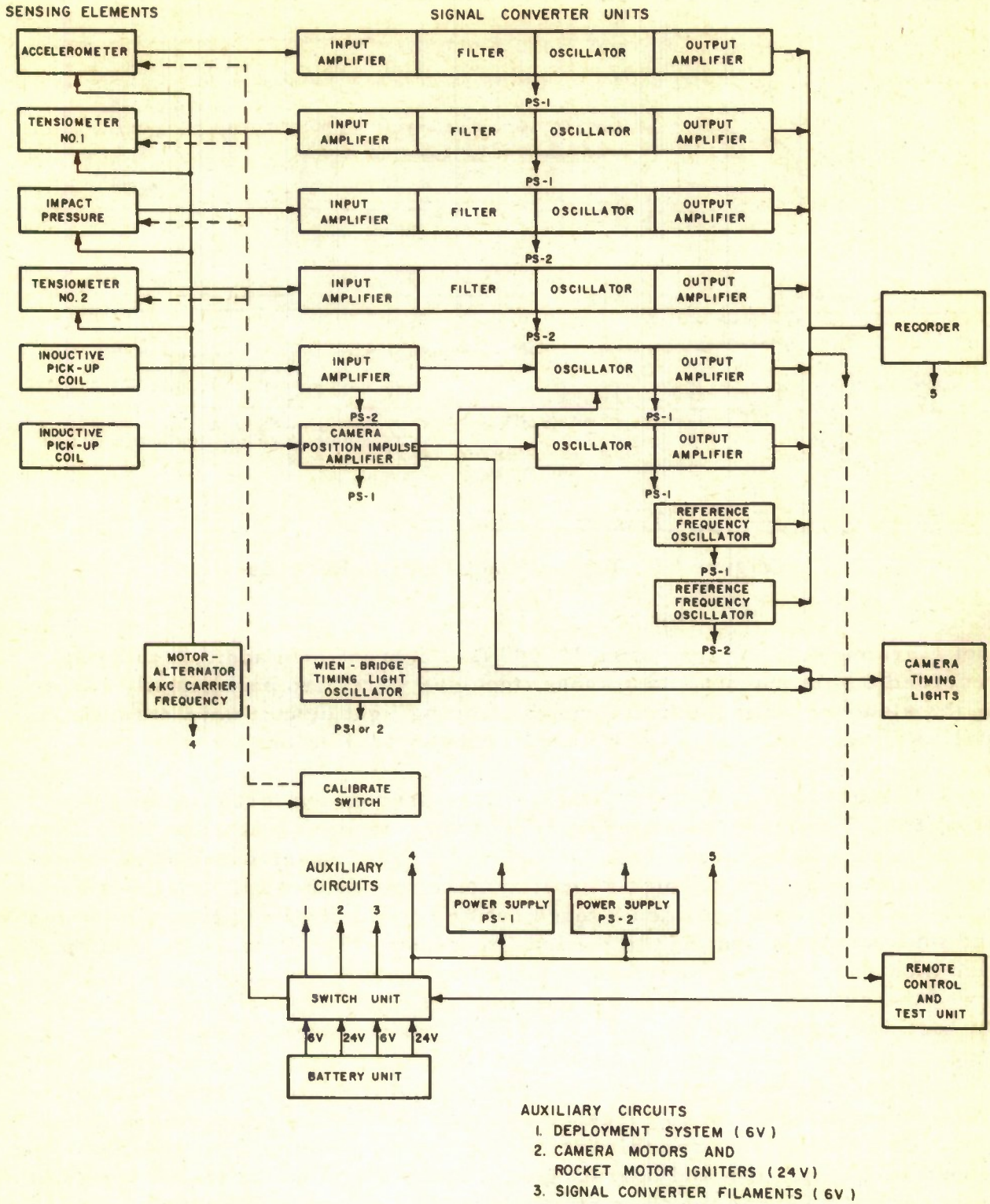

Figure 81 Instrumentation Block Diagram

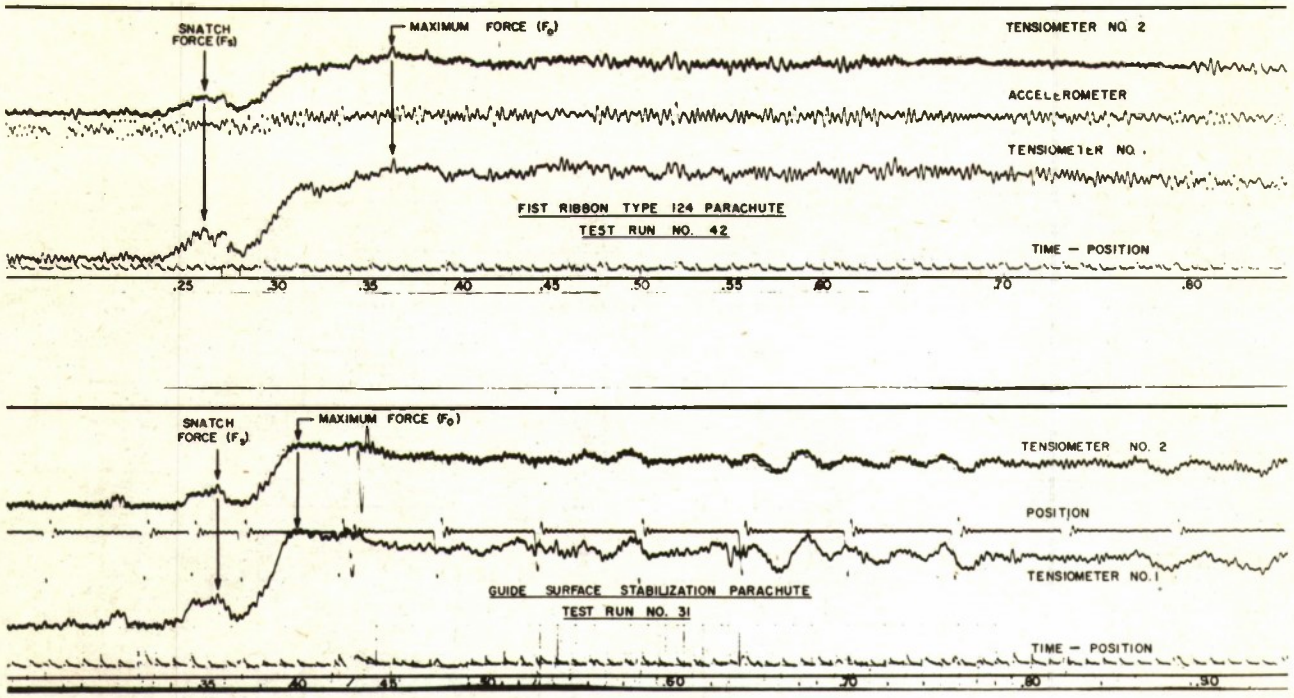

Figure 82 Typical Oscillograph Records

foot increments along the entire 10,000 feet of track. In addition to being recorded on the magnetic tape these impulses were also permanently recorded on the sledborne camera film through a timing light circuit developed and installed in the cameras by Cook Research Laboratories' engineers.

Various motion picture cameras were used on the test vehicle during the program. These are identified by type, frame speed, location on the vehicle and test run numbers in Table 25. Sufficient illumination was present at the test site to allow use of color film at camera speeds up to 1000 frames per second. Color film provided a much better record of events than simple black and white contrast, but due to the long processing time required one of the sled mounted cameras was usually loaded with black and white film. This allowed the examination of at least one photographic record a few hours after the test was completed.

In addition to the sled mounted motion picture cameras a number of track side motion picture, sequence and still cameras were employed on each test. On a typical test run this included several individually panned cameras loaded with color film and operating at a frame speed of 128 fps, a series of stationary high-speed motion picture cameras loaded with black and white

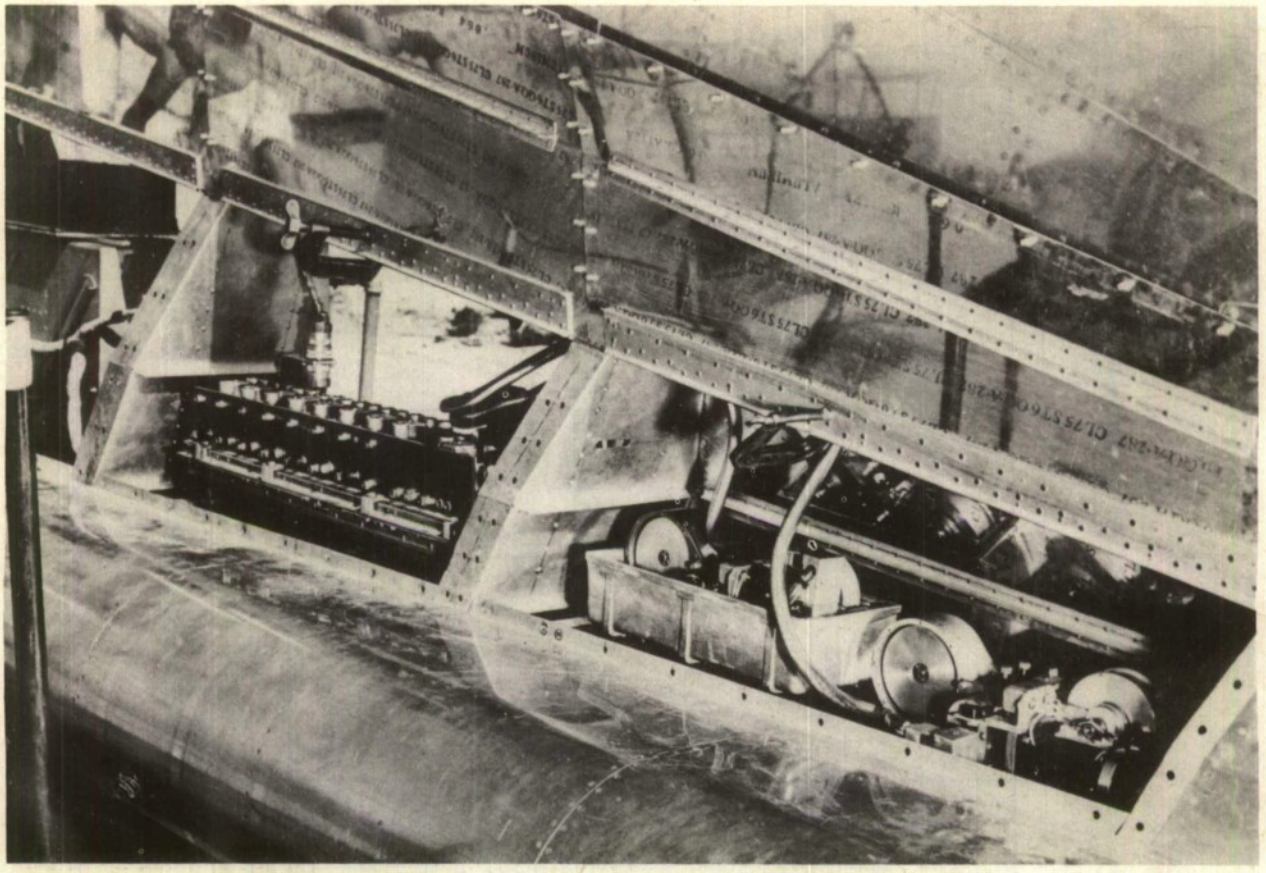

Figure 83 Test Vehicle Instrumentation Compartments

film and operating at a frame speed of approximately 1000 fps, a hand operated sequence camera used to record a peak action shot and any still photography deemed essential. The diagram in Fig. 86 illustrates the placement of photographic coverage on a typical high-speed sled test run.

During the early part of the test program several burnouts were experienced in the rocket engine injector and chamber assemblies. Examination of the oscillographic records revealed the excessive pressure pulsation had been present in the engine on all runs where rough engine combustion had led to engine burnout. An automatic engine shutdown device which detected rough engine performance and shut down the rocket engine was designed and installed in the engine circuit by the engineers of the Cook Research Laboratories Field Test Section. This unit was designed so that it would count the pressure pulsations present in improper engine combustion but would not be actuated by the normal pressure variations in the rocket thrust chamber. When a preset number of abnormal pulsations had occurred

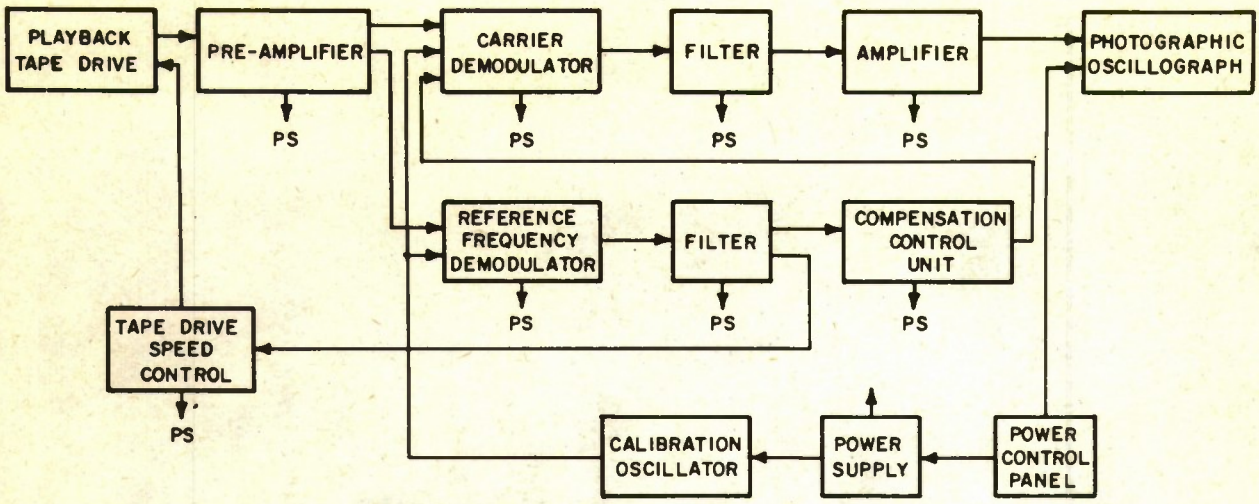

MAGNETIC TAPE PLAYBACK SYSTEM

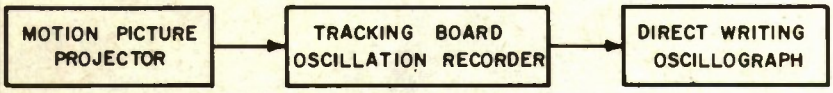

MOTION PICTURE PLAYBACK SYSTEM

Figure 84 Playback System Block Diagram

the device automatically initiated the engine shutdown circuit and prevented eventual damage to the rocket engine. A schematic diagram of the automatic shutdown device is shown in Fig. 87

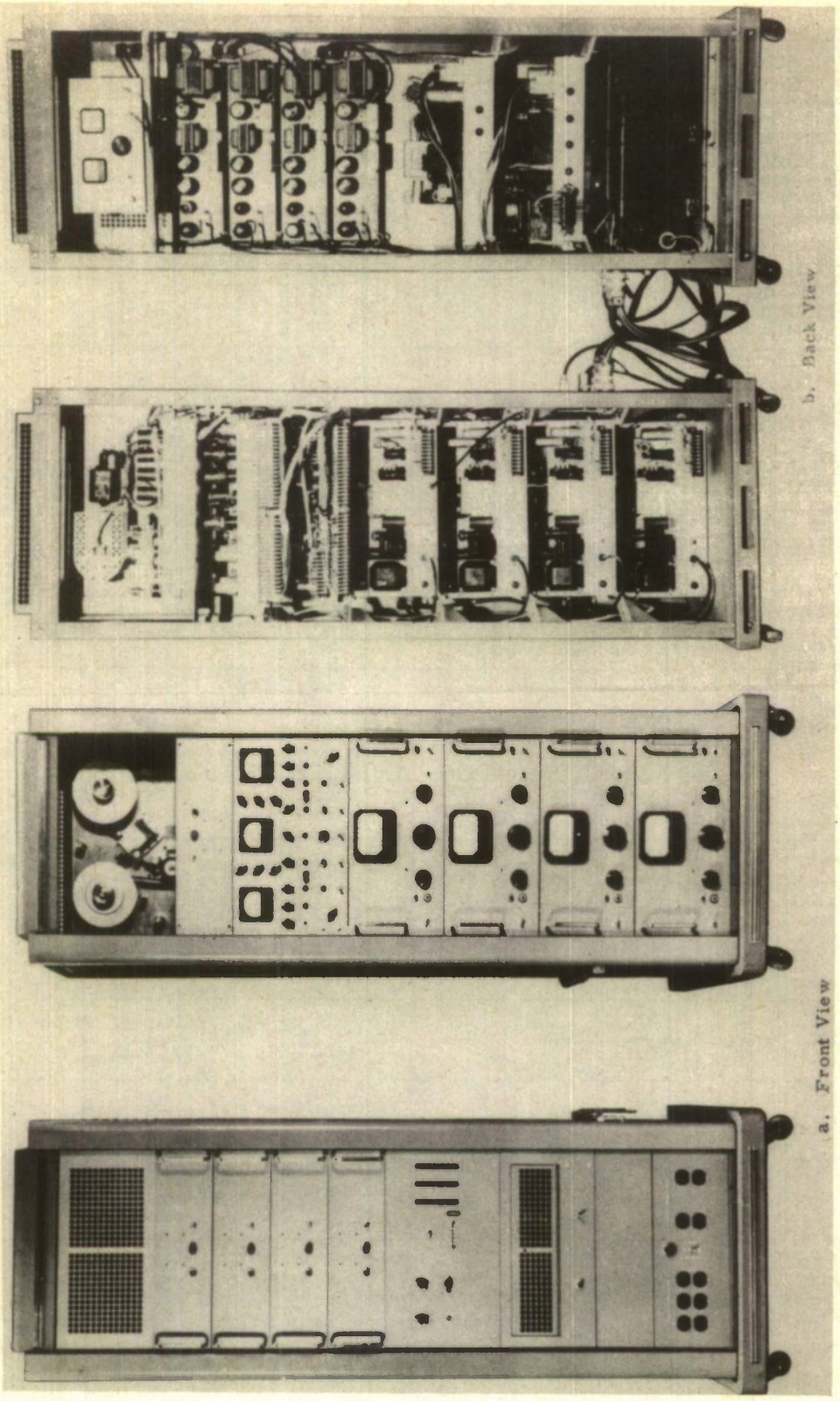

Figure 85 Playback Consoles

TABLE 24

TRANSDUCERS AND QUANTITIES MEASURED

QUANTITY MEASURED	SENSING ELEMENT	RATED FULL SCALE OF SENSING ELEMENT	APPROXIMATE FULL SCALE OUTPUT *	LOCATION OF SENSING ELEMENT OR COMPONENT	REMARKS
PARACHUTE DRAG FORCE	BALDWIN SR-4 RESISTANCE STRAIN GAGE BRIDGE TENSIOMETERS	30,000 lb 50,000 lb 100,000 lb	15 MV 15 MV 15 MV	CONNECTING LINK BETWEEN PARACHUTE RISERS AND SLED ATTACHMENT.	TENSION LINK OF STEEL WITH 120,000 PSI YIELD STRENGTH. RATED FULL SCALE LOAD CORRESPONDED TO STRESS OF 60,000 PSI.
IMPACT PRESSURE	STATHAM P96-20D-350 WIANCO 3 PAD-10 (P1405)	0-20 PSIg 0-10 PSIg	20MV 1V	IN NOSE SECTION COMPARTMENT OF TEST VEHICLE.	NOT USED AFTER RUN NO. 48.
ACCELERATION	STATHAM A5A-15-350 STATHAM A5A-50-350	± 15 Gs ± 50 Gs	20 MV 20 MV	ON FORWARD SPAR BULKHEAD FACING REAR CONTROL COMPARTMENT. APPROXIMATE LATERAL C.G. OF VEHICLE.	
TIME	10KC OSCILLATOR	——	——	INSTRUMENTATION COMPARTMENT	SEE TEXT
POSITION	INDUCTIVE PICKUP COIL	——	——	ON LEFT FORWARD SLIPPER OF TEST VEHICLE.	SEE TEXT
STABILITY & GENERAL PARACHUTE BEHAVIOR.	MOTION PICTURE CAMERAS	——	——	ON CAMERA COMPARTMENT ON REAR OF SLED UPRIGHT.	SEE TABLE

* FOR 10V INPUT TO BRIDGE. SUFFICIENT AMPLIFICATION WAS AVAILABLE THAT FULL FREQUENCY SHIFT COULD BE OBTAINED WITH 3.5 MV.

TABLE 25

SLEDBORNE PHOTOGRAPHIC EQUIPMENT

RUN NO.	CAMERA TYPE	FILM	FRAME SPEED	TIMING LIGHTS *	LOCATION	COVERAGE
1-37	FASTAX	16MM COLOR	1000	YES	CAMERA COMPARTMENT UPPER	PARACHUTE INFLATION OPERATION AND STABILITY DATA
	BELL & HOWELL 70 G	16 MM COLOR	128	YES	CAMERA COMPARTMENT LOWER	PARACHUTE INFLATION OPERATION AND STABILITY DATA
38-48	FASTAX	16MM COLOR	1000	YES	CAMERA COMPARTMENT LOWER	PARACHUTE INFLATION OPERATION AND STABILITY DATA
	GSAP N-9	16MM COLOR	64 ($\frac{1}{1000}$ sec. exp.)	NO	CAMERA COMPARTMENT UPPER	GENERAL PARACHUTE OPERATION
49-63	BELL & HOWELL 70 G	16 MM COLOR	128	YES	MODIFIED CAMERA COMPARTMENT BELOW ELECTRICAL DISCONNECT	PARACHUTE INFLATION OPERATION AND STABILITY DATA
	GSAP N-6	16MM COLOR	64 ($\frac{1}{128}$ sec. exp.)	NO	FORWARD PART OF PARACHUTE COMPARTMENT	PARACHUTE PACK TRAJECTORY DURING DEPLOYMENT

* 100 CYCLE LIGHT IMPULSE RECORDED ON FILM AND ON MAGNETIC TAPE TO PROVIDE RECORD SYNCRONIZATION.

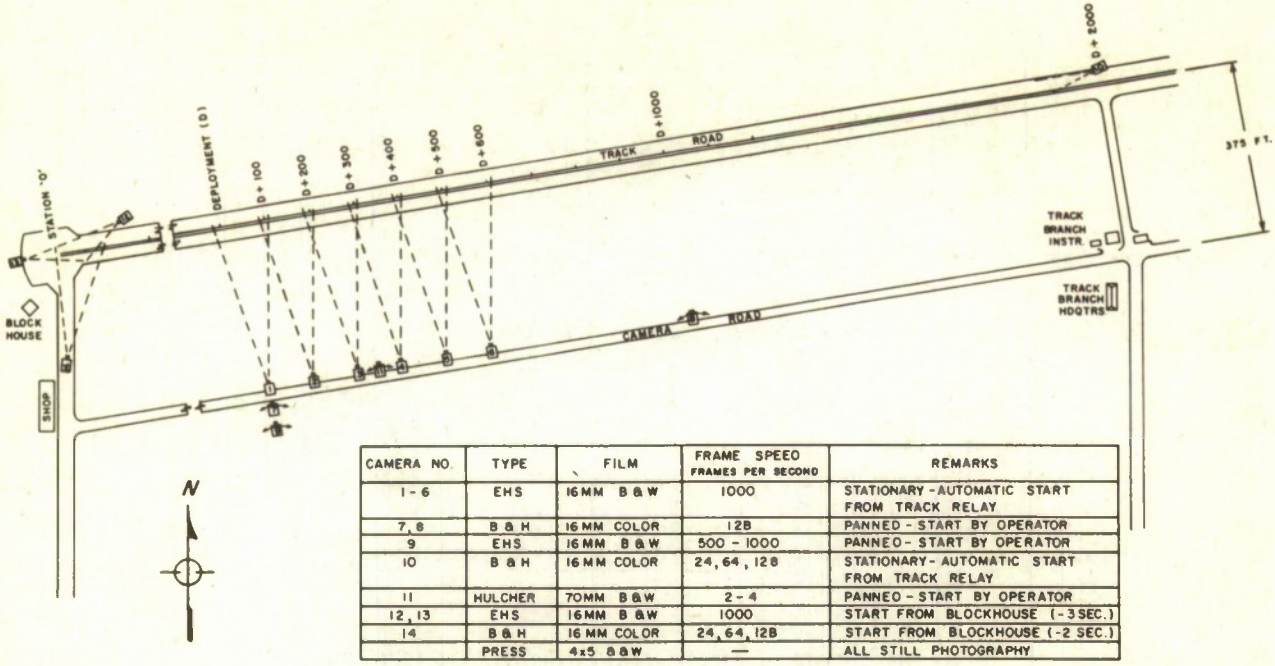

CAMERA NO.	TYPE	FILM	FRAME SPEED FRAMES PER SECOND	REMARKS
1-6	EHS	16MM B&W	1000	STATIONARY - AUTOMATIC START FROM TRACK RELAY
7, 8	B & H	16 MM COLOR	128	PANNED - START BY OPERATOR
9	EHS	16MM B&W	500 - 1000	PANNED - START BY OPERATOR
10	B&H	16MM COLOR	24, 64, 128	STATIONARY - AUTOMATIC START FROM TRACK RELAY
11	HULCHER	70MM B&W	2-4	PANNED - START BY OPERATOR
12, 13	EHS	16MM B&W	1000	START FROM BLOCKHOUSE (-3 SEC.)
14	B&H	16 MM COLOR	24, 64, 128	START FROM BLOCKHOUSE (-2 SEC.)
	PRESS	4x5 B&W	—	ALL STILL PHOTOGRAPHY

EHS - EASTMAN HIGH SPEED
B&H - BELL & HOWELL MODEL 70G

Figure 86 Trackside Photographic Coverage

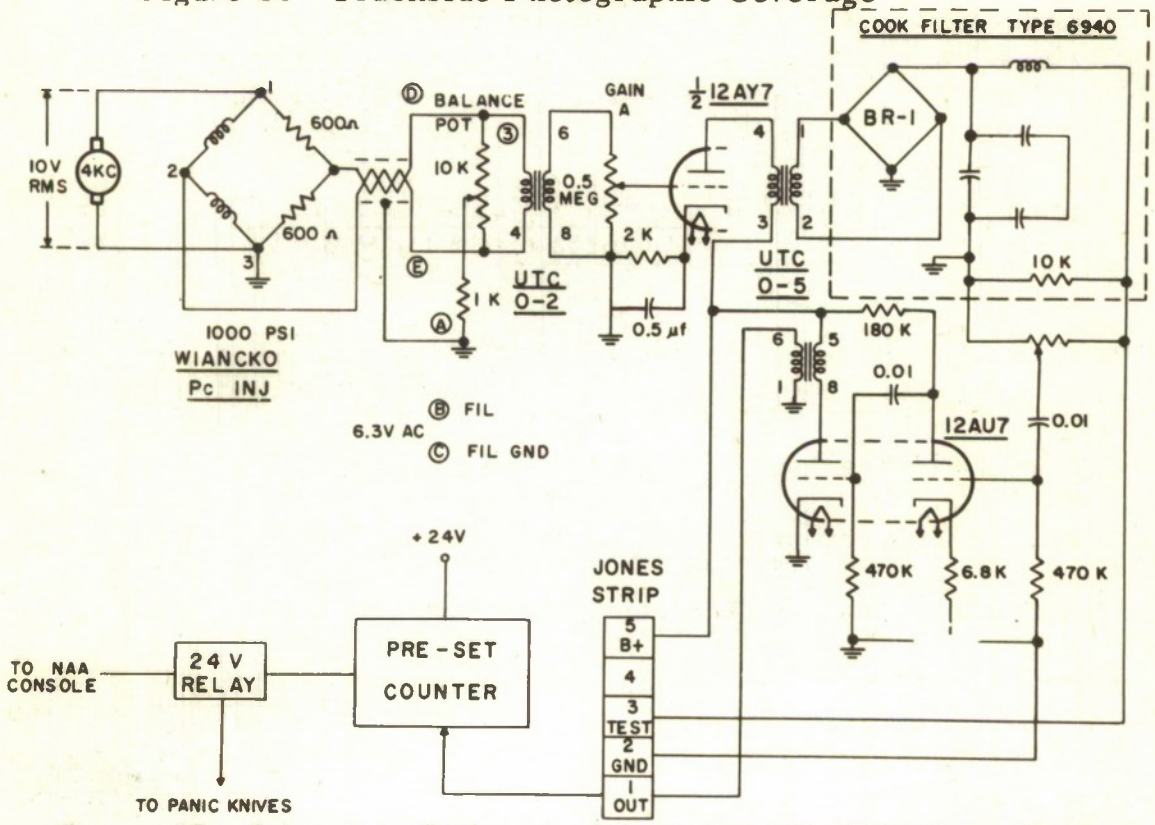

Figure 87 Schematic Diagram of Automatic Sled Shutdown Device

BIBLIOGRAPHY

1. Barnes, R. W. United States Air Force Parachute Handbook. AMC Engineering Division, Parachute Branch, Equipment Laboratory Wright-Patterson Air Force Base, Ohio. March 1951. (CADO ATI No. 35532)

2. Freeman, H. F. Determination of Parachute Diameter. AMC Engineering Division. Report No. MCREXE-672-12H. Wright-Patterson Air Force Base, Ohio. 1 April 1950

3. Heinrich, Dr. H. G. Guide Surface Parachutes. AMC, Engineering Division, Equipment Laboratory. Report No. MCREXE-672-25F. Wright-Patterson Air Force Base, Ohio. February 1948

4. Heinrich, Dr. H. G. Experimental Parameters in Parachute Opening Theory

5. Knacke, T. Design, Use and Construction of FIST Type Parachute. AMC, Engineering Division, Report No. MCREXE-672-19LL. Wright-Patterson Air Force Base, Ohio. June 1948

6. McComb, W. J. Porosity of Ribbon Parachutes. AMC, Technical Note No. I-12. Wright-Patterson Air Force Base, Ohio. November 1951

7. Military Specification. Parachute, Ribbed Guide Surface, General Specification for Construction of. MIL-P-5905A. 29 February 1952

8. Military Specification. Parachute, FIST Ribbon, General Specification for Construction of. MIL-P-6635 (USAF). 27 July 1951

9. Military Specification. Nylon Cord. MIL-C-5040

10. Military Specification. Nylon Tubular Webbing. MIL-W-5625

11. Military Specification. Parachute Nylon Ribbon. MIL-R-5608

12. Air Force - Navy Aeronautical Specification. Nylon Thread

13. U. S. Air Force Specification. Drag Parachute Nylon Cloth

14. Cook Research Laboratories. Recovery Systems for Missiles and Target Aircraft, Parts I and II, WADC TR 5853

15. Cook Research Laboratories. Interim Progress Report PR 3-1 through PR 3-35

16. Radioplane Co., Rotafoil Performance Evaluation Report No. 705 January 1953